

INFORMATION TO USERS

This manuscript has been reproduced from the microfilm master. UMI films the text directly from the original or copy submitted. Thus, some thesis and dissertation copies are in typewriter face, while others may be from any type of computer printer.

The quality of this reproduction is dependent upon the quality of the copy submitted. Broken or indistinct print, colored or poor quality illustrations and photographs, print bleedthrough, substandard margins, and improper alignment can adversely affect reproduction.

In the unlikely event that the author did not send UMI a complete manuscript and there are missing pages, these will be noted. Also, if unauthorized copyright material had to be removed, a note will indicate the deletion.

Oversize materials (e.g., maps, drawings, charts) are reproduced by sectioning the original, beginning at the upper left-hand corner and continuing from left to right in equal sections with small overlaps. Each original is also photographed in one exposure and is included in reduced form at the back of the book.

Photographs included in the original manuscript have been reproduced xerographically in this copy. Higher quality 6" x 9" black and white photographic prints are available for any photographs or illustrations appearing in this copy for an additional charge. Contact UMI directly to order.

UMI

A Bell & Howell Information Company
300 North Zeeb Road, Ann Arbor MI 48106-1346 USA
313/761-4700 800/521-0600

RICE UNIVERSITY

**ELUCIDATION OF THE FORMATION AND
DECOMPOSITION OF CLATHRATE HYDRATES OF
NATURAL GASES THROUGH GAS SOLUBILITY
MEASUREMENTS**

**by
GUILLAUME FENEYROU**

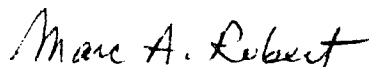
**A THESIS SUBMITTED
IN PARTIAL FULFILLMENT OF THE
REQUIREMENTS FOR THE DEGREE**

MASTER OF SCIENCE

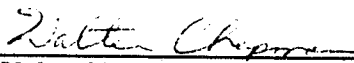
APPROVED, THESIS COMMITTEE:



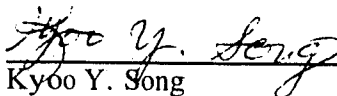
Riki Kobayashi, Director
Professor of Chemical Engineering



Marc A. Robert
Professor of Chemical Engineering



Walter Chapman
Associate Professor of Chemical Engineering



Kyoo Y. Song
Senior Research Associate in Chemical
Engineering

Houston, Texas
May, 1996

UMI Number: 1379494

UMI Microform 1379494
Copyright 1996, by UMI Company. All rights reserved.

**This microform edition is protected against unauthorized
copying under Title 17, United States Code.**

UMI
300 North Zeeb Road
Ann Arbor, MI 48103

ABSTRACT

Elucidation of the Formation and Decomposition of Clathrate Hydrates of Natural Gases through Gas Solubility Measurements

by
Guillaume Feneyrou

Through isobaric temperature ramping experiments, the solubility of pure methane, ethane, propane, carbon dioxide gases and a methane-propane gas mixture in pure liquid water has been measured. The experiments are conducted at low temperatures and pressures corresponding to the clathrate hydrate formation and decomposition region.

The inhibitory effect of a 10 weight percent methanol aqueous solution and a 0.5 weight percent polyvinylpyrrolidone aqueous solution on the hydrate formation and decomposition conditions has been estimated. A study of the pH-induced change in the hydrate stability has also been performed.

The isobaric solubility data obtained show a significant divergence from Henry's law prior to and during hydrate formation. A molecular mechanism of hydrate nucleation is hypothesized, based on an analysis of the gas supersaturation observed and the current knowledge on the structure of liquid water.

ACKNOWLEDGMENTS

I wish to express my sincere gratitude to the following persons and organizations.

Professor Riki Kobayashi, for fostering a research environment that encourages creativity, individual initiative and trust; for his professional and unselfish guidance as principal thesis advisor.

Dr. Kyoo Y. Song, whose rigorous methodology, experience and friendship supported me throughout this project.

Mr. Raymond Martin, for his expert maintenance of the experimental apparatus.

Dr. Doug Elliott (IPS Inc.), for his assistance and financial support.

Professors Marc Robert and Walter Chapman for serving on my oral committee.

Most of all, to my fiancée, Lurdes, and my family, for their continuous interest, encouragement and affection.

TABLE OF CONTENTS

RICE UNIVERSITY	i
ABSTRACT	ii
ACKNOWLEDGMENTS	iii
TABLE OF CONTENTS	iv
LIST OF TABLES	vii
LIST OF FIGURES	viii
INTRODUCTION	1
1. EXPERIMENTAL PROGRAM	6
<i>1.1. Experimental Method</i>	6
1.1.1. Previous Experimental Methods.....	6
1.1.2. Isobaric Volume-Temperature Loops: "Ramping Experiments".....	10
1.1.3. Experimental Procedure.....	11
<i>1.2. Experimental Apparatus</i>	13
1.2.1. Current Equipment.....	13
1.2.2. Future Modifications.....	17
2. THE SOLUBILITY OF PURE HYDROCARBON GASES IN PURE WATER IN THE HYDRATE REGION	18
<i>2.1. Experimental Results</i>	18
2.1.1. Objective.....	18
2.1.2. First Set of Experiments.....	18
2.1.3. Second Set of Experiments.....	22

2.2. <i>Data Analysis and Discussion</i>	30
2.2.1. Mass Balances	31
2.2.2. Results.....	34
2.2.3. Enthalpies and Entropies of Solution.....	41
2.2.4. Discussion.....	49
3. EFFECT OF INHIBITORS ON HYDRATE FORMATION AND DECOMPOSITION	56
3.1. <i>Experimental Results</i>	56
3.2. <i>Data Analysis and Discussion</i>	65
4. INFLUENCE OF THE pH OF THE WATER ON THE CATASTROPHIC CONDITIONS	71
4.1. <i>Results</i>	71
4.2. <i>T_c and FHDT as a Function of the pH of Water</i>	86
4.2.1. Comparisons of T _c and FHDT.....	86
4.2.2. Phase Rule.....	88
4.3. <i>Gas Solubility at T_c</i>	89
4.4. <i>Low Temperature CH₄-C₃H₈ Runs</i>	92
5. MOLECULAR INSIGHTS ON THE DISSOLUTION OF HYDROCARBON GASES IN LIQUID WATER.....	95
5.1. <i>Primary Nucleation, Crystal Growth and Metastability</i>	95
5.2. <i>Previous Investigations on Hydrate Nucleation</i>	98
5.3. <i>The Structure of Water upon Cooling and Hydrocarbon dissolution</i>	102
5.3.1. The Structure of Liquid Water.....	102
5.3.2. Dissolution of Non-polar Gases in Water: A Molecular Mechanism for Gas Hydrate Nucleation ?.....	104

CONCLUSIONS AND FUTURE WORK.....	108
<u>APPENDIX A:</u> SAMPLE CALCULATIONS OF MASS BALANCES, HYDRATE DENSITIES AND EXPERIMENTAL ACCURACY	110
<u>APPENDIX B:</u> THERMODYNAMIC RELATIONS FOR ENTHALPIES AND ENTROPIES OF SOLUTION.....	114
<u>APPENDIX C:</u> IMPACT OF NEW SOLUBILITY DATA ON STATISTICAL THERMODYNAMICS PREDICTIONS	116
BIBLIOGRAPHY	119

LIST OF TABLES

TABLE 2-1	CONSTANT PRESSURE EXPERIMENTS.....	23
TABLE 2-2	VOLUME CHANGE UPON CONVERTING WATER TO HYDRATE.....	35
TABLE 2-3	ENTHALPIES AND ENTROPIES OF SOLUTION OF CH ₄ IN LIQUID WATER	42
TABLE 2-4	ENTHALPIES AND ENTROPIES OF SOLUTION OF C ₂ H ₆ IN LIQUID WATER.....	42
TABLE 2-5	ENTHALPIES AND ENTROPIES OF SOLUTION OF C ₃ H ₈ IN LIQUID WATER.....	43
TABLE 2-6	ENTHALPIES AND ENTROPIES OF SOLUTION OF CO ₂ IN LIQUID WATER.....	43
TABLE 2-7	ENTHALPIES AND ENTROPIES OF SOLUTION OF PURE HYDROCARBONS IN LIQUID WATER.....	44
TABLE 2-8	CATASTROPHIC AND FINAL HYDRATE DECOMPOSITION TEMPERATURES	52
TABLE 2-9	ENTHALPIES OF DISSOCIATION OF HYDRATE TO LIQUID WATER AND VAPOR.....	54
TABLE 3-1	COMPRESSIBILITY FACTORS AND PHASES OF METHANE-PROPANE MIXTURES AT 300 PSIA.....	58
TABLE 3-2	TC AND FHDT OF CH ₄ -AQUEOUS SOLUTION SYSTEMS.....	59
TABLE 3-3	TC AND FHDT OF C ₂ H ₆ -AQUEOUS SOLUTION SYSTEMS.....	60
TABLE 3-4	TC OF CH ₄ -C ₃ H ₈ IN AQUEOUS SOLUTIONS	60
TABLE 3-5	FHDT OF CH ₄ -C ₃ H ₈ IN AQUEOUS SOLUTIONS	61
TABLE 3-6	TC AND FHDT OF CO ₂ -AQUEOUS SOLUTION SYSTEMS.....	61
TABLE 3-7	RELATIVE DIFFERENCES BETWEEN TC AND FHDT	66
TABLE 4-1	PH-TEMPERATURE RAMPING EXPERIMENTS.....	71
TABLE 4-2	MEAN pH OVER THE RANGE OF TEMPERATURE CONSIDERED AND THE STANDARD DEVIATION FROM THE MEAN.....	72
TABLE 4-3	CATASTROPHIC TEMPERATURES IN VARIOUS pH SOLUTIONS.....	80
TABLE 4-4	FINAL HYDRATE DECOMPOSITION TEMPERATURES IN VARIOUS pH SOLUTIONS.....	81
TABLE 4-5	GAS CONCENTRATION IN THE LIQUID PHASE AT TC FOR SEVERAL SYSTEMS.....	91
TABLE 4-6	SECOND CATASTROPHIC INCREASE IN CH ₄ -C ₃ H ₈ RUNS	92
TABLE 5-1	CONSUMPTION OF METHANE GAS AT 55 BARS AND 274.3 K FROM BISHNOI ET AL. .	99

LIST OF FIGURES

FIGURE 1	HYDRATE OCCURRENCES IN THE WORLD.....	2
FIGURE 2	(H ₂ O) _n HOST STRUCTURES I,II AND H OF THE CLATHRATE "GAS" HYDRATES.....	3
FIGURE 1-1	THE THERMOSTATED HYDRATE UNIT	14
FIGURE 2-1	METHANE HYDRATE RUN IN PURE WATER (FIRST SET)	20
FIGURE 2-2	ETHANE HYDRATE RUN IN PURE WATER (FIRST SET)	21
FIGURE 2-3	PRESSURE-TEMPERATURE DIAGRAM FOR PROPANE AND WATER.....	25
FIGURE 2-4	ETHANE HYDRATE RUN IN PURE WATER.....	26
FIGURE 2-5	PROPANE HYDRATE RUN IN PURE WATER.....	27
FIGURE 2-6	PROPANE HYDRATE RUN IN PURE WATER. VOLUME AS FUNCTION OF TIME..	28
FIGURE 2-7	PROPANE HYDRATE RUN IN PURE WATER. TEMPERATURE AS FUNCTION OF TIME.....	29
FIGURE 2-8	PROPANE SOLUBILITY IN PURE WATER AT 60 PSIA.....	37
FIGURE 2-9	CARBON DIOXIDE SOLUBILITY IN PURE WATER AT 500 PSIA.....	38
FIGURE 2-10	METHANE SOLUBILITY IN PURE WATER AT 500 PSIA.....	39
FIGURE 2-11	ETHANE SOLUBILITY IN PURE WATER AT 500 PSIA.....	40
FIGURE 2-12	ENTHALPY OF SOLUTION OF METHANE IN PURE WATER.....	45
FIGURE 2-13	ENTHALPY OF SOLUTION OF ETHANE IN PURE WATER.....	46
FIGURE 2-14	ENTROPY OF SOLUTION OF METHANE IN PURE WATER	47
FIGURE 2-15	ENTROPY OF SOLUTION OF ETHANE IN PURE WATER	48
FIGURE 2-16	DISSOCIATION ENERGIES OF SINGLE-COMPONENT GAS HYDRATES	55
FIGURE 3-1	METHANE HYDRATE RUN IN A 10 WT% METHANOL AQ. SOLUTION.....	62
FIGURE 3-2	ETHANE HYDRATE RUN IN A 0.5 WT% PVP AQ. SOLUTION	63
FIGURE 3-3	CARBON DIOXIDE HYDRATE RUN IN A 10 WT% METHANOL AQ. SOLUTION ...	64
FIGURE 4-1	METHANE HYDRATE RUN IN A PH 7 BUFFER SOLUTION.....	74
FIGURE 4-2	HYDRATE RUN OF A MIXTURE OF CH ₄ AND C ₃ H ₈ (19.98 MOL %) IN A PH 5 BUFFER SOLUTION	75
FIGURE 4-3	METHANE HYDRATE RUN IN A PH 4 BUFFER SOLUTION.....	76
FIGURE 4-4	HYDRATE RUN OF A MIXTURE OF CH ₄ AND C ₃ H ₈ (19.98 MOL %) IN A PH 3 BUFFER SOLUTION	77
FIGURE 4-5	HYDRATE RUN OF A MIXTURE OF CH ₄ AND C ₃ H ₈ (19.98 MOL %) IN A PH 5 BUFFER SOLUTION	78

FIGURE 4-6	HYDRATE RUN OF A MIXTURE OF CH_4 AND C_3H_8 (19.98 MOL %) IN A PH 3 BUFFER SOLUTION	79
FIGURE 4-7	CATASTROPHIC TEMPERATURES OF CH_4 -BUFFER SOLUTIONS SYSTEMS.....	82
FIGURE 4-8	FHDT OF CH_4 -BUFFER SOLUTIONS SYSTEMS	83
FIGURE 4-9	CATASTROPHIC TEMPERATURES OF CH_4 - C_3H_8 -BUFFER SOLUTIONS SYSTEMS.....	84
FIGURE 4-10	FHDT OF CH_4 - C_3H_8 -BUFFER SOLUTIONS SYSTEMS.....	85
FIGURE 5-1	WATER CLUSTER FORMATION AROUND A DISSOLVED APOLAR MOLECULE..	107

INTRODUCTION

One of the most exciting research areas in chemical physics deals with the most common life-sustaining compound—water.¹

The smallest estimate of potential resources of natural gas contained in oceanic hydrate deposits is $1.5 \times 10^{16} \text{ m}^3$ [Makogon 1984]. About 50 hydrate occurrences with total gas reserves of 700 trillion m^3 are estimated in the world oceans [Fig. 1]. The energy density—volume of methane at standard conditions per volume of rock—of methane hydrate is two to five times greater than the energy density of conventional sources of gas. Thus, harvesting that energy resource without harming the environment may be one of the great engineering challenges of the future.

In addition, in 1934 when Hammerschmidt found hydrates to be the cause of plugged natural gas pipelines, industrial interest in preventing hydrate formation arose. The cost of hydrate inhibition through pipeline insulation, methanol or glycol injection ranges from 2×10^6 \$ to 50×10^6 \$. Hence, industrial needs in hydrate prevention during exploration, production, transmission and processing of natural gas are tremendous.

¹ E. Dendy Sloan, Jr. in his address to the International Conference on Natural Gas Hydrates (1993).

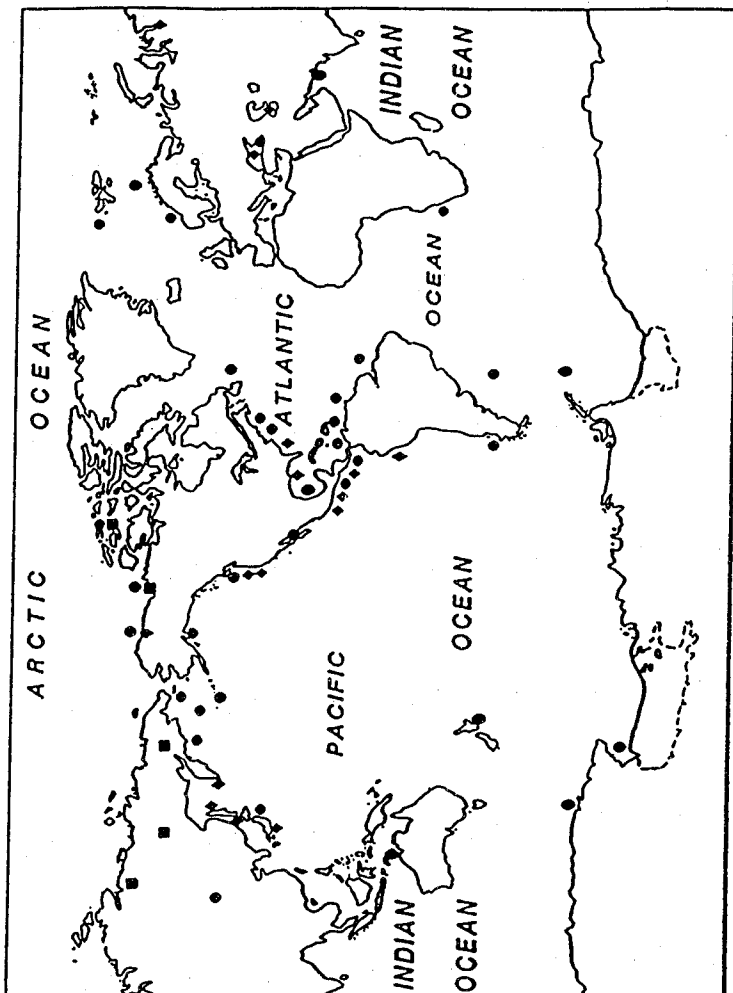
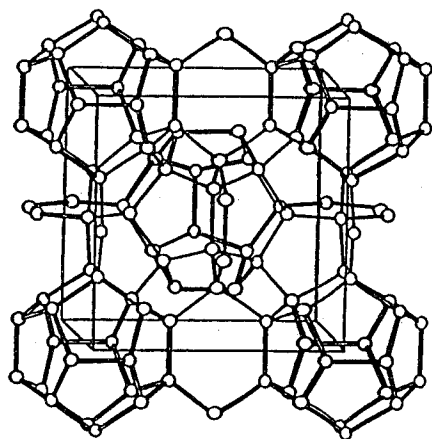
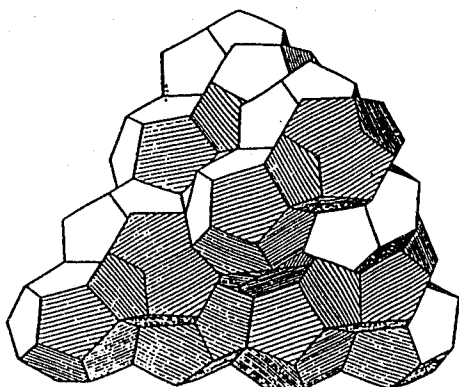


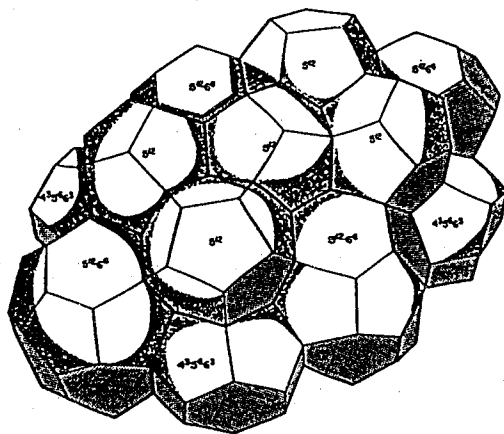
Fig. 1 Hydrate Occurrences in the World
(source: Kvenvolden, 1993)



Structure I



Structure II



Structure H

**Fig. 2 $(\text{H}_2\text{O})_n$ Host Structures I,II and H of the Clathrate
“Gas” Hydrates**
(source: Sloan, 1993)

Gas hydrates are crystalline materials composed of natural gas molecules trapped in a solid lattice of water molecules. The gas components filling the cavities are not directly bonded to the water molecules of the framework and accordingly are clathrate compounds. Hydrates form at moderate temperatures and high pressures when low molecular weight gas molecules are brought into contact with water.

Via diffraction experiments, two hydrate structures were first determined [von Stackleberg 1949, Jeffrey 1984]. Structure I is characteristic of hydrates of relatively small gas molecules [Fig. 2]. The unit cell is formed by the linkage of 46 water molecules resulting in 2 pentagonal-dodecahedral cavities and 6 tetrakaidcahedral cavities of 20 and 24 water molecules, respectively. Upon total occupation of the cavities, the empirical formula of the resulting gas hydrate is $X \cdot 5.75 \text{ H}_2\text{O}$ where X denotes the hydrate forming molecule. Structure II consists of 136 water molecules in the unit cell, enclosing 16 pentagonal-dodecahedral and 8 hexakaidecahedral cavities. The coordination numbers of these cavities are 20 and 28, respectively.

Only in 1987 was another structure discovered by Ripmeester et al. through X-ray diffraction and NMR studies which was named "structure H" [Fig. 2]. Other structures may still have gone unnoticed [Dyadin 1991].

Once identified "what" clathrate hydrates are, a better understanding on "how" they form and decompose represents the most challenging goal in the area of hydrate research. Very little data exist on the solubility of hydrocarbon gases in liquid water at low temperatures and high pressures due to the experimental difficulty involved in the hydrate formation studies.

In this work, isobaric solubility data of five gas mixtures in seven different aqueous solutions are measured through temperature ramping experiments. The high pressure and versatile apparatus used provides a large number of precise valuable data and gives a unique perspective in the "dynamics" of hydrate formation and decomposition.

1. EXPERIMENTAL PROGRAM

1.1. EXPERIMENTAL METHOD

1.1.1. Previous Experimental Methods

During the last fifty years, most of the apparatus used to measure hydrate phase equilibria are more or less based on the high pressure visual cell developed by Deaton and Frost in 1937. Their apparatus consisted in a high-pressure hydrate cell, the main dimensions being $2.5 \times 3.2 \times 15.2 \text{ cm}^3$, provided with a window made from glass which resisted pressures up to 180 bars. A valve system regulated the inlet and outlet gas flow. The cell was located in a thermostated bath and thermocouples built into the cell recorded the gas and liquid phases temperatures.

In more than a century since the first hydrates were scientifically studied [de Forcrand 1882, Villard 1888], few data exist on hydrate phase equilibria. Many requirements exist to build a high-pressure apparatus where temperature is controlled and agitation is sufficient to provide renewal of the gas-liquid surface. Without proper mixing, occlusion of liquid water in the hydrate phase as well as long nucleation periods due to liquid metastability can occur.

Thus, on later versions of the apparatus of Deaton and Frost—as those used by Katz and coworkers, Kobayashi et al., Makogon or more

recently Holder and Bishnoi—one or several of the following features have been developed:

- ♦ The sight glass was modified or removed to carry out experiments at higher pressures.
- ♦ Mercury displacement of liquids was used.
- ♦ An air-bath replaced the fluid-bath. The cooling and heating systems were improved to increase the operating temperature range
- ♦ Thermocouples and pressure transducers were used.
- ♦ Mixing is improved by several means such as rotating or rocking the cell, bubbling gas through the liquid phase, and mechanical, magnetic or ultrasonic agitation.
- ♦ Filming the inside of the cell provided a better visual observation of the formation and decomposition process.

The apparatus have mainly been used at temperatures above the ice point that is in the three phases Lw-H-V or Lw-H-LHC region or in the four and five phases Lw-H-V-LHC and Lw-HI-HII-V-LHC regions.

Regarding the experimental procedure, the measure of macroscopic thermodynamic properties involved three modes of operation.

At isothermal conditions, hydrates are slowly formed at a pressure higher than the equilibrium value. The pressure is maintained constant by exchange of gas or liquid with an external reservoir. Once hydrates are fully formed, the pressure is gradually reduced until the last crystal particle has disappeared.

The results consist in the pressure and temperature at which this final hydrate crystal is observed.

In the isobaric mode, once hydrate is formed as previously, the temperature is slowly increased maintaining the same constant pressure until the last visual particle is observed.

Finally, the isochoric experiment is carried out in a closed cell. The temperature is gradually decreased until a marked depression occurs which corresponds to the formation of a hydrate phase. The temperature is then gradually increased above the point where the last visual hydrate particle is observed.

Thus all three operations measure the conditions at which the final hydrate crystal is visually observed. In addition, in the isochoric experiment, the pressure and the temperature are recorded throughout the cycle. Since the pressure increases up to its initial value upon hydrate decomposition, the final hydrate decomposition is taken as the intersection between the cooling and the heating curve.

The heats associated with the formation or decomposition of hydrates are even more difficult to measure, mainly due to the difficulty in obtaining a "pure" hydrate phase. Only three such sets of experiments are reported up to date [Handa 1986, Lievois 1987, Rueff 1987]. The remaining heats available have been computed via the Clausius-Clapeyron equation by differentiation of three phase equilibrium pressure-temperature data:

$$\frac{dp}{dT} = \frac{\Delta H}{T\Delta V} \quad (1-1)$$

where ΔH is the quantity of heat absorbed or released in the process, ΔV the volume change during the reaction, and dp/dT is the variation of the equilibrium pressure with respect to the temperature. But the reported values are only an estimate since the formation of hydrates involves energetic processes taking place before the measured final hydrate crystal conditions are reached. In particular, the heat related to the water evaporation in the hydrocarbon gas phase, measured by Song and Kobayashi [Song 1994], and to the dissolution of hydrocarbons in the water-rich phase are not taken into account.

Statistical thermodynamic investigations, starting with the solid solution theory of van der Waals and Platteeuw, lead to a widely used computerized approach as an alternative to the painstaking experimental measurements. This theory is partially based on the assumption that all clathrates are solid solutions of the entrapped solute molecules in a metastable lattice of the host solvent². In 40 years, many refinements of the theory have been made—in particular by Kobayashi et al. at Rice University—and the current commercially available computer programs give a good description of the phase equilibria of clathrates [Appendix C].

However, the theory is based on hydrocarbon solubility data extrapolated from Henry's law. Since our work reports a large

² For more details, see van der Waals (1959) and Sloan (1991).

deviation of experimental solubilities from the previously assumed values, a revision of the theory needs to be made.

Moreover, these statistical thermodynamic predictions do not give information on the kinetics of hydrate formation or decomposition. After studying the time-independent properties of clathrate hydrates, a growing body of research is very recently directed towards understanding the time-dependency of hydrate formation and decomposition properties [Barrer 1967, Falabella 1975, Vysniauskas 1983 and 1985, Sloan 1991, Dholabhai 1993].

So far, three techniques to prevent hydrate formation have emerged: dehydration to remove excess water from the system, heating to raise the system temperature above the hydrate formation temperature and lowering of the latter temperature by alcohols, glycols, salts...The use of kinetic inhibitors such as polymers [Yousif 1994] may lead to a better control of the nucleation and growth of hydrate crystals and consequently to tremendous industrial applications.

1.1.2. Isobaric Volume-Temperature Loops: “Ramping Experiments”

The phase equilibria as well as the kinetics are involved in the process of hydrate formation and decomposition. Thus, the ramping of one of the state variables such as the temperature of one the phases provides substantial information.

Since the formation and decomposition of a hydrate phase is marked respectively by a decrease and an increase in pressure in the

constant volume mode, an isobaric experiment should exhibit the opposite features as the temperature is lowered. In this work, such isobaric temperature cycles are made possible by using a state-of-the-art digital positive displacement pumps which maintains a constant pressure in a visible cell located in an air bath. The results show an abnormal increase of the hydrocarbon gas solubility as the temperature is lowered. Hydrate formation and decomposition are revealed by catastrophic increases and decreases in the gas intake similar to the pressure changes in isochoric experiments. Previous experimental investigations did not report high solubility data at high pressure and low temperatures [Kobayashi 1951, Culberson 1950 and 1951, Dodds 1956], even though a departure from high temperature data was sometimes expected [Shinoda 1968]. The results obtained in this work are the first reported solubility measurements accurate enough to show a marked increase as the hydrate formation conditions are approached.

1.1.3. Experimental Procedure

The cylinder of the pump is filled with the gas mixture at the chosen pressure, several hours prior to starting the experiment. Heaters located in the cylinder walls heat and maintain the gas mixture at a chosen temperature of 90°F. During that time, the cell is first cleaned with distilled water. The whole system volume inside the air bath is evacuated. The cell is then filled with 23 ml of the solution studied before being pressurized with the gas mixture at the desired pressure.

The temperature and the pressure of the pump and the cell unit are recorded separately until thermal equilibrium is reached. It is only after attaining this equilibrium at which no gas leak is detected that the temperature is ramped at a constant rate. The pump automatically adjusts the pressure at the desired value while the two data logging computers collect information concerning the cylinder position, and the actual pressure and temperatures at desired time intervals which are usually five minutes each.

When the first series of experiment is completed, the liquid solution is purged out of the cell followed by a total evacuation of the gas phase. For pH measurements, the solution is collected in order to check for its final volume and final pH. The temperature effect on the pH of the buffer solutions was estimated by measuring the pH of the solution, located in the air bath, as the temperature is ramped.

The automation of the apparatus allows very long experiments that are often conducted continuously for several days. The numerous data collected in the computers give a very accurate estimation of the temperature behavior upon hydrate formation and decomposition. Since the time elapsed is known, the apparatus is also suitable for kinetics experiments at constant temperature.

On the other hand, these high pressure experiments are difficult since pressure leaks can occur in many places along the tubing network. A single run requires many checks for pressure leaks. And when one occurs, it is painstaking to find the exact location. Also, the temperature controlling system is very precise over a wide range of

temperature, but erratic electronic behavior can sometimes cause the temperature control to fail.

12. EXPERIMENTAL APPARATUS

12.1. Current Equipment

Hydrate formation and decomposition takes place in a visual cell similar to the one used in previous work starting with Deaton and Frost. This Jerguson-type cell is built in steel and two glass windows on each side enable visual observation of the phase transitions, its volume being 91.5 ml [Fig. 1-1].

A motor placed on top of the air bath rocks the cell in which 1/2 in type 440 stainless steel balls roll back and forth along a 5/8 in bore. Two small Beryllium springs are mounted to cushion and protect the platinum resistance thermometer—PRT—inserted into the cell on the side walls. The speed of rotation of the cell can be varied, but a speed at which the cell makes 25 cycles per minute is usually chosen.

In addition, a magnetic pump recirculates the gas present in the cell at a variable rate. When the position of the cell corresponds to the time when the gas flows into the cell, the gas bubbles through the liquid phase to provide a good gas-liquid surface contact. Both rocking and bubbling renew the gas-liquid interfacial surface where hydrates used to form in previous work when such mixing was not provided. It has been proven [Vysniauskas 1983] that better mixing of the system delays the appearance of a critical nuclei.

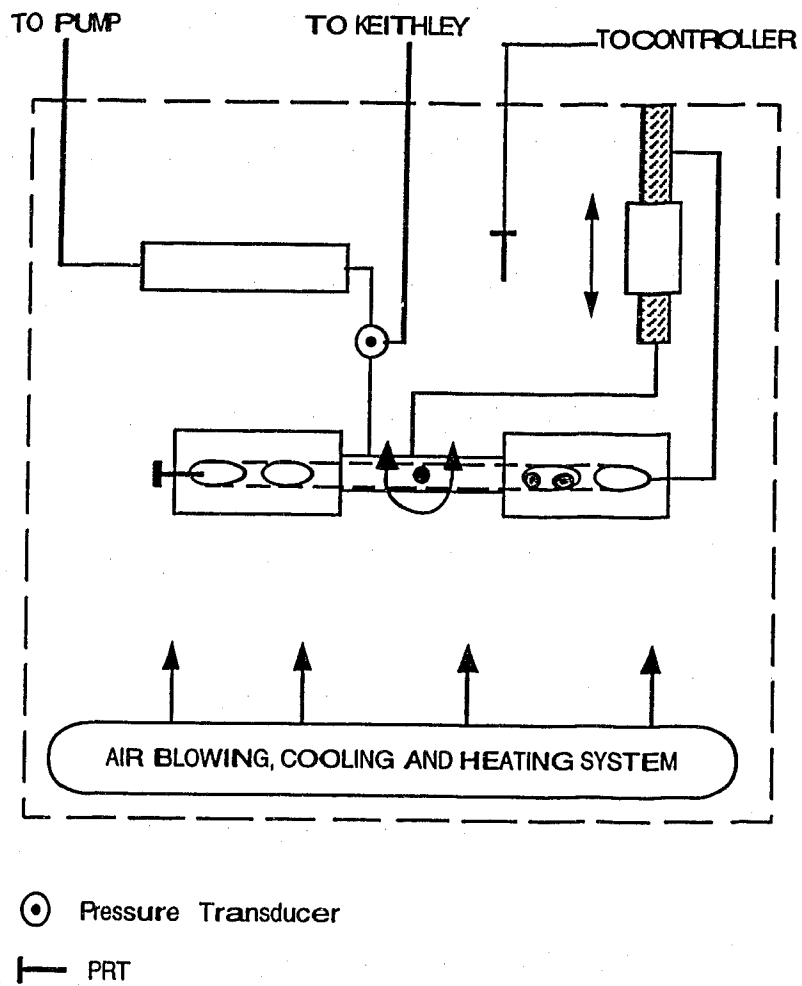


Fig. 1-1 The Thermostated Hydrate Unit

An air bath unit houses the visual cell. It has evolved in our laboratory over the last four decades. The bath is thermodynamically controlled providing both heat and refrigeration. Through careful design it has been possible to develop a temperature control system that can achieve temperatures as high as 40°C and as low as -12°C with a millidegree precision. Nevertheless, since Freon is present in the cooling system, air bath temperatures higher than room temperature require a simultaneous cooling of the system coupled to the heating which could damage the apparatus. The air temperature is maintained uniform with the help of two blowers that recirculate the air inside the bath.

The temperature is measured by three PRT's placed in the air bath, on the cell wall, and in the water-rich liquid phase. They are calibrated to $\pm 3 \times 10^{-3}$ K via a NIST certified PRT. A computer program controls the temperature via an interface. The upper and lower temperature limits as well as the ramping rate serve as parameters while the actual air temperature is displayed at chosen intervals.

Most central to our measurements are the two fully automated "Digital Positive Displacement" pumps: a two-cylinders RUSKA pump and a RUSKA/AMOCO pump. With the RUSKA pump, numerous operations can be programmed through the on-board membrane keypad or via a computer interface. Some of the standard operations include absolute and incremental discharges at preset rates and variable speed forward or reverse jog. Depending on the maximum pressure requirements, the digital control system provides variable rates up to 2400 ml/h and feed ratios as wide as 1/20,000. Feed

rates are selectable in 0.001 ml/min. This work is made possible by the constant pressure option which varies the speed of the pump to maintain the desired pressure. The AMOCO pump exhibit the same main features via a "home-made" computer interface.

The accuracy of the controlled pressure depends largely on the transducer that closes the control loop. The RUSKA pump has a 10,000 psia range HEISE pressure transducer that is rated at 0.07 percent accuracy at full scale. The AMOCO pump has a 1000 psia range with a similar rating. Thus the precision of the AMOCO pump is greater than the precision of the RUSKA pump.

A reservoir bottle is located inside the air bath between the pump and the visual cell. The total reservoir size was either 150 ml or 300 ml. Since these volumes are big in comparison to the gas phase volume in the cell, these bottles help bringing the added gas from the pump at the cell temperature.

Vacuum is created when needed throughout the system with a small vacuum pump temporarily hooked to the cell. The signals from the PRT's and the pressure transducers are collected by two personal computers at desired time intervals. In addition, three KEITHLEY'S display the instantaneous values to be converted to temperature and pressure units.

The following gas mixtures are used in this work:

- ♦ CH_4 : ultra high purity grade from LINDE (UNION CARBIDE).
- ♦ C_2H_6 : pure grade from PHILLIPS PETROLEUM COMPANY.
- ♦ C_3H_8 : research grade also from PHILLIPS.

- ♦ CO₂: anaerobic grade from AIRCO.
- ♦ CH₄ (80.02 mol%)-C₃H₈(19.98 mol%) gas mixture, prepared by IWECO.

Pure water runs are performed with deionized water.

The pH of the buffer solutions is measured with a high temperature and high pressure combination electrode that features a porous Teflon liquid junction and allows use over a broad spectrum of pH.

1.2.2. Future Modifications

A major modification has already been made to the system, the addition of a gas chromatograph that provides the possibility of analyzing the gas phase composition on-line, while the temperature is ramped. A sophisticated tubing network and valves provide very small samples that scarcely affect the gas phase pressure.

The addition of a second cell above the existing one is currently under study. Simultaneous solubility measurements of the same gas mixture in two different aqueous solutions will then be possible. Thus, this "piggy-back" cell should increase the productivity of the current apparatus.

2. THE SOLUBILITY OF PURE HYDROCARBON GASES IN PURE WATER IN THE HYDRATE REGION

2.1. EXPERIMENTAL RESULTS

2.1.1. Objective

At high pressure, the solubility of hydrocarbons in water is greatly promoted as the temperature decreases. Our first purpose is to quantify the increase in gas consumption as a function of temperature for each of the following pure components: methane, ethane, propane and carbon dioxide. The resulting plots along with an evaluation of the enthalpies and entropies of solution will provide new and more accurate solubility measurements in the hydrate region. It is not until reproducible and reliable data are obtained with pure components in pure liquid water that future experiments involving hydrocarbons mixtures and aqueous solutions can be justified.

2.1.2. First Set of Experiments

The solubility of pure methane and pure ethane gases in pure liquid water has been measured. The pressure was maintained constant using a digitally controlled positive displacement RUSKA pump. In order to form hydrates in the temperature range 0°C-15°C, the corresponding constant pressure are chosen to be 583 psia for pure methane and 217 psia for pure ethane. Both components are in the gaseous state at these conditions. The accuracy of the controlled

pressure depends largely on the transducer that closes the control loop. The RUSKA pump is installed with a 10,000 psia range pressure transducer rated at 0.07 percent full scale accuracy. Therefore, the precision of the controlled pressure is estimated at ± 7 psia which is rather poor at our operating pressures. Mixing of the liquid and the gas phases is ensured only by rocking the cell in which the stainless steel balls roll back and forth. The results are shown in Fig. 2.1 and 2-2 where the Y-axis represent the volume added at a constant temperature of 82°F and constant pressure. The independent variable is either the time elapsed since the cooling of the cell started or the temperature inside the cell. These plots clearly exhibit several distinctive regions.

- ◆ As the temperature is lowered, the volume of pure gas added to the cell increases linearly.
- ◆ At one point, the volume added to the cell increases suddenly. The starting point is referred as the Catastrophic Temperature of hydrate formation, T_c .
- ◆ A sudden increase in volume added as part of the catastrophic formation takes place. The partial solidification of the liquid phase stops the movement of the ball bearings.
- ◆ No gas is released when first heating the liquid water-hydrate-vapor system.
- ◆ A catastrophic point of hydrate decomposition is detected.
- ◆ A sudden volume decrease.

Fig. 2-1 Methane Hydrate Run in Pure Water (First Set)

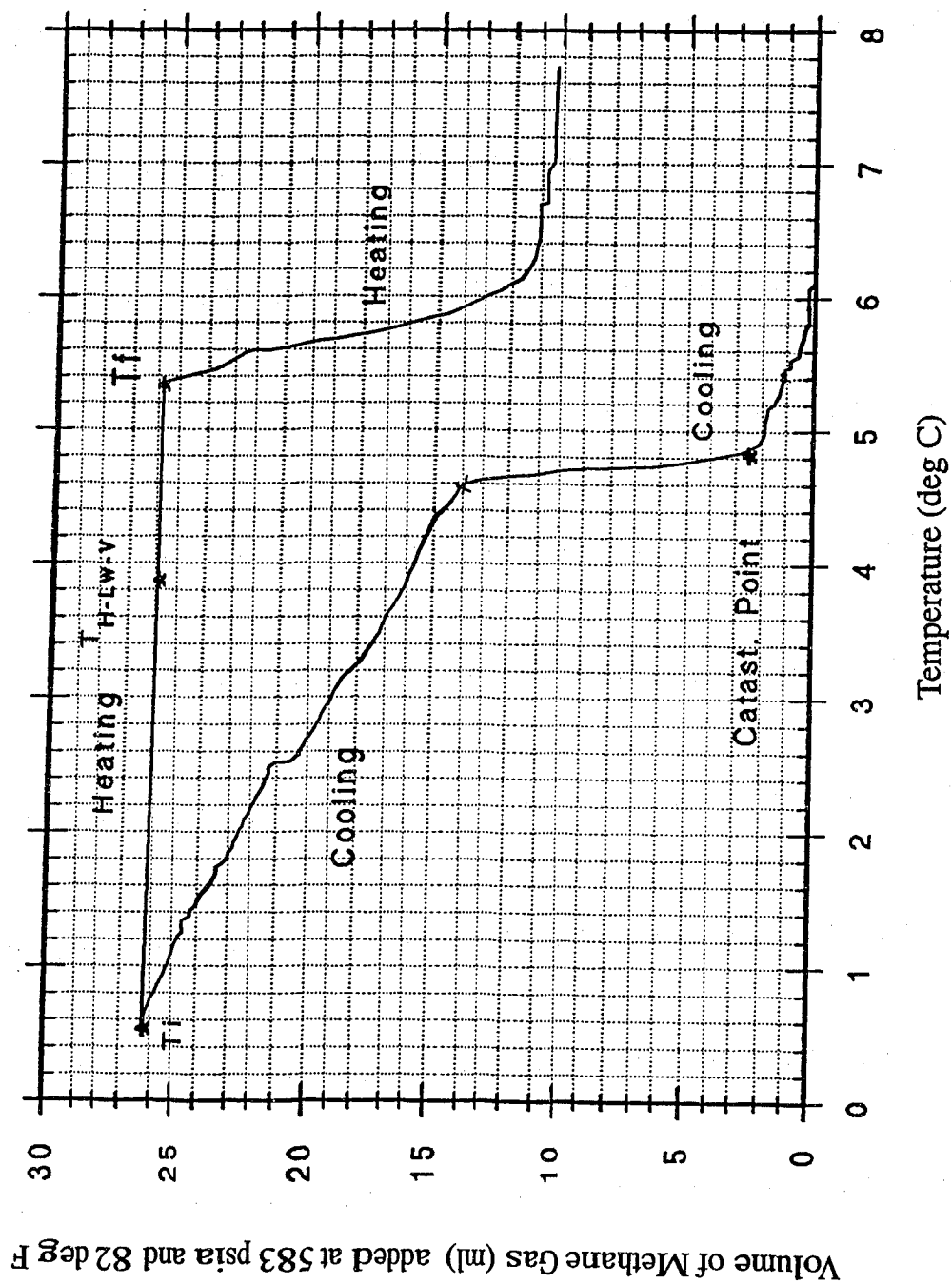
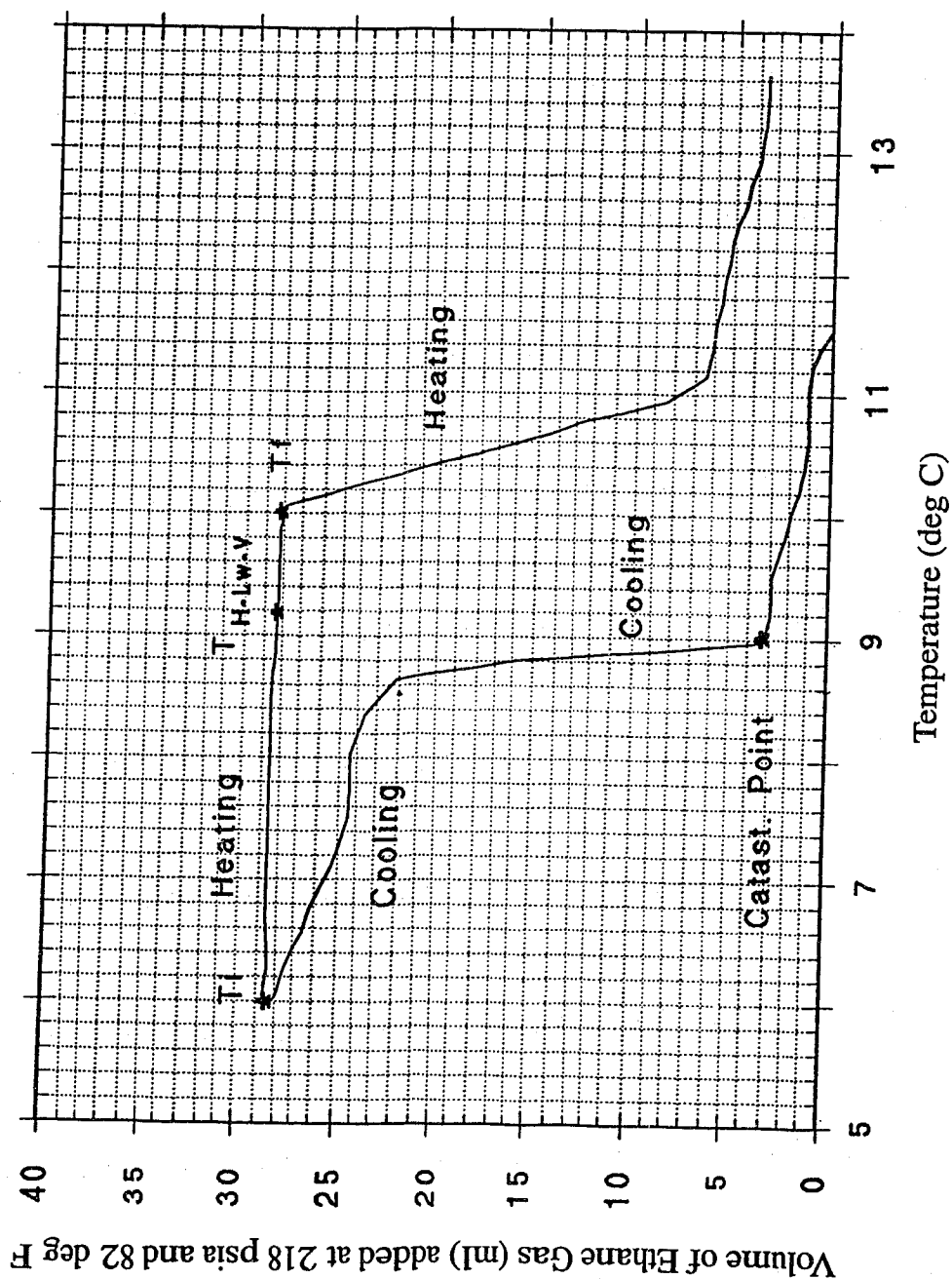


Fig. 2-2 Ethane Hydrate Run in Pure Water (First Set)



- ◆ At one point the volume starts decreasing linearly with increasing temperature with a different slope than the one obtained during the heating process. This point is called the Final Hydrate Decomposition Temperature, FHDT. There, the movement of the balls resumes.
- ◆ The volume does not reach its initial value when the temperature comes back to its initial state.

Hydrate formation and decomposition runs for methane and ethane are performed at two different ramping rates of 1°C/h and 0.5°C/h, all other parameters identical.

2.1.3. Second Set of Experiments

The previous methane and ethane runs clearly exhibited an increase in solubility as the temperature approached hydrate formation conditions at constant pressure. In order to achieve reproducibility of these measurements, an improved mixing of the gas and the liquid phases and a higher sensitivity of the pressure control was needed. Thus, two major modifications of the experimental apparatus had been made.

A magnetic pump was added to recirculate the gas phase from top of the cell to the bottom where the gas bubbles through the liquid phase. The gas recirculation rate is 366 ml/min. In addition, the rocking of the cell moves the balls back and forth at a rate of 25 cycles/min. The gas phase is therefore homogenized and the interfacial surface area is increased.

The AMOCO pump replaced the RUSKA pump. The 1000 psia range pressure transducer increased the precision by a factor of 10. Also, the system volume was increased by adding a 300 ml reservoir bottle that preconditioned the temperature of the added gas to the system temperature before being contacted with the liquid water.

It was decided to run pure methane, pure ethane as well as pure propane and pure carbon dioxide in pure liquid water. These measurements were performed at the following constant pressures and ramping rates.

Table 2-1 Constant Pressure Experiments

GAS	CH₄	C₂H₆	C₃H₈	CO₂
PRESSURE (psia)	500	95	60	500
RAMPING RATES (°C/h)	2	2	1	2

A low pressure was needed for C₃H₈-H₂O system because of the low vapor pressures of propane. It is important to stay on the L_W-H-V_{HC} three phase line shown in Fig. 2-3 to avert the formation of ice and liquid hydrocarbons that would interfere with our visual account of the experiment. A more typical pressure was chosen for methane and carbon dioxide that enables direct comparisons with

solubility measurements from other investigators and field experiences.

The results are displayed in plots 2-4 through 2-6 where the Y-axis represent the volume of gas added at a constant temperature of 90°F and constant pressure. Propane runs show very good reproducibility with respect to volume and temperature. This remains true for all systems, providing that the water present in the cell is either replaced before each run or carefully evacuated. If the loops are performed continuously, the amount of gas added during the first run will be greater than for the successive attempts. Thus, to enable good comparisons, fresh water or gas-free water was used as much as possible. The behavior of the temperature controlling system is checked by plotting the temperature inside the cell versus time [Fig. 2-7]. The temperature should decrease and increase regularly with a constant slope defined by the chosen ramping rate. The upper and lower temperature limits are also fixed as parameters.

Methane, ethane and propane exhibit the same characteristic behavior:

- ♦ a linear gas consumption upon cooling,
- ♦ a catastrophic increase in gas consumption,
- ♦ a small gas release upon first heating,
- ♦ a catastrophic decrease in the added gas volume,
- ♦ a linear gas release upon heating.

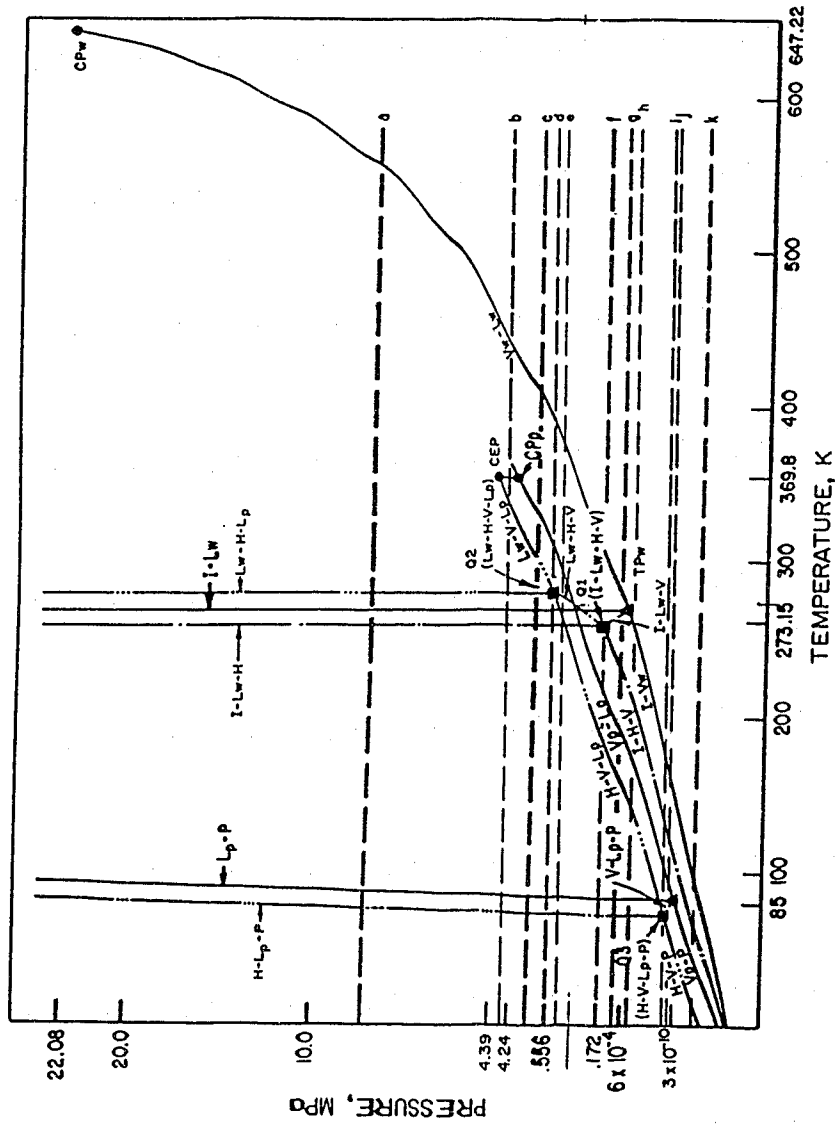


Fig. 2-3 Pressure-Temperature Diagram for Propane and Water
(source: Sloan, 1990)

Fig. 2-4 Ethane Hydrate Run in Pure Water
(Amoco pump; Run #2; Ramping 2 °C/h)

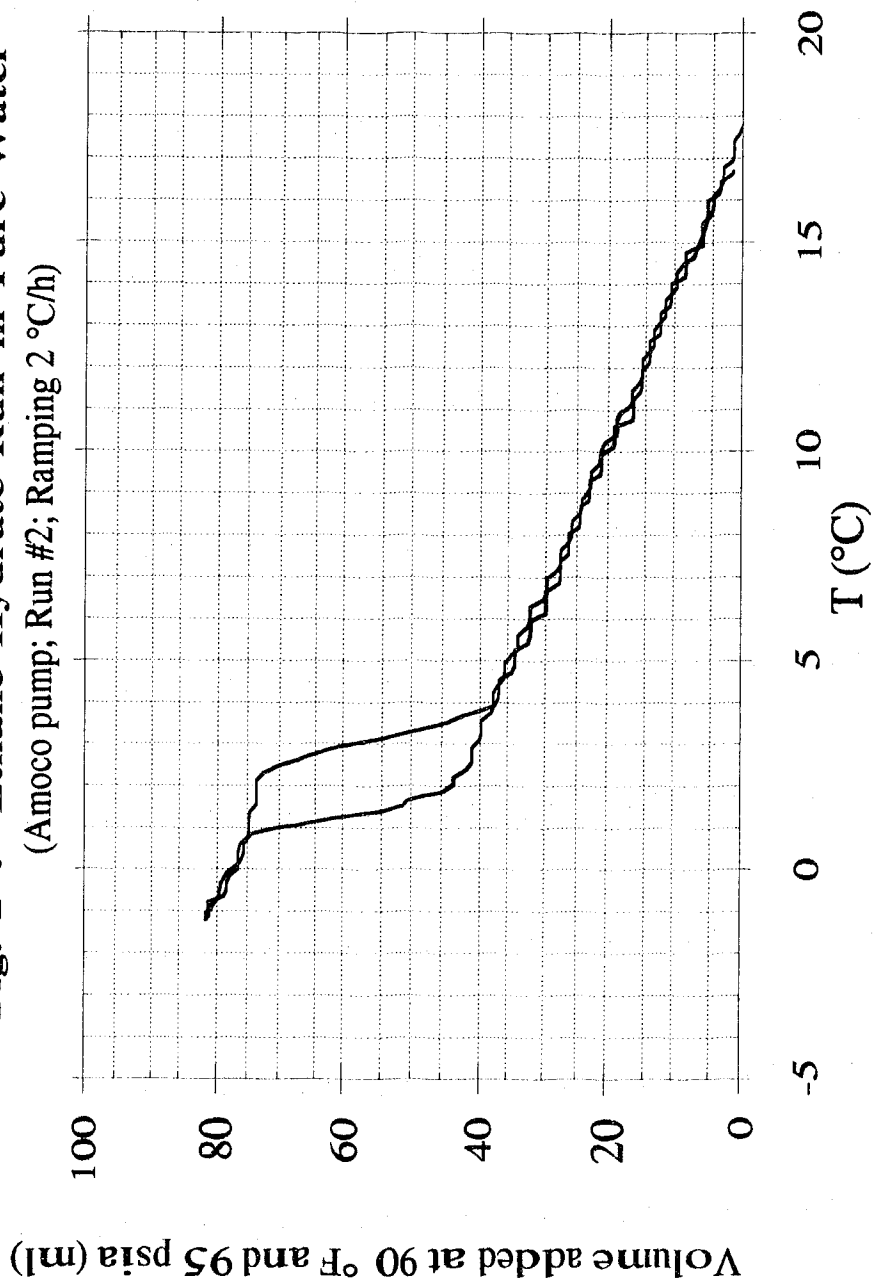
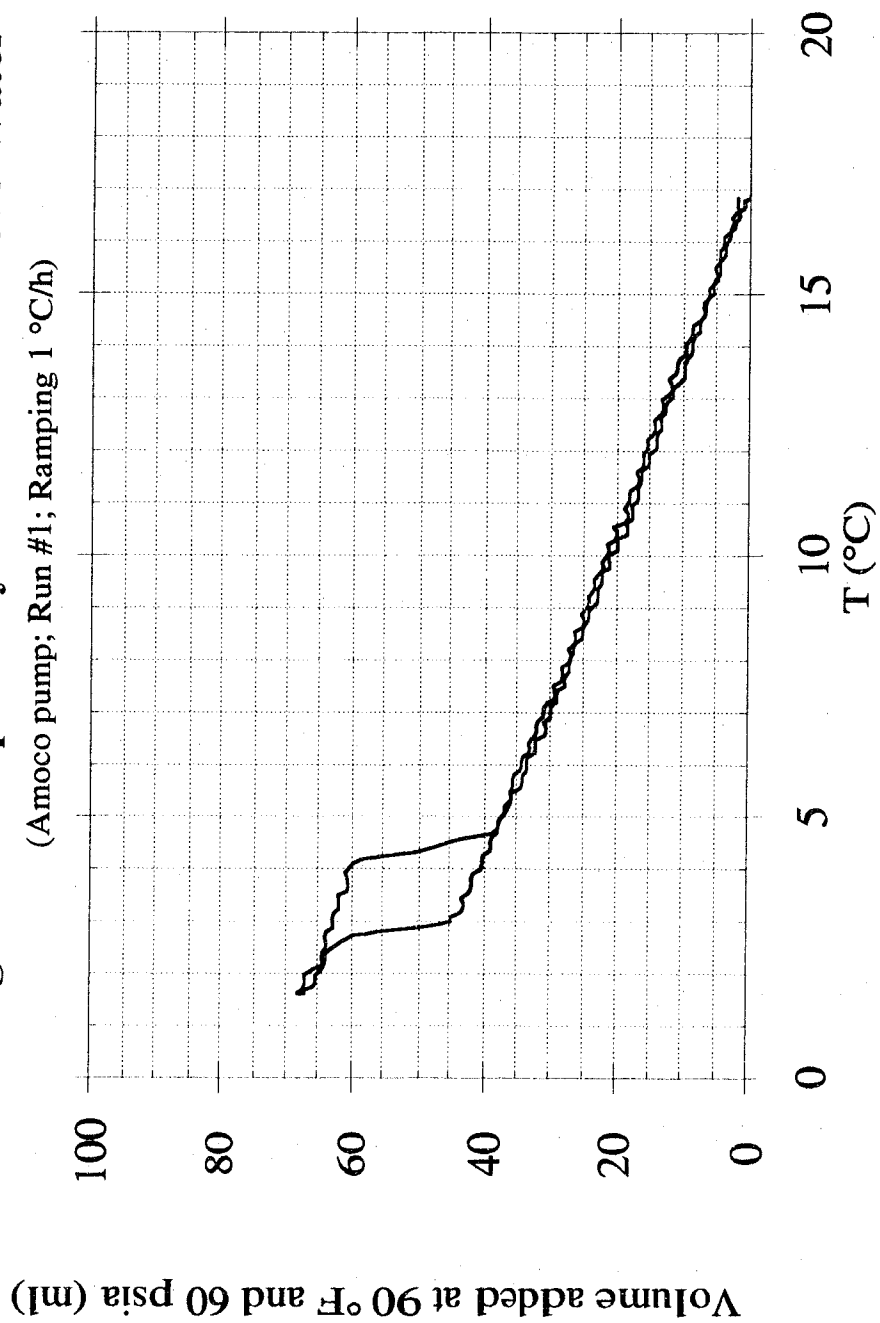
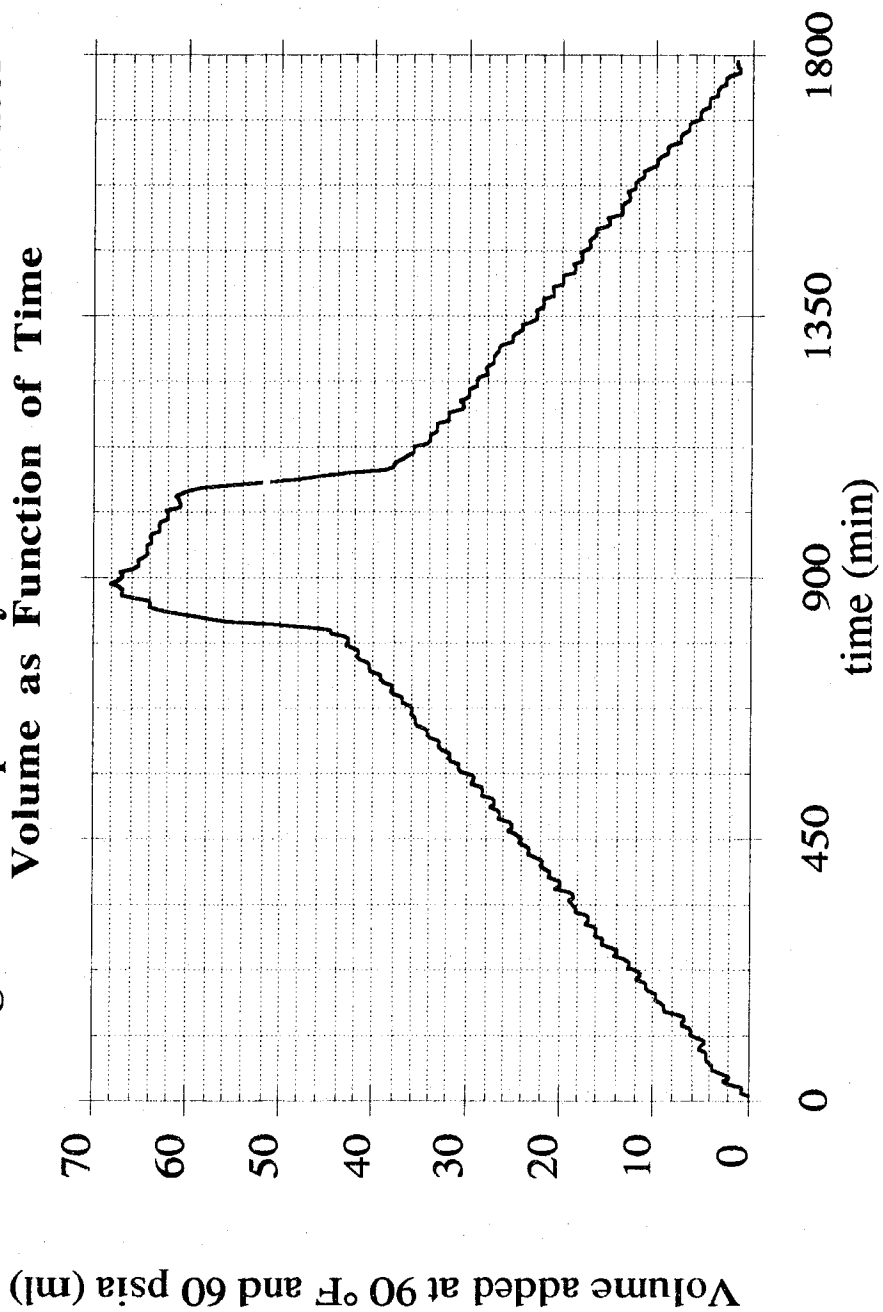


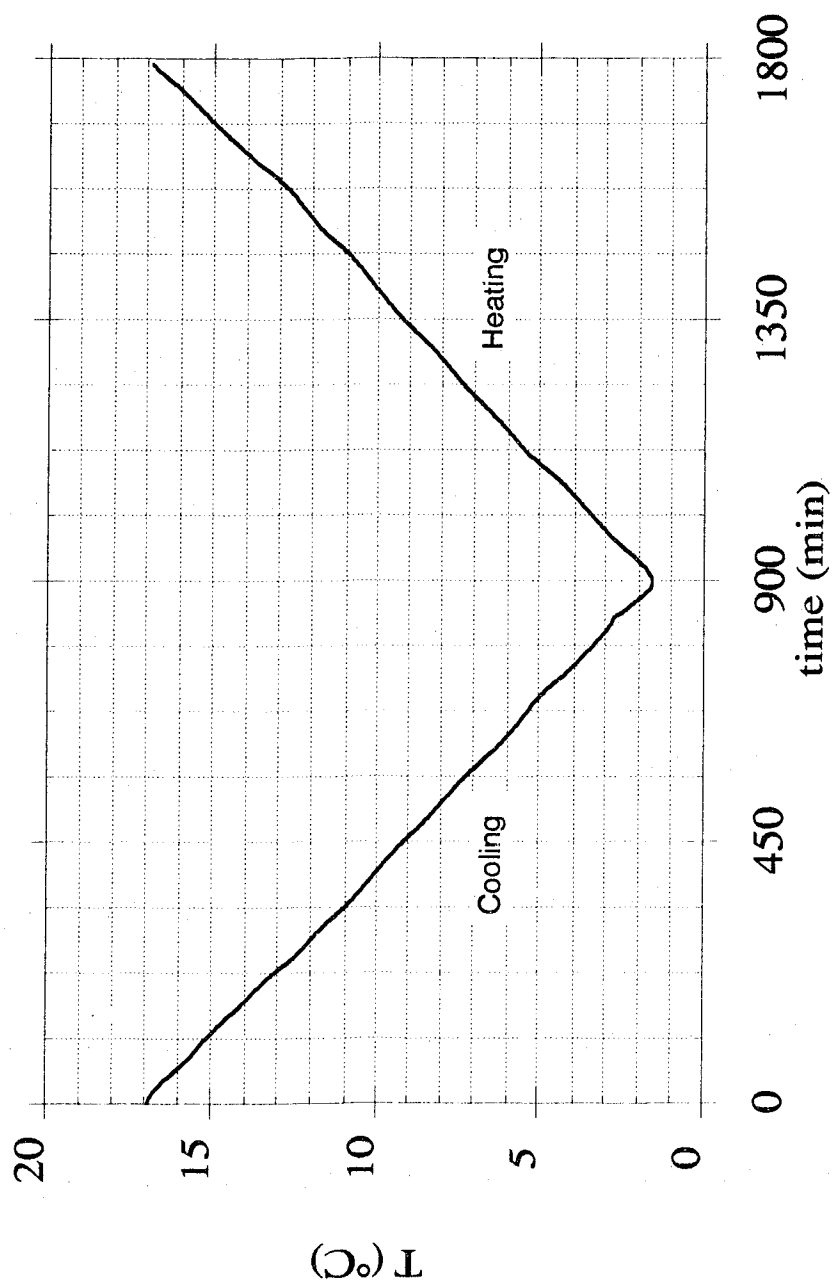
Fig. 2-5 Propane Hydrate Run in Pure Water
(Amoco pump; Run #1; Ramping 1 °C/h)



**Fig. 2-6 Propane Hydrate Run in Pure Water
Volume as Function of Time**



**Fig. 2-7 Propane Hydrate Run in Pure Water
Temperature as Function of Time**



The hysteresis obtained in the cycle is a common feature to all runs made with methane, ethane and propane without exception and whatever the experimental parameters are. Carbon dioxide measurements, on the other hand, show an inverse tendency: the gas is released as soon as the hydrate part lies under the cooling part. There is a separation between the cooling and the heating curve for methane at higher temperatures. This fact must be regarded carefully since it may be due to poor smoothing of the electronic glitches that occurred at the end of the methane run. For all other runs, the heating and the cooling curves superimpose well on each other. Propane plots show a sharp hysteresis curve and precise catastrophic and final hydrate decomposition temperatures. The change in solubility of ethane in water was measured at high temperatures up to 30°C upon heating. At the turning point, when the hydrate phase is heated, some results indicate the existence of a small loop. After hydrate formation, the balls are stuck and the bubbling stops due to solidification of the liquid phase. Heat is released as a result of exothermic hydrate formation. Both phenomena account for the occurrence of this small loop [Fig. 2-5].

2.2. DATA ANALYSIS AND DISCUSSION

The system inside the air bath can be regarded as an open reactor exchanging material with the outside at a constant pressure. The temperature inside the reactor is uniform at any given time. The cell in which the phase transition takes place is rather small, but

the total gas phase volume of the system is $V_{\text{sys}}^v = 531.2$ ml as measured in the previous pure components experiments. Assuming a small volume change of the gas phase, as temperature is lowered the pump adds Δn_{HC} moles of hydrocarbon to the gas phase to maintain a constant pressure. Therefore, the actual solubility of the hydrocarbon in the liquid phase is the net difference between what is added to the whole reactor and what is added to the gas phase due to gas compression. For the determination of the actual solubility of hydrocarbons in water, rigorous mass balances need to be derived.

22.1. Mass Balances

Let there be ϕ phases and C components in the system. The maximum number of variables needed to specify the state of all phases is $\phi(C+1)$. Assuming the system is in a state of internal equilibrium, then among the $\phi(C+1)$ variables there are $(\phi-1)(C+2)$ equilibrium relations. Thus the number of degrees of freedom, F , is given by the Gibbs Phase Rule:

$$F + \phi = C + 2 \quad (2-1)$$

The present experiments involve two components—water and one hydrocarbon—and two phases before hydrate formation. Thus the state is specified by the controlled pressure and temperature. The complete conversion of liquid water and gas to hydrates is a very slow process due to inclusion of liquid water in the hydrate crystals [Galloway 1968, Lievois 1987]. Hence, equilibrium is not

achieved immediately after T_c and the Gibbs Phase Rule does not strictly apply.

Let n_i^P be the net amount of hydrocarbon i exchanged between the pump and the system from state 1 ($T_{sys}=T_1$ and $P_{sys}=P_1$) to state 2 ($T_{sys}=T_2$ and $P_{sys}=P_2$). If n_i^P is positive, the pump has added gas to the system and vice-versa.

Mass Balance on water

The system exchanges only pure hydrocarbon gases with the pump. The amount of water in the system throughout the process is fixed:

$$(n_w^{sys})_1 = (n_w^{sys})_2 \quad (2-2)$$

that is:

$$(n_w^H + n_w^L + n_w^V)_1 = (n_w^H + n_w^L + n_w^V)_2 \quad (2-3)$$

Assuming

$$\Delta_1^2 n_w^V \approx 0 \quad (2-4)$$

then,

$$\Delta_1^2 (n_w^H + n_w^L) = 0 \quad (2-5)$$

Mass Balance on component i

No chemical reaction takes place in the reactor.

$$n_i^P = (n_i^{sys})_2 - (n_i^{sys})_1 \quad (2-6)$$

$$n_i^{sys} = n_i^H + n_i^L + n_i^V \quad (2-7)$$

Take state 1 as the initial state (T_i, P). Because no hydrates are present initially³,

$$(n_w^H + n_w^L)_2 = (n_w^L)_1 \quad (2-8)$$

$(n_w^L)_1$ is the amount of water initially introduced. And,

$$(n_i^{sys})_1 = (n_i^L + n_i^V)_1 \quad (2-9)$$

$(n_i^V)_1$ is known from the density of component i at T_i . $(n_i^L)_1$

must be taken from reported measurements.

Before hydrate formation

$$(n_i^H)_2 = 0 \quad (2-10)$$

Thus,

$$(n_i^L)_2 = n_i^P + (n_i^L)_1 + (n_i^V)_1 - (n_i^V)_2 \quad (2-11)$$

Using the compressibility factors:

$$(n_i^V)_2 = \left(\frac{P}{Z_i RT} \right)_2 \times (V^V)_2 \quad (2-12)$$

$$\text{where } V^{sys} = V^L + V^V \quad (2-13)$$

$$(n_i^V)_2 = \left(\frac{P}{Z_i RT} \right)_2 \times \left(V^{sys} - \left(\frac{Z_w RT}{P} \right)_2 n_w^L \right) \quad (2-14)$$

$$\text{since } (n_w^L)_1 = (n_w^L)_2 = \text{constant} = n_w^L \quad (2-15)$$

³ Although our hypothesis does assume that a distribution of pentagonal dodecahedra microcrystals does occur even in liquid water.

And finally:

$$(n_i^L)_2 = n_i^P + (n_i^{sys})_1 - \left(\left(\frac{P}{Z_i RT} \right)_2 \times \left(V^{sys} - \left(\frac{Z_W RT}{P} \right)_2 n_W^L \right) \right) \quad (2-16)$$

After hydrate formation

$$(n_i^{sys})_2 = (n_i^H + n_i^L + n_i^V)_2 \quad (2-17)$$

So the volume of the vapor phase is:

$$V^V = V^{sys} - V^L$$

$$V^V = V^{sys} - \left(\frac{Z_W RT}{P} \right)_2 n_W^L \frac{\rho_W}{\rho_H} \quad (2-18)$$

And the solubility of component i in liquid water at (T₂,P) is:

$$(n_i^L)_2 = n_i^P + (n_i^{sys})_1 - \left(\left(\frac{P}{Z_i RT} \right)_2 \times \left(V^{sys} - \left(\frac{Z_W RT}{P} \right)_2 n_W^L \frac{\rho_W}{\rho_H} \right) \right) \quad (2-19)$$

The amount of gas exchanged with the pump is given by:

$$n_i^P = \left(\frac{P}{Z_i RT} \right)_{(T^P, P^P)} \times \left((V^P)_2 - (V^P)_1 \right) \quad (2-20)$$

and the amount of water in the system is:

$$n_W^L = \left(\frac{P}{Z_W RT} \right)_{\text{ambient (TP)}} \times V^W \quad (2-21)$$

where V^W is the volume of water introduced.

2.2.2. Results

The compressibility factors are obtained from reference tables [Goodwin 1974 and 1977, IUPAC 1973] and with DDMIX, a NIST computer program that calculates thermodynamic and transport

properties based on the Peng-Robinson equation of state and the NIST extended corresponding states model.

The change in the volume of water corresponding to $\left(n_w^L\right)_1$ moles is computed for the $C_3H_8-H_2O$ system. This change has a maximum value lower than the experimental uncertainty given in Appendix A. Therefore, the volume of water before hydrate formation is taken as constant. Table 2-2 reports the volume change upon converting water to hydrate. In our experiment, the volume change after hydrate formation is estimated at 0.6 ml.

Table 2-2 Volume Change Upon Converting Water to Hydrate in ml/mol [Handbook of Gas Hydrate Properties and Occurrence]

STRUCTURE	$T < 0^\circ\text{C}$	$T > 0^\circ\text{C}$
I	3.0	4.6
II	3.4	5.0

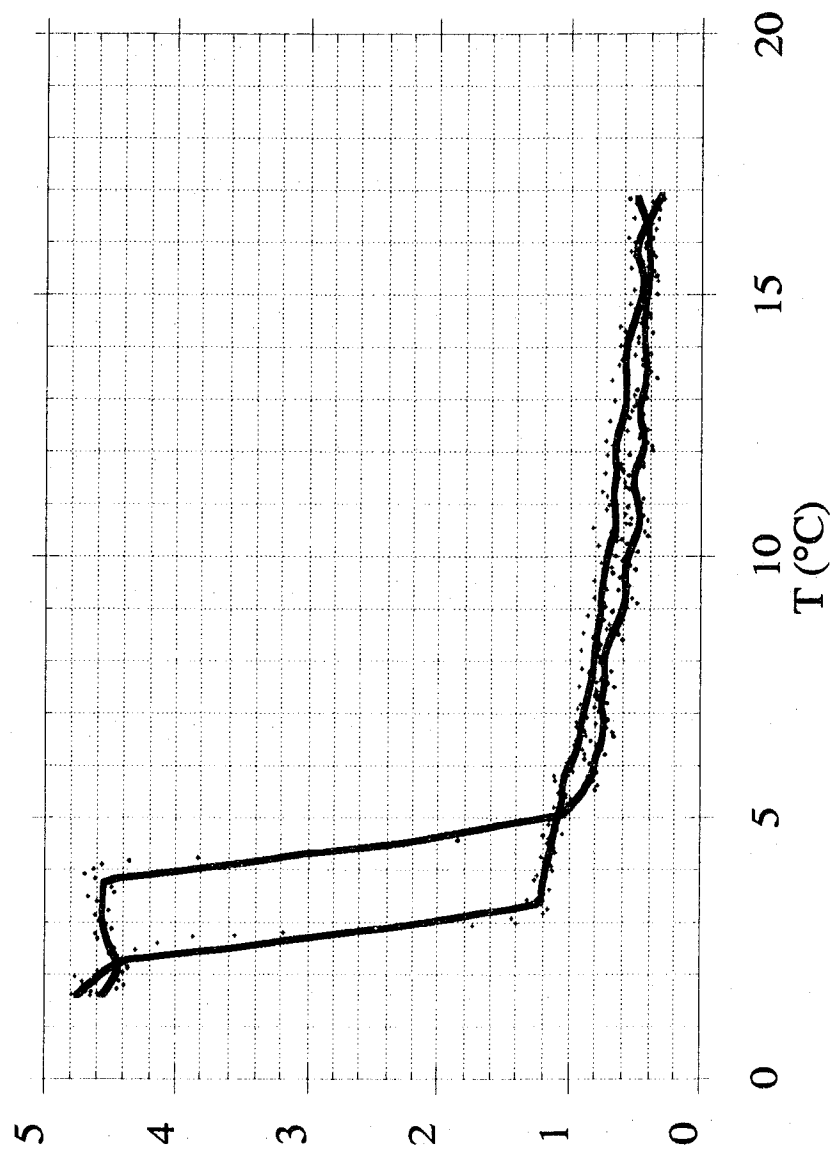
The density of the hydrate phase has never been measured. Yet, it is possible to give an estimate based on the statistical theory of Van der Waals and Platteeuw as seen in Appendix C. The calculated hydrate densities for any of the pure hydrocarbon-water system seem rather close to the water density. Moreover, only 6.2 percent of water is estimated to be transformed in $C_3H_8-H_2O$ hydrate at our lowest operating temperature as computed in Appendix A.

Galloway waited 40 to 70 hours to obtain complete conversion of 15 ml of water at a constant subcooled temperature of hydrate formation. Song needed 5 days to complete conversion of a liquid volume five times the volume used in this experiment. Hence, this low conversion value is not surprising and in the following calculations the volume of the condensed phase after hydrate formation is assumed equal to the volume of $\left(n_w^L\right)_1$ moles of liquid at the same conditions.

A sample calculation based on the previous mass balances is given in Appendix A. As a result, Fig. 2-8 to 2-11 represent the first reported values of the solubility of methane, ethane, propane and carbon dioxide in pure liquid water at low temperature and high pressure. The shape of these plots differ slightly from the previous Volume-Temperature plots, but the main characteristics remain. Some solubility data of methane in liquid water and ethane in liquid water exist in the literature [Kobayashi 1951, Culberson 1950 and 1951]. Moreover, it has been a common practice to estimate solubilities from extrapolated Henry's constants at low temperature and high pressure. Battino et al. have derived Henry's constants at low temperatures and low pressures [Rettich 1981]. By applying a small Poynting correction factor, the high pressures solubility data are computed. The compared mole fractions values both with reported literature data and computed data are shown in Fig. 2-10 and 2-11.

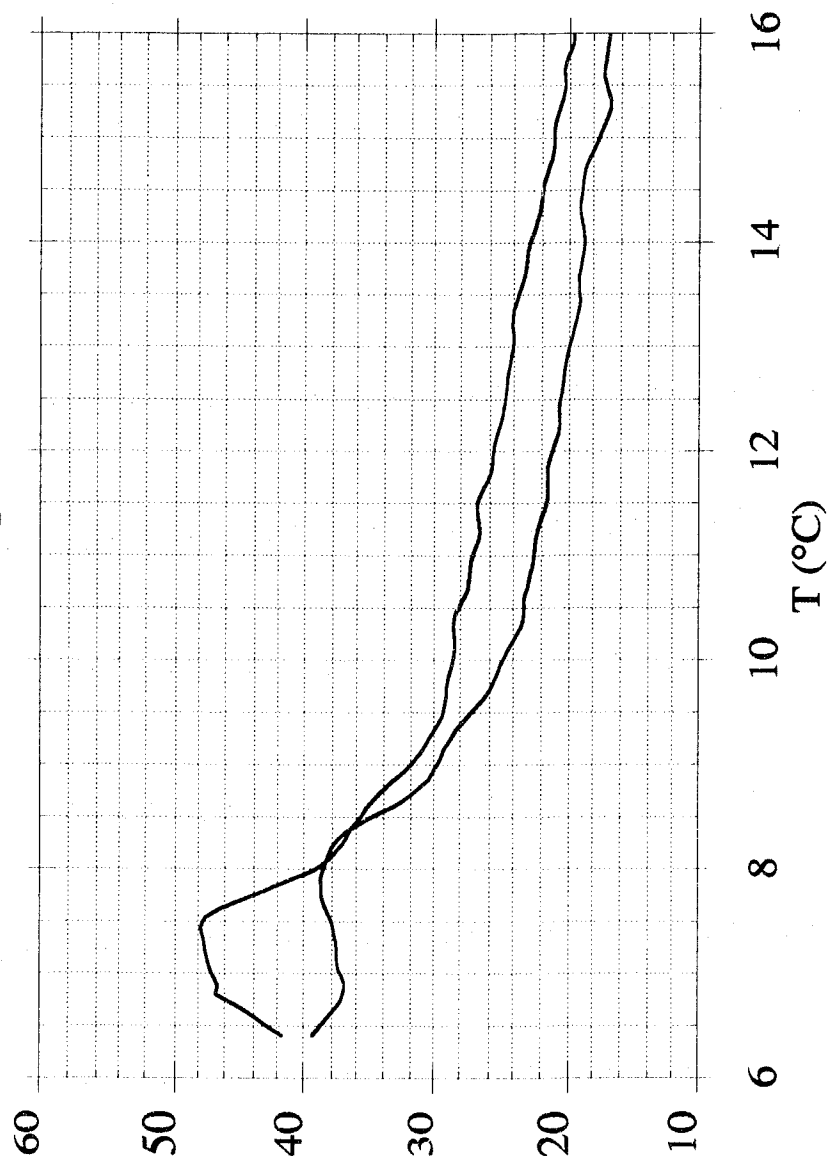
C_3H_8 in 23 cc of liquid water (molx1000)

Fig. 2-8 Propane Solubility in Pure Water at 60 psia



**Fig. 2-9 Carbon Dioxide Solubility in Pure Water
at 500 psia**

CO_2 in 23 cc of liquid water (molx1000)



**Fig. 2-10 Methane Solubility in Pure Water
at 500 psia**

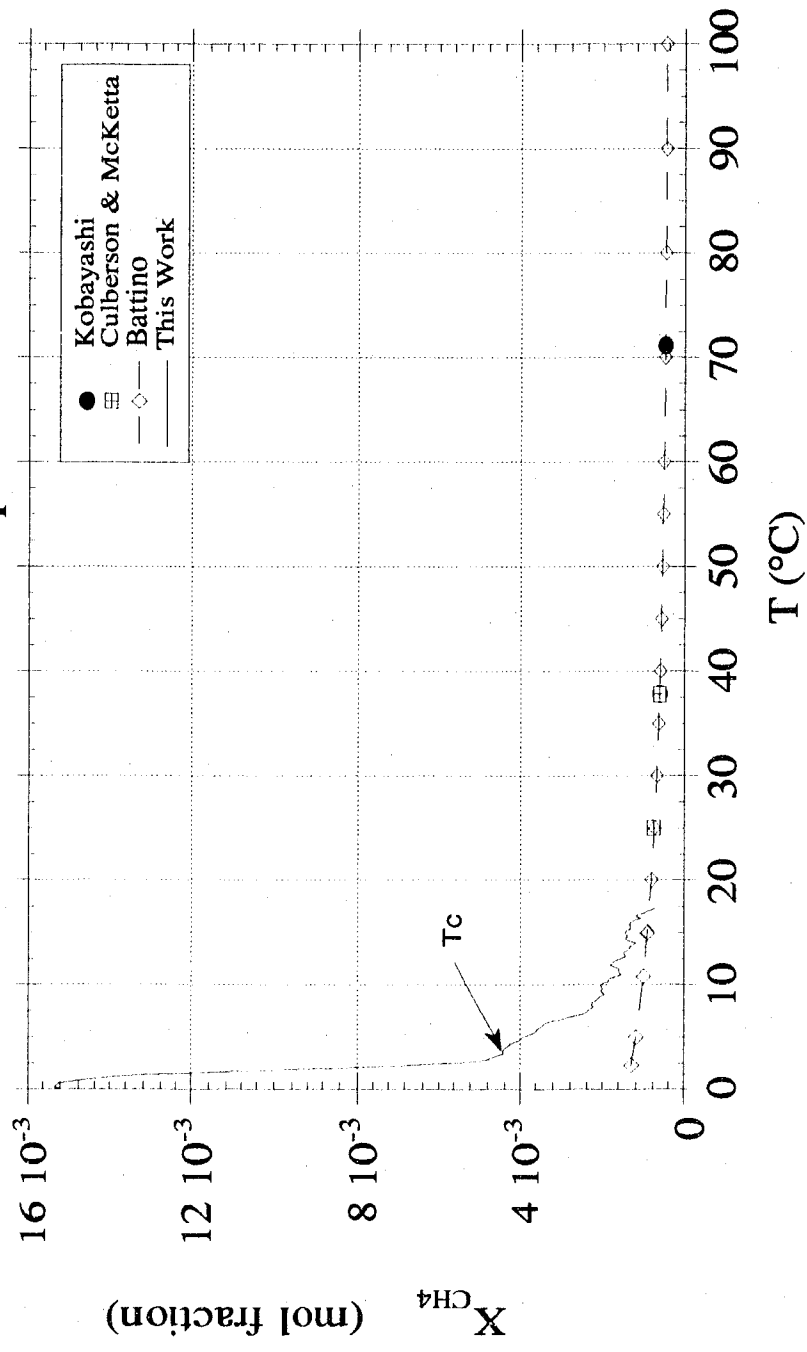
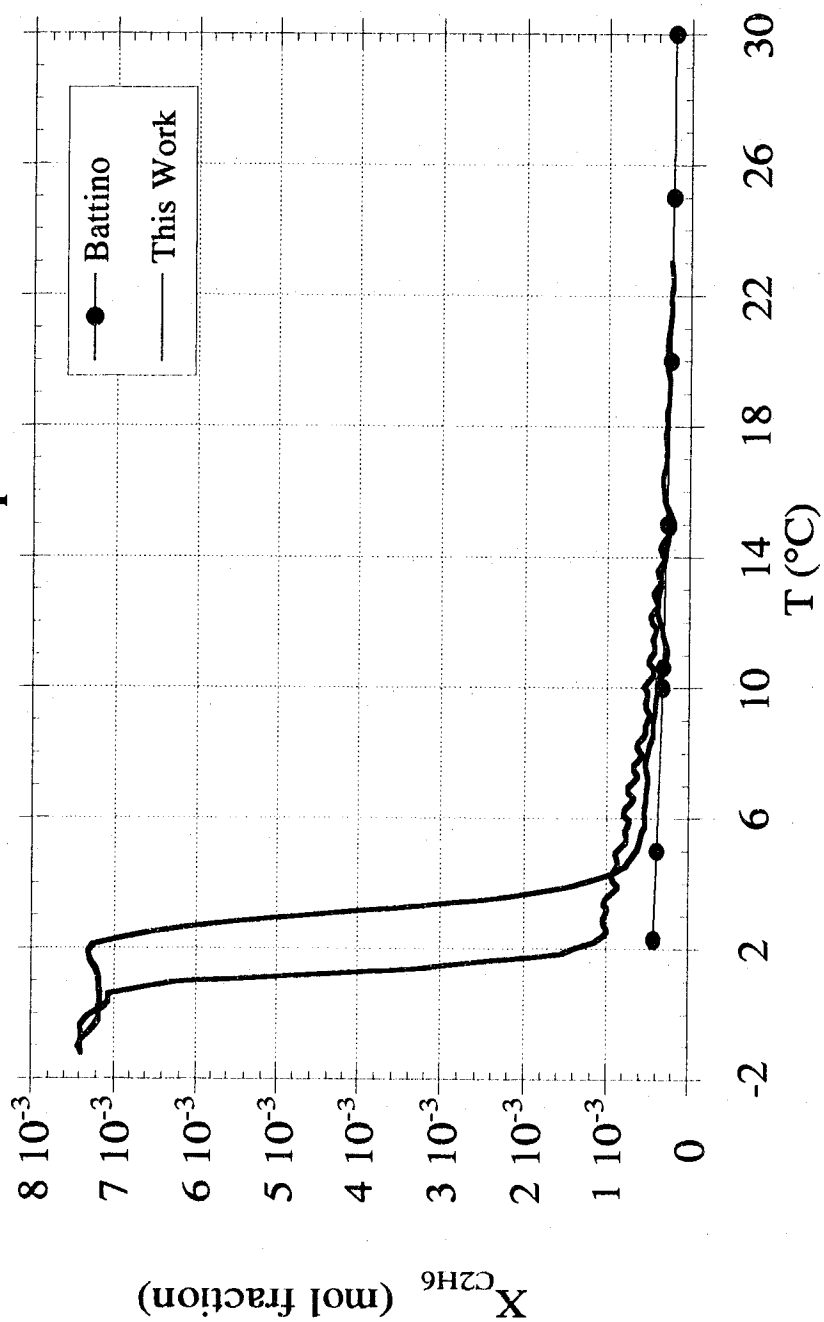


Fig. 2-11 Ethane Solubility in Pure Water
at 500 psia



2.2.3. Enthalpies and Entropies of Solution

Assuming equilibrium is reached at each temperature, the enthalpies and entropies of solution of hydrocarbon gases in liquid water are derived from the following thermodynamic relationships [Appendix B]:

$$\bar{h}_i^{L\infty} - h_i^{V_0} = -R \left(\frac{\partial \ln x_i}{\partial 1/T} \right)_{P, \text{sat}} = \Delta \bar{h}_i \quad (2-22)$$

$$\bar{s}_i^{L\infty} - s_i^{V_0} = R \left(\frac{\partial \ln x_i}{\partial \ln T} \right)_{P, \text{sat}} = \Delta \bar{s}_i \quad (2-23)$$

Standard state for Eq. 2-22 is an infinitely dilute solution and for Eq. 2-23 a solution above which the fugacity of the solute gas is one atmosphere. Hence, whenever plots of $\ln x_i$ vs $\ln T$ and $\ln x_i$ vs $1/T$ give an approximately straight line, the enthalpies and entropies of solution are constant over the considered temperature range and can be derived from Eq. 2-22 and Eq. 2-23. Because these thermodynamic relationships assume that equilibrium is established between the phases, enthalpies and entropies of solution have only been derived at temperatures above the catastrophic hydrate formation temperature, T_c . Table 2-3 to Table 2-6 show the calculated $\Delta \bar{h}_i/R$ and $\Delta \bar{s}_i/R$ values, constant over the corresponding temperature ranges, for each of the pure hydrocarbon gases.

The low regression coefficients of methane and ethane are due to the appearance of some electronic glitches during the experiments, since these coefficients are calculated directly from raw experimental data and not from the previous smoothed solubility curves. Before hydrate formation, these curves can be divided into two major linear

parts: a high temperature solubility line, far from hydrate formation and a low temperature solubility line which ends just before T_c . The resulting enthalpies and entropies of solution are reported in Table 2-7.

Table 2-3 Enthalpies and Entropies of Solution of CH_4 in Liquid Water

Temperature Range ($^{\circ}\text{C}$)	Regression Coefficient	$-\Delta\bar{h}_i/R$ (K)	$-\Delta\bar{s}_i/R$
17.27 — 7.35	0.17	3228.4	11.3
7.3 — 3	0.43	9106.9	32.7

Table 2-4 Enthalpies and Entropies of Solution of C_2H_6 in Liquid Water

Temperature Range ($^{\circ}\text{C}$)	Regression Coefficient	$-\Delta\bar{h}_i/R$ (K)	$-\Delta\bar{s}_i/R$
7 — 21	0.58	3958.2	13.8
7 — 12	0.60	9827.0	34.7
13 — 21	0.26	2802.8	9.6

Table 2-5 Enthalpies and Entropies of Solution of C_3H_8 in Liquid Water

Temperature Range (°C)	Regression Coefficient	$-\Delta \bar{h}_i/R$ (K)	$-\Delta \bar{s}_i/R$
16.5 — 3.7	0.95	6028.9	21.3
6 — 16.8	0.86	5275.4	18.5
6 — 10.5	0.83	8165.3	29.0
11 — 16	0.51	3482.5	12.1
6 — 16	0.88	5820.4	20.5

Table 2-6 Enthalpies and Entropies of Solution of CO_2 in Liquid Water

Temperature Range (°C)	Regression Coefficient	$-\Delta \bar{h}_i/R$ (K)	$-\Delta \bar{s}_i/R$
16 — 10	0.80	5142.9	18.0
9.25 — 8	0.61	11822.0	42.0
7.8 — 10.25	0.88	18461.0	65.4
10.5 — 16.5	0.72	5230.7	18.3

Table 2-7 Enthalpies and Entropies of Solution of Pure Hydrocarbons in Liquid Water

	Far from Tc		Close to Tc	
	$\Delta \bar{h}_i$	$\Delta \bar{s}_i$	$\Delta \bar{h}_i$	$\Delta \bar{s}_i$
CH ₄	-6.4	-22.4	-18.1	-65.0
C ₂ H ₆	-5.6	-19.1	-19.5	-69.0
C ₃ H ₈	-6.9	-24.0	-16.2	-57.7
CO ₂	-10.2	-35.7	-23.5	-83.4

$\Delta \bar{h}_i$ in kcal/mol of gas

$\Delta \bar{s}_i$ in cal/mol of gas

Himmelblau and Battino et al. calculated these enthalpies and entropies of solution for methane and ethane from solubility data at low temperatures and atmospheric pressures. The reported values along with our calculations are shown in Fig 2-12 to 2-15.

Fig. 2-12 Enthalpy of Solution of Methane in Pure Water

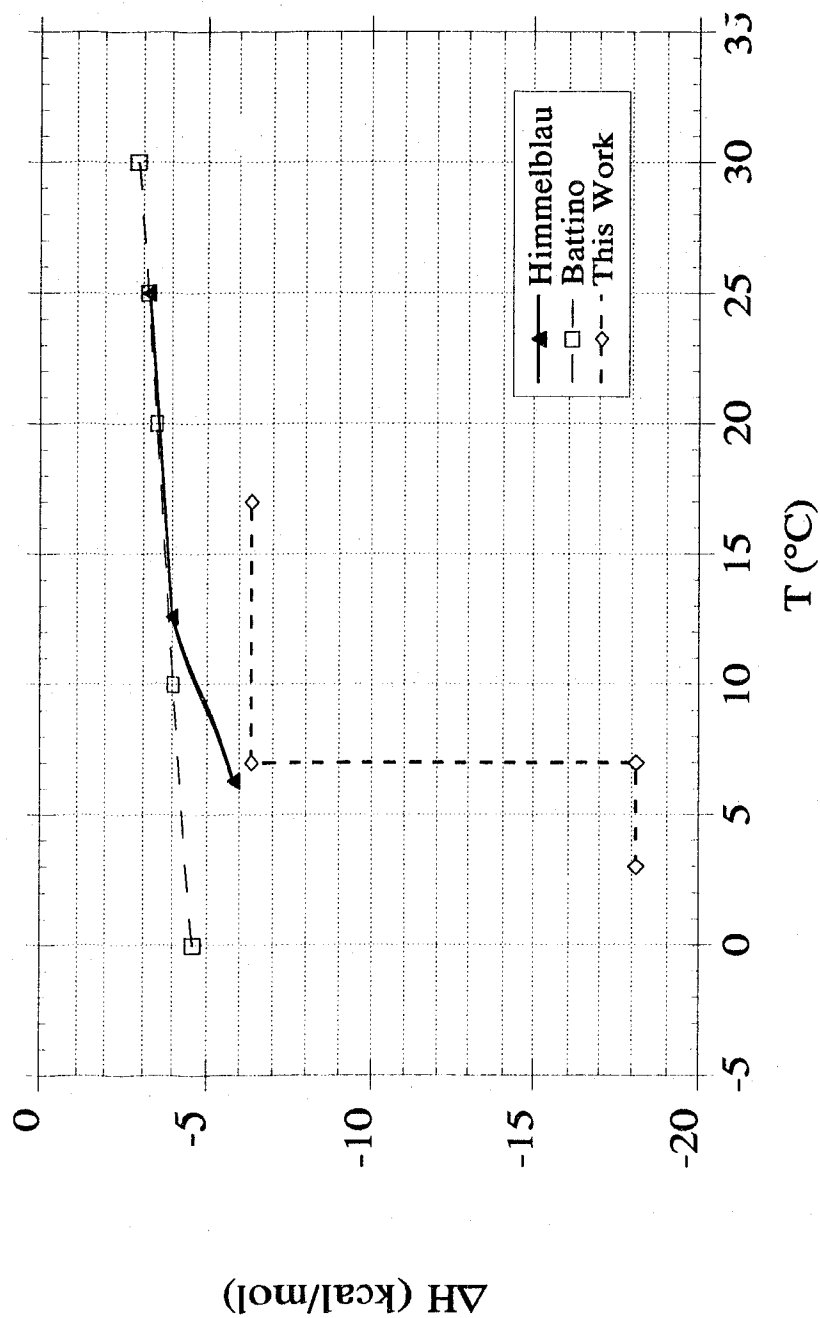


Fig. 2-13 Enthalpy of Solution of Ethane in Pure Water

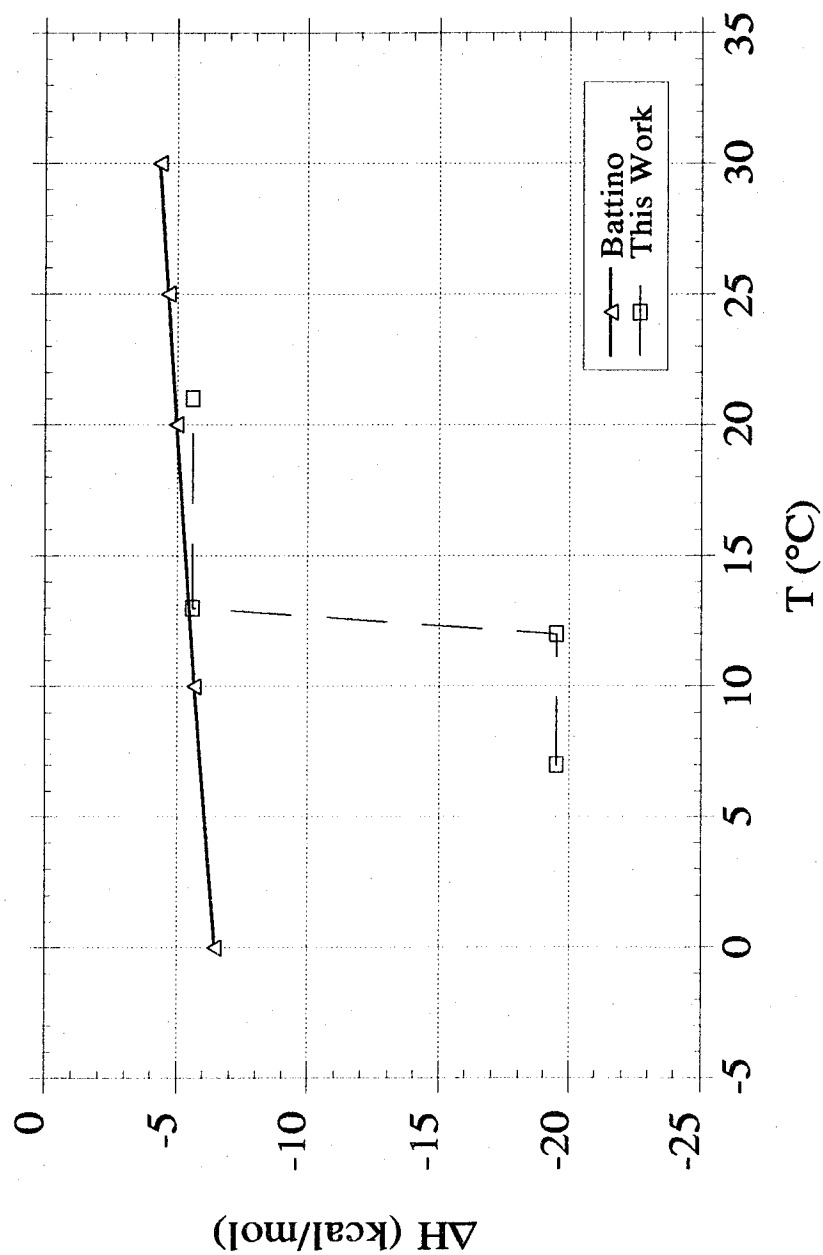


Fig. 2-14 Entropy of Solution of Methane in Pure Water

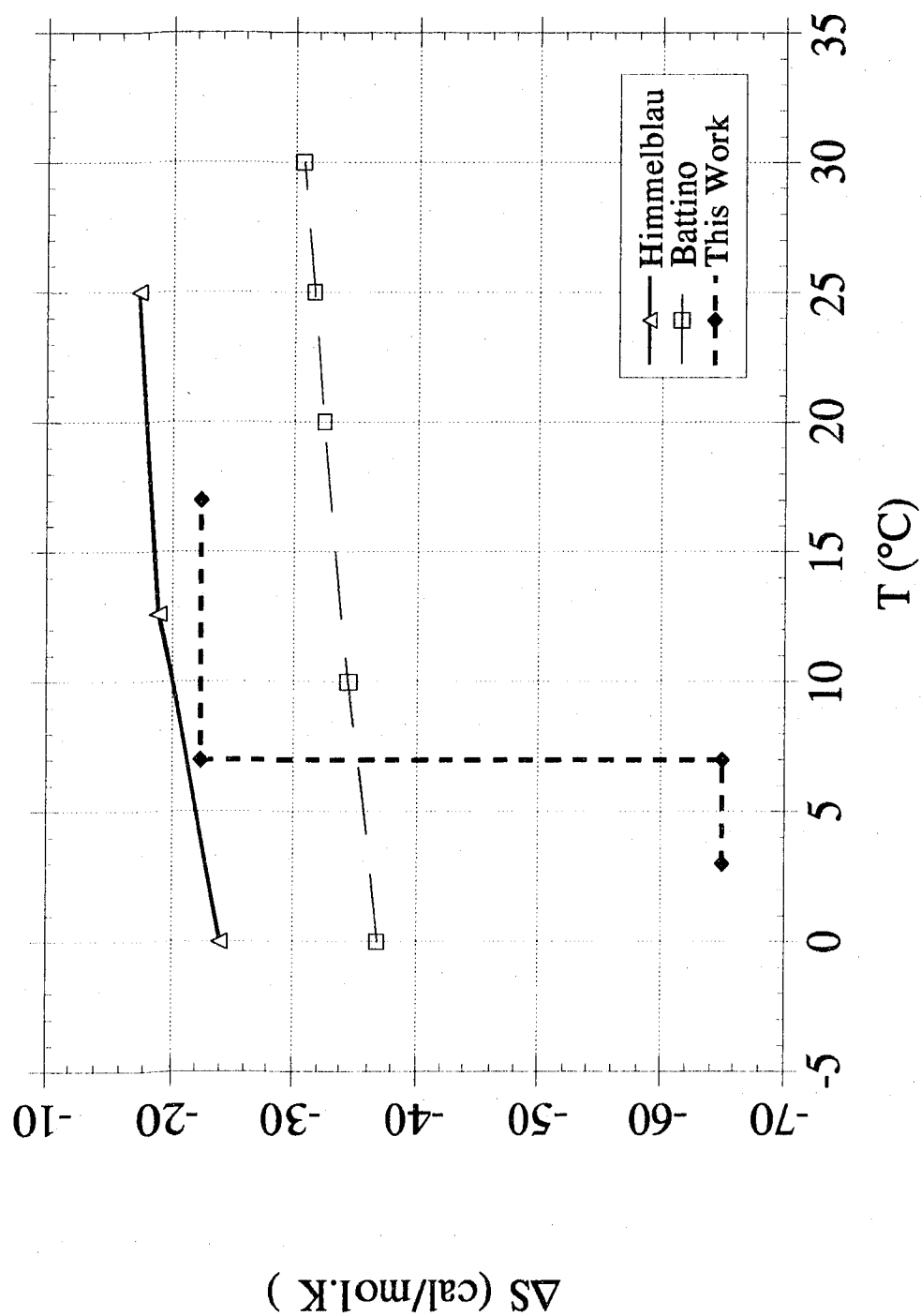
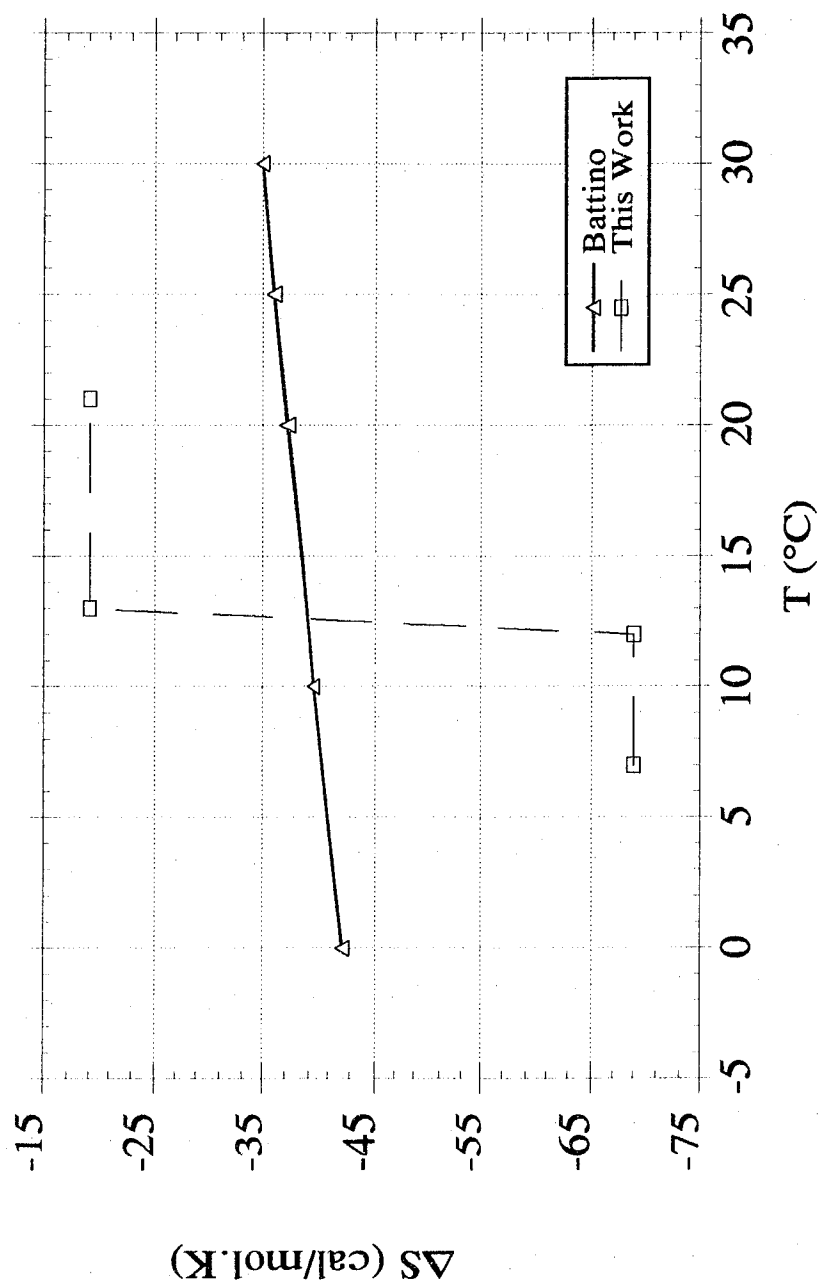


Fig. 2-15 Entropy of Solution of Ethane in Pure Water



2.2.4. Discussion

Fig. 2-10 and 2-11 clearly show a sudden increase in gas solubility from higher temperature—or extrapolated low temperature—solubility data. Data obtained with the $C_2H_6-H_2O$ system go high enough in temperature to provide a direct comparison with reported data. In Fig. 2-11 our solubility measurements superimpose perfectly on reported data from literature at temperatures up to $23^\circ C$, after completing the entire hydrate formation and decomposition cycle. This constitutes an encouraging validation of our experimental measurements. Below $15^\circ C$, the liquid solution becomes supersaturated with hydrocarbon gases. At T_c , this supersaturation corresponds to an increase by 150 percent of the predicted Henry's law solubility of ethane at the same temperature. Concerning methane, our data are 300 percent higher than Henry's law values. After hydrate formation, the amount of gas in the condensed phase is as high as 15.2×10^{-3} mol of methane and 7.4×10^{-3} mol of ethane. That is respectively 3.4 times and 7.4 times as high as the solubility at T_c . A high level of supersaturation of any hydrocarbon gas in liquid water is, therefore, achieved a few degrees before and after hydrate formation.

Our solubility measurements highlight the crystallization process that takes place during hydrate formation. Among the conditions of formation of gas hydrate, the solubility of the gas in water plays an important role, since the dissolved gas particles form the nuclei which initiate the process of hydrate precipitation and crystal growth. Thus, in Fig. 2-8 to 2-11, the gas supersaturation observed

down to T_c corresponds to a nucleation period, while after T_c , crystal growth takes place. According to the homogeneous nucleation theory, once a crystal grows to a critical size, further growth decreases the free energy of the system [Knight 1967] and is thus thermodynamically favored. The critical nuclei radius can be expressed as a function of the latent heat of crystallization (ΔH_c), the interfacial free energy σ and the extent of supercooling $\Delta T = T_{eq} - T$:

$$r_{cr} = \frac{2\sigma T_{eq}}{(-\Delta H_c)\Delta T} \quad (2-24)$$

The growth of a spherical crystal in the bulk liquid from zero radius to the critical radius r_{cr} involves a free energy increase and therefore, according to thermodynamics, should not happen. One may then state that around T_c , nucleation occurs as a result of a fluctuation in free energy, due to local temperature and pressure fluctuations, of sufficient magnitude to surmount the free energy barrier. Once a sufficient number of crystals is reached, they assemble together. Hydrate grows in a similar way to the freezing of ice at a approximately constant temperature, as observed in this study by the sudden increase in solubility after T_c . By visual observation, crystals first appear on the window of the cell where the temperature is lower than in the bulk of liquid or close to the metallic surface.

One of the major differences between the first set of experiments and the second is that after hydrate formation and decomposition the solubility comes back close to its initial value, providing that good mixing is achieved and high temperatures are

reached. Thus the amount of metastability of the liquid solution at high temperature does not depend on the thermal history of the water. The volume jump measured in this work corresponds to a low conversion of water to hydrates. As already stated, once hydrate formation happens, mixing is not achieved further and liquid water is trapped into hydrate crystals in a way that growth is inhibited. Therefore it is interesting to consider the sizes of the hysteresis curves obtained. A direct comparison is possible. Big increase (or decrease) in solubility corresponds to many hydrate cages stabilized and assembling together (respectively disassembling) requiring more hydrocarbon solute molecules to participate. Our results show a process more important for methane than for carbon dioxide and even more for ethane. The smallest hysteresis is for $C_3H_8-H_2O$ system. Propane participates only in the formation of large cages of structure II, Hexakaidecahedra, while ethane participates only in the formation of large cages of structure I, Tetrakaidecahedra; but methane and carbon dioxide participate in the formation of two types of cages and a bigger amount of these gases is needed for crystal growth. Furthermore, Table 2-8 reports the catastrophic and final hydrate decomposition temperatures along with the statistical thermodynamic predictions of hydrate formation for each of the hydrocarbon-water systems. The predicted values are obtained by using the Colorado School of Mines hydrate prediction program [Sloan 1990] which is based on the statistical theory of van der Waals and Platteeuw [van der Waals 1959].

Table 2-8 Catastrophic and Final Hydrate Decomposition Temperatures

Temperatures (°C)	CH₄	C₂H₆	C₃H₈	CO₂
Tc	2.1	2	3	8.0
FHDT	3.2	3.9	4.7	8.7
Stat. Thermo.	1.1	1.9	1.7	0.7
FHDT-Tc	2.81	3.13	4.23	8.44
Stat Thermo-FHDT	0.39	0.77	0.47	0.26
Stat. Thermo-Tc	0.71	1.13	1.23	0.44

The computed data are closer to the FHDT than to Tc which is consistent with the fact that statistical thermodynamic predictions rely on experimental FHDT data. Also the temperature difference between Tc and FHDT is very similar between comparable systems. This difference may be interpreted as the necessary subcooling of the liquid before nucleation occurs. The mean subcooling is 1.35°C with a standard deviation of 0.55°C.

From an energetic point of view, the experimental enthalpies and entropies of solution are negative and in very good agreement at higher temperatures with reported values from other investigators [Himmelblau 1959, Rettich 1981]. Previous solubility measurements were conducted at atmospheric pressure, which accounts for the small difference in $\Delta \bar{h}_i$ and $\Delta \bar{s}_i$. At lower temperature, these energies shift down and diverge from the atmospheric enthalpies

and entropies even though no hydrate formation takes place yet. The shifts in enthalpies and entropies as T_c is approached can be compared with ice formation on one hand and experimental heats of dissociation on the other [Handbook 1983].

The heat associated with the formation of one mol of liquid water from ice is about 1.4 kcal. Not all water molecules participate in cage formation. Once hydrate is formed, the minimum coordination of methane molecules is $n=5\frac{3}{4}$ molecules of H_2O per molecule of CH_4 . In liquid water this number must logically be higher. Nemethy and Sheraga suggest $n=13$. Thus the heat associated with the formation of one mol of liquid water from ice is at least $1.4 \times 5.75 = 8$ kcal/mol of hypothetical methane gas present in the liquid water. This heat is comparable with the lowering of enthalpy of solution as hydrate formation is approached. Table 2-9 along with Fig. 2-16 show experimental and correlated dissociation energies of single component gas hydrates.

One may first remark that the increasing order in the dissociation energies— CH_4 , CO_2 , C_2H_6 and C_3H_8 —is the same as the decreasing order in the hysteresis sizes previously mentioned. So the dissociation energy of methane hydrate is close to the shift in enthalpy when T_c is approached. But these energies become large for $C_2H_6-H_2O$ hydrate and very large for $C_3H_8-H_2O$ hydrate. Propane is more soluble in water than methane at low temperatures. But propane solubility decreases suddenly when the temperature is increased, becomes lower than the methane solubility above $100^\circ F$

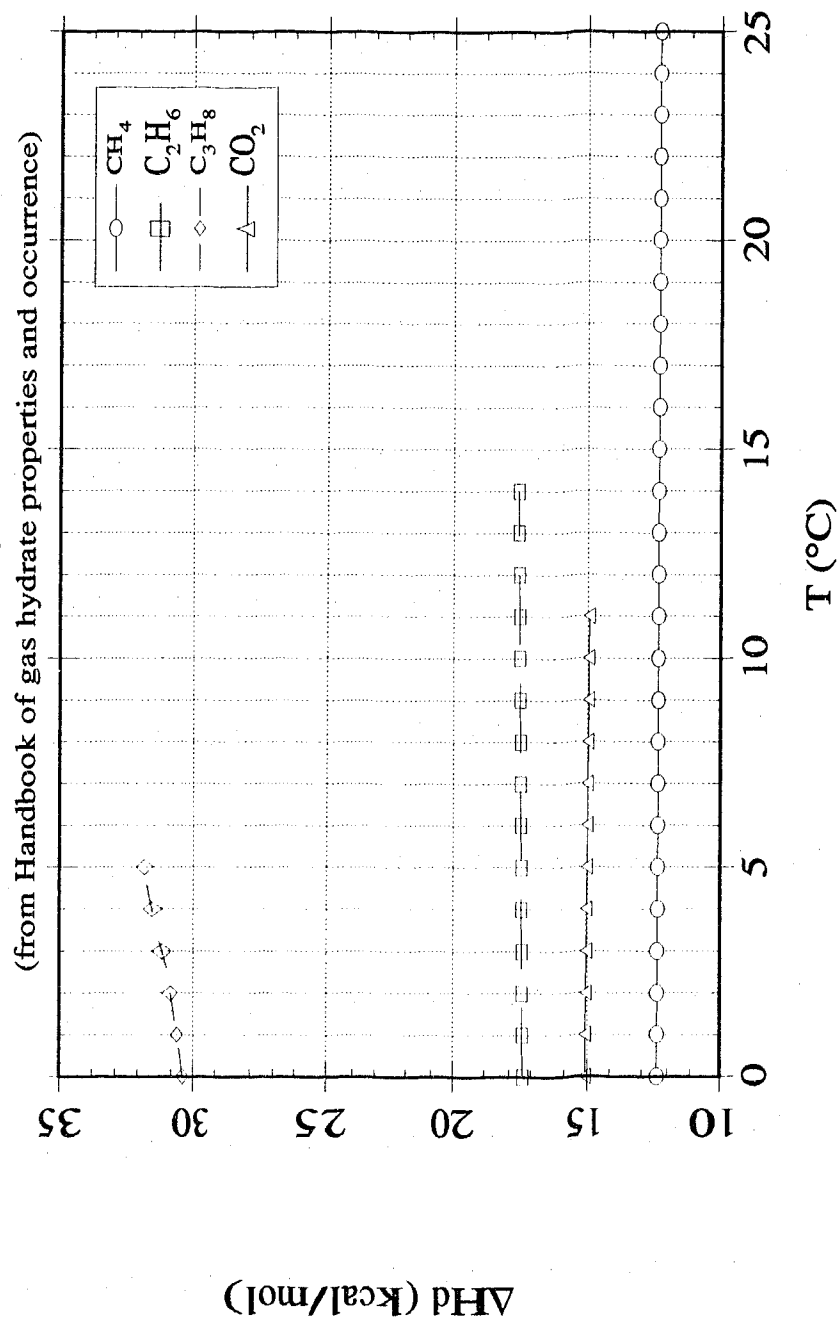
and finds a minimum around 200°F [Kobayashi 1951]. Thus the change in enthalpy and entropy of solution considering a wider range of temperature is bigger than our experimental values and may be close to the enthalpy of dissociation of hydrates.

Table 2-9 Enthalpies of Dissociation of Hydrate to Liquid Water and Vapor

Temperature range (K)	CH ₄	C ₂ H ₆	C ₃ H ₈	Reference
160 — 210	12.94	/	/	[Handa]
190 — 250	/	17.15	/	id
210 — 260	/	/	30.86	id
278.15	13.77	/	/	[Lievois]
283.15	12.72	/	/	id
?	12.83	/	/	[Davidson]
?	/	17.98	/	id
?	/	/	32.1	id

After studying hydrate formation from pure hydrocarbon gas and pure liquid water, the next chapter deals with the change in the catastrophic conditions brought by the presence of inhibitors in the aqueous solutions such as methanol and PVP.

Fig. 2-16 Dissociation Energies of Single-Component Gas Hydrates



3. EFFECT OF INHIBITORS ON HYDRATE FORMATION AND DECOMPOSITION

Methanol is widely used in the natural gas industry to prevent hydrate formation due to its cost and effectiveness. The introduction of methanol into gas pipelines commonly encountered range from a few weight percent up to 25 weight percent. Since very few data exist on the hydrate inhibition via polyvinylpyrrolidone—namely PVP—such experiments are carried out. These concern systems containing methane, ethane, carbon dioxide and a mixture of methane and propane in a 0.5 weight percent aqueous solution of PVP. The results are then compared with those obtained with pure water and an aqueous methanol solution.

3.1. EXPERIMENTAL RESULTS

Solubilities of pure methane, pure ethane, pure carbon dioxide and a mixture of methane and propane are measured in two aqueous solutions, one containing 10 weight percent of methanol and the other 0.5 weight percent of PVP K-90. For the last few runs, a reservoir bottle of 300 ml was removed thus reducing the total system volume to 231.2 ml. Otherwise, the experimental apparatus and procedure remain the same as stated in chapter 2. The operating pressure for the $\text{CH}_4\text{-C}_3\text{H}_8\text{-H}_2\text{O}$ system is set at 300 psia. Using DDMIX—the NIST computer program—the phases of a mixture of methane and propane are computed for propane mol fractions ranging from 10 percent to 30 percent and reported in Table 3-1.

A liquid phase appears only for 30 percent of propane at 0°C and higher concentrations. From higher temperature solubility data [Kobayashi 1951], propane solubility increases more than methane solubility as temperature is lowered under 200°F. Moreover, hydrate formation usually depletes the gas phase of its heavy components in a consistent way with the "Bucky-Ball" formation theory [Chapter 5]. Thus the propane mol fraction in the gas phase decreases upon cooling; a rule of thumb is a maximum 5 percent decrease. The hydrocarbon mixture is then a vapor phase all the way down to low temperatures.

Pure methane, ethane and carbon dioxide operating pressures remain the same as previously that is respectively 500, 95 and 500 psia.

In PVP aqueous solution at 500 psia, methane hydrate was observed after ice formed. And the freezing of a large part of the liquid water modified the temperature behavior of the liquid solution usually observed. Balls became stuck and ceased mixing the condensed phases, ice formed around the PRT, and as a result, the temperature data collected fluctuated. It was then difficult to determine correctly the catastrophic temperature and the final hydrate decomposition temperature. At 95 psia, the same phenomena happened during ethane hydrate formation. Hence, in order to form hydrates on the 3 phase line Lw-H-V, the pressure was increased to 700 psia for CH₄-PVP system and to 160 psia for C₂H₆-PVP system.

Table 3-1 Compressibility Factors and Phases of Methane-Propane Mixtures at 300 psia

10 mol % of C ₃ H ₈				
0 °C	5 °C	10 °C	15 °C	20 °C
Vapor	Vapor	Vapor	Vapor	Vapor
0.93144	0.93566	0.93957	0.94321	0.94660
15 mol % of C ₃ H ₈				
0 °C	5 °C	10 °C	15 °C	20 °C
V	V	V	V	V
0.92014	0.92504	0.92957	0.93377	0.93768
19.98 mol % of C ₃ H ₈				
0 °C	5 °C	10 °C	15 °C	20 °C
V	V	V	V	V
0.90760	0.91327	0.91851	0.92336	0.92785
25 mol % of C ₃ H ₈				
0 °C	5 °C	10 °C	15 °C	20 °C
V	V	V	V	V
0.89348	0.90007	0.90613	0.91173	0.91690
30 mol % of C ₃ H ₈				
0 °C	5 °C	15 °C	20 °C	
L+V	V	V	V	
0.07455/0.88482	0.88538	0.89887	0.90483	

This problem does not occur using methanol solutions since 10 weight percent of methanol in liquid water lowers the ice formation temperature in such a way that hydrates form before ice as temperature is lowered.

Fig 3-1 to 3-3 show a sample of the resulting plots. And in Tables 3-2 to 3-6 are reported the catastrophic temperatures and the final hydrate decomposition temperatures for all systems. The computed predictions are added for systems containing pure water or a 10 weight percent methanol aqueous solution.

Table 3-2 Tc and FHDT of CH₄-Aqueous Solution Systems

	Pure H ₂ O	Methanol	PVP ⁴
Tc (°C)	2.1	0.5	2.2
FHDT (°C)	3.2	0.8	7.2
CSMHYD (°C)	2.82	-1.9	/
Ramping rate (°C/h)	2	2	2

⁴ Run carried out at 700 psia.

Table 3-3 Tc and FHDT of C₂H₆-Aqueous Solution Systems

	Pure H ₂ O	Methanol	PVP ⁵	
Tc (°C)	2	-1	0.8	1.5
FHDT (°C)	3.9	1.1	8.7	8.5
CSMHYD (°C)	3.12	-1.48	/	/
Ramping rate (°C/h)	2	2	2	2

Table 3-4 Tc of CH₄-C₃H₈ in Aqueous Solutions

Tc (°C)	Ramping rate (°C/h)	Pure H ₂ O	Methanol	PVP
Run #1	2	13.4	10.1	7
Run #2	1.5	12.2	/	/
Run #3	4	13	/	/
Run #4	4	12	/	/
Run #5	5	11.8	/	/
Run #6	3	12.3	11.1	/
Run #7	3	13.5	11.7	/
CSMHYD	/	14.06	9.41	/

⁵ Two runs carried out at 160 psia.

Table 3-5 FHDT of $\text{CH}_4\text{-C}_3\text{H}_8$ in Aqueous Solutions

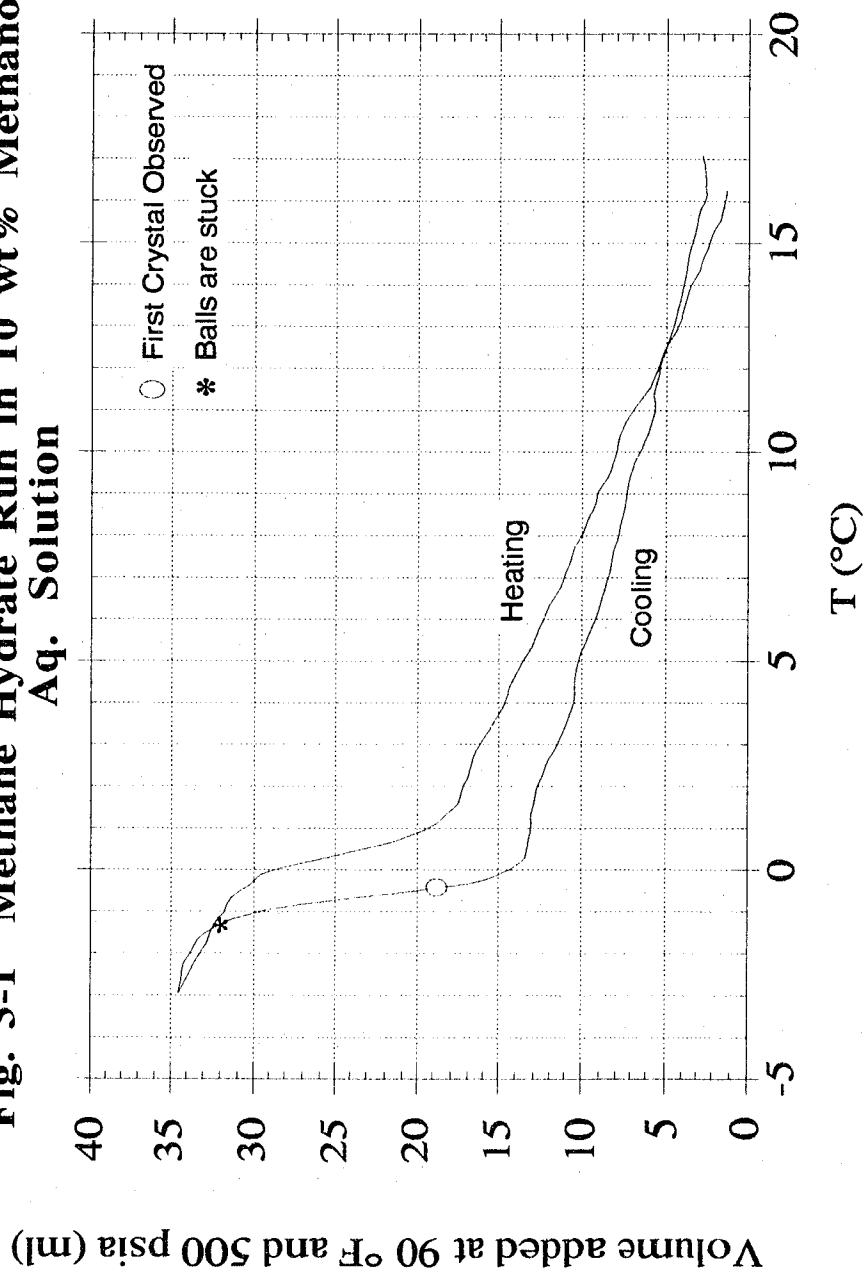
FHDT ($^{\circ}\text{C}$)	Ramping rate ($^{\circ}\text{C}$)	Pure H_2O	Methanol	PVP
Run #1	2	15.3	12.5	14.7
Run #2	1.5	15	/	/
Run #3	3	15.3	12.8	/
Run #4	3	15.1	/	/

Table 3-6 Tc and FHDT of CO_2 -Aqueous Solution Systems

	Pure H_2O	Methanol			PVP ⁶
Tc ($^{\circ}\text{C}$)	8	5.5	5.2	5.5	7.5
FHDT ($^{\circ}\text{C}$)	8.7	5.7	5.7	5.7	8.8
CSMHYD ($^{\circ}\text{C}$)	8.43		5.62		/
Ramping rate ($^{\circ}\text{C/h}$)	2	2	2 / 0.5 ⁷	2	2

⁶ Run carried out at 500 psia.⁷ Ramping rate is changed throughout the cycle.

Fig. 3-1 Methane Hydrate Run in 10 wt % Methanol Aq. Solution



**Fig. 3-2 Ethane Hydrate Run in 0.5 wt % PVP
Aq. Solution**

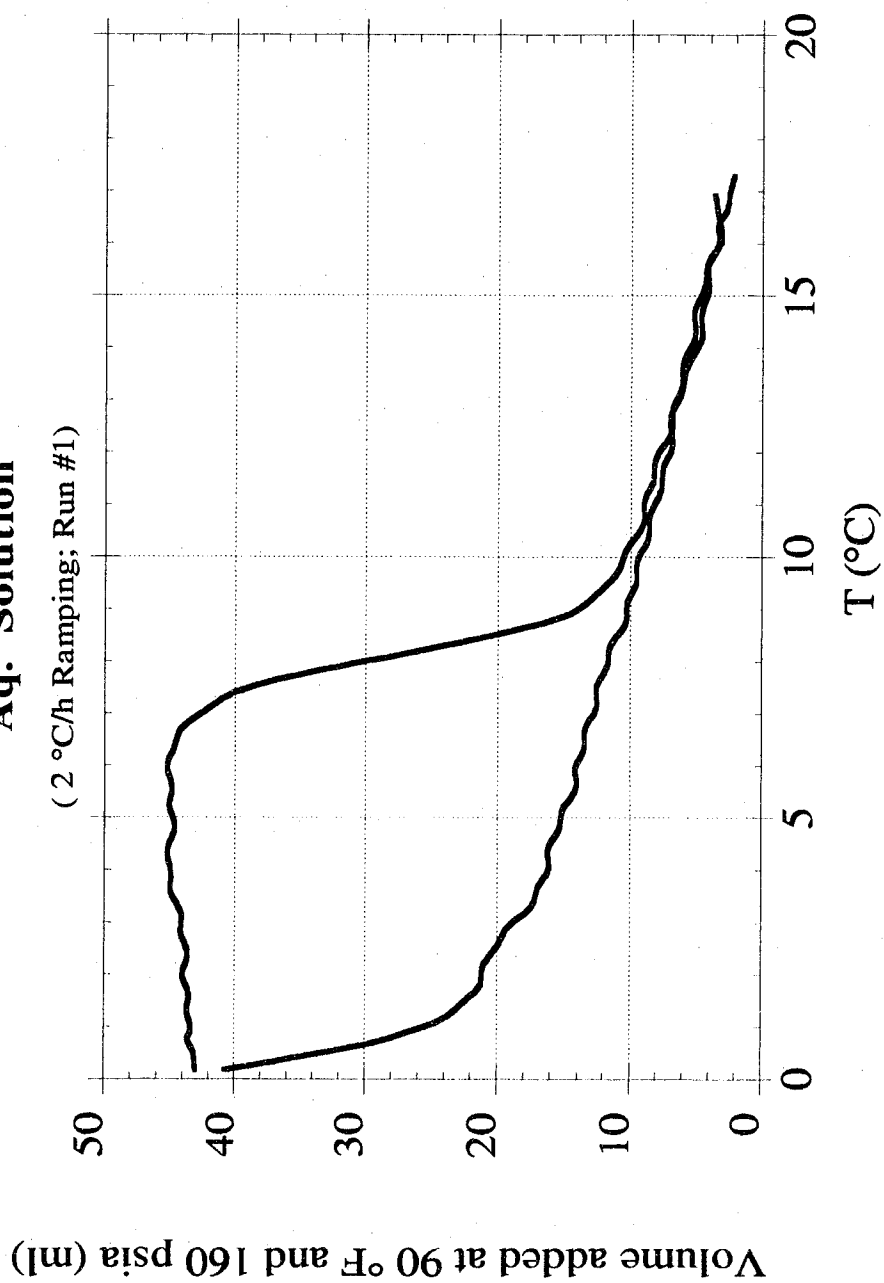
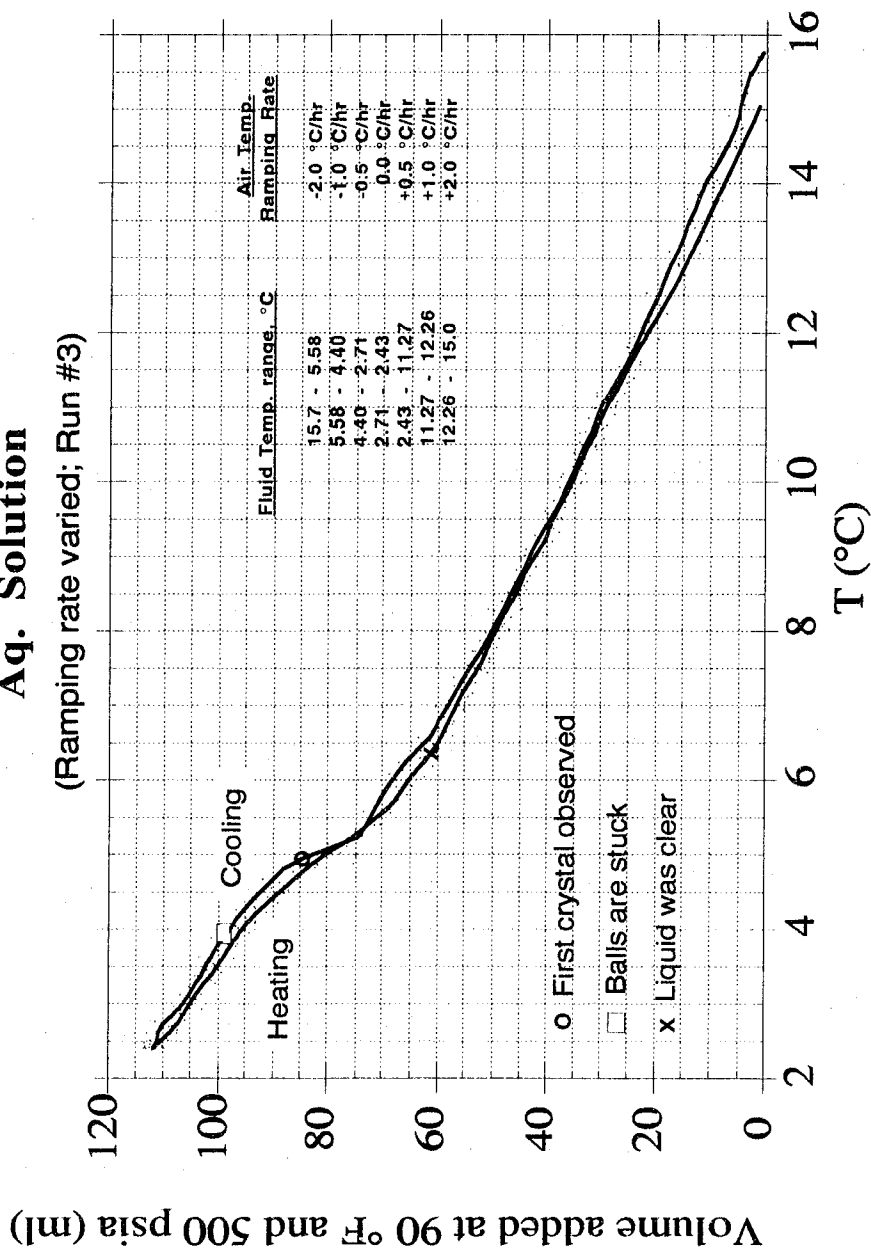


Fig. 3-3 Carbon Dioxide Hydrate Run in a 10 wt % Methanol Aq. Solution
(Ramping rate varied; Run #3)



3.2. DATA ANALYSIS AND DISCUSSION

CSMHYD predicts lower temperature of hydrate stability than our experimental FHDT when a 10 weight percent methanol aqueous solution is used. A comparison of T_c , FHDT with predicted temperatures is given in Table 3-7.

Methanol is a highly volatile substance and is added in pure liquid water at ambient temperature and pressure before being introduced in the cell. So the actual methanol concentration in the liquid phase is lower than 10 weight percent and the inhibition effect is less than expected. Some techniques, useful to the gas industry, exist to estimate the amount of methanol to be injected in natural gas pipelines. In comparison, the FHDT is relatively well predicted for pure water systems with a deviation from our experimental data ranging from 3 to 20 percent [Table 3-7].

Concerning $\text{CH}_4\text{-C}_3\text{H}_8$ hydrate, the predicted temperature of hydrate stability is for a gas phase above the condensed phase at a given composition. The reported values in the tables correspond to the initial gas phase composition, that is approximately 80 percent of methane and 20 percent of propane. As previously mentioned, the gas phase content of propane around the catastrophic temperature is lower than 20 mol percent and therefore the corresponding predicted hydrate formation temperature is lower than the reported values. Thus the predicted temperatures using CSMHYD represent an upper estimate of the actual hydrate formation temperature.

Table 3-7 Relative Differences Between Tc and FHDT

		CH₄	C₂H₆	CO₂	CH₄-C₃H₈
FHDT-Tc	<i>Pure H₂O</i>	1.1	1.9	0.7	1.9
	<i>Methanol</i>	0.3	2.1	0.2/0.5 ⁸	2.4
	<i>PVP</i>	5.0	7.9/6.0 ⁸	1.3	7.7
FHDT - CSMHYD	<i>Pure H₂O</i>	0.38	0.78	0.27	1.24
	<i>Absolute Deviation</i>	11.8%	20%	3.1%	8.1%
	<i>Methanol</i>	2.7	2.58	0.08	3.09
ΔFHDT (Pure H₂O-Methanol)⁹		2.4	2.8	3	2.8
ΔT (Pure H₂O-Methanol)¹⁰		1.6	3	2.5/2.8 ⁸	3.3
ΔFHDT (Pure H₂O-PVP)		-4	-4.8/-4.6 ⁸	-0.1	0.6
ΔTc (Pure H₂O-PVP)¹¹		-0.1	1.2/0.5 ⁸	0.5	6.4

⁸ Two runs.⁹ Mean=2.75°C; Standard Deviation=0.25°C; Variance=0.06.¹⁰ Mean=2.80°C; Standard Deviation=0.81°C; Variance=0.66.¹¹ Mean=0.53°C; Standard Deviation=0.53°C; Variance=0.82.

T_c is difficult to determine properly when hydrate is formed from a $\text{CH}_4\text{-C}_3\text{H}_8$ gas mixture. As a matter of facts, the slope of the solubility plots increase gradually as temperature is ramped down and the increase in gas solubility is not so sudden nor so high as previously noticed with pure components gas hydrates. It is known that the addition of a small amount of propane to methane causes the hydrate structure to switch from structure I to structure II. So propane fits into the large cavity of structure II—Hexakaidecahedra—and methane the small cavity of structure II. The induction time, for the simple methane hydrate observed by Falabella and caused by a vacillation of methane molecules between structures before a critical nucleus size is achieved, disappears. The high T_c observed in the $\text{CH}_4\text{-C}_3\text{H}_8\text{-H}_2\text{O}$ system run confirm that propane stabilizes the large cages of the structure II hydrate and enhances hydrate formation.

One may interpret the slow change in solubility upon hydrate formation as due to the separate formation of two types of cages. A first part may be the increase in propane solubility; during the second part at lower temperature, methane is dissolved in the aqueous solution to stabilize small cages of structure II. A future gas chromatograph analysis will lead to a better understanding of the process occurring in the formation of $\text{CH}_4\text{-C}_3\text{H}_8$ hydrate.

On the other hand, the sharp changes upon heating the hydrate solution provides a precise determination of the FHDT as shown in Table 3-5. Once again, crystal decomposition is a less random process than crystal formation

The inhibitory effect of methanol on hydrate formation is very consistent in all systems. The mean catastrophic temperature depression on 10 weight percent methanol inhibition is estimated at 2.8°C and is readily comparable with the 2.75°C change in final hydrate decomposition temperature.

Even though methane and propane runs in PVP aqueous solution are carried out at higher pressures, the catastrophic temperatures are slightly lower or equal as in a pure water system. Carbon dioxide hydrate formation at 500 psia both in pure water and PVP solution, show a difference in T_c of only 0.5°C . So our measurements indicate a better inhibitory effect using a 10 weight percent methanol solution than with a 0.5 weight percent PVP aqueous solution.

On the other hand, PVP seems to inhibit hydrate decomposition. All FHDT are above the pure water data and as a result the hysteresis observed are very wide in comparison with the two other liquid solutions.

Three CO_2 -methanol runs are performed: one with a 231.2 ml system volume and two with a 531.2 ml system volume. Following Eq. 2-1 to 2-21, mol fractions of hydrocarbon gas in solution are calculated using the corresponding system volumes. The resulting solubilities are similar with a maximum deviation of 10.2 percent at the lower temperatures. Some of this error may be due to an inaccuracy in the determination of the system volumes. Thus CO_2 -methanol runs reasonably validate the derivation of the mass balances.

Also, in Fig. 3-3 the ramping rate is lowered in two steps down to 0.5°C/h as the temperature decreases. The measured T_c and FHDT [Table 3-6] remain the same and only a slight change in the solubility occurs. The heating part still lies under the cooling part and the hysteresis is smaller but also remains. So when the cooling rate is changed, the overall picture of the process is similar, with only slight changes in the solubility measurements. $\text{CH}_4\text{-C}_3\text{H}_8$ runs are performed at several ramping rates ranging from 1.5°C/h to 5°C/h . It appears that no direct relation exists between the catastrophic temperature and the ramping rate. In run #2 at 1.5°C/h , T_c is only 0.2°C higher than at 5°C/h . FHDT data are scatter between 15°C to 17°C with a small standard deviation of 0.15°C . The same analysis can be made with methanol aqueous solution runs. Thus one can assume that nucleation and decomposition are independent of the cooling rate. The small fluctuations may be due either to experimental inaccuracy in the data logging, or the presence of non-melted crystal seeds that act as nucleating agents.

This statement is consistent with the heterogeneous nucleation of ice. According to Knight, supercooled liquid water is nucleated by foreign particles and the cooling rate of water has no effect whatsoever upon nucleation temperature.

The time interval of data logging for each experiment is 5 minutes regardless of the ramping rate. Hence, at low ramping rates more data points are available and the catastrophic conditions may be determined more precisely. By extrapolating to 0°C/h several

runs made with fresh solution at different ramping rates, one may obtain an absolute nucleation temperature.

4. INFLUENCE OF THE pH OF THE WATER ON THE CATASTROPHIC CONDITIONS

The effect of the pH of the water on the hydrate formation and decomposition conditions has been studied. Temperature ramping experiments at constant pressure involving low pH aqueous solutions for methane gas and a gaseous mixture of methane and propane were conducted according to Table 4-1.

Table 4-1 pH-Temperature Ramping Experiments

GAS	PRESSURE (psia)	pH			
		7	5	4	3
CH ₄	500	7	5	4	3
CH ₄ -C ₃ H ₈	300	7	5	4	3

A comparison of the catastrophic temperatures, T_c , obtained will reveal whether or not hydrate formation is a function of the pH of the water forming the hydrates.

4.1. RESULTS

Two series of experiments were performed. One was conducted with the RUSKA pump. Hydrate formation and decomposition of CH₄ and a mixture of CH₄ and C₃H₈ (19.98 mol%) in pH 7, pH 5, and pH 4 were measured. The other series of experiment was performed on

the same gas mixtures in pH 5 and pH 3 aqueous solutions using the AMOCO pump.

In order to obtain a stable pH solution throughout the run, commercial pH-buffer solutions are used. pH 7 and pH 4 buffer solutions were obtained from BAXTER DIAGNOSTICS; pH 7 buffer solution consists of Sodium Phosphate, dibasic and pH 4 is an aqueous solution of Potassium Acid Phthalate. pH 5 is an ACROS ORGANICS product with composition unknown.

For each pH-buffer solution, the temperature dependence is estimated through pH measurements of the solution placed inside the air bath. According to Le Châtelier's Law, the dissociation constants of weak acids and bases will increase with increasing pressure. However, this effect assumes importance only at very high pressures and we will neglect the pressure dependence of pH.

The temperature dependence of the pH of the buffer solutions is found to be very low. Table 4-2 gives the mean value and standard deviation for each set of measurements.

Table 4-2 Mean pH over the Range of Temperature Considered and the Standard Deviation from the Mean

pH-Buffer	7	5	5	4	4
Mean pH	6.994	4.882	4.979	3.955	3.898
σ	0.031	0.028	0.018	0.010	0.030

The pH of buffer solutions depends on the pKa of the buffer weak acid and the concentration ratio of the acid [AH] and its conjugate base [A]:

$$\text{pH} = \text{pKa} + \log([A]/[AH]) \quad (4-1)$$

When the buffer concentration is sufficiently high, pressure-induced changes in pH do not significantly alter the concentration ratio term and can be attributed directly to the changes in pKa. Zipp et al. estimated the changes in the pH of buffer solutions under pressure [Neuman 1973]. This change is less than 0.1 at 7000 psia.

Thus the pH of the buffer-solutions are considered as constant throughout the run and equal to the rounded values—7, 5, 4, and 3.

Figures 4-1 to 4-6 show a sample of the resulting hydrate runs. Hydrate formation of $\text{CH}_4\text{-C}_3\text{H}_8$ in pH 7, pH 5 and pH 3 aqueous solutions has been conducted at low temperature. Remarkably, a second sudden increase in gas solubility is observed a few degrees below the first catastrophic temperature [Section 4.4].

Except for this feature, the other plots exhibit the same general behavior as in the previous chapters. Catastrophic temperature and final hydrate decomposition temperature along with the corresponding ramping rates and thermal history of the solution are reported in Table 4-3 and Table 4-4. The plots 4-7 to 4-10 help to achieve an estimate of the pH-induced temperature changes.

Fig. 4-1 Methane Hydrate Run in a pH 7 Buffer Solution

Volume added at 90 °F and 500 psia (ml)

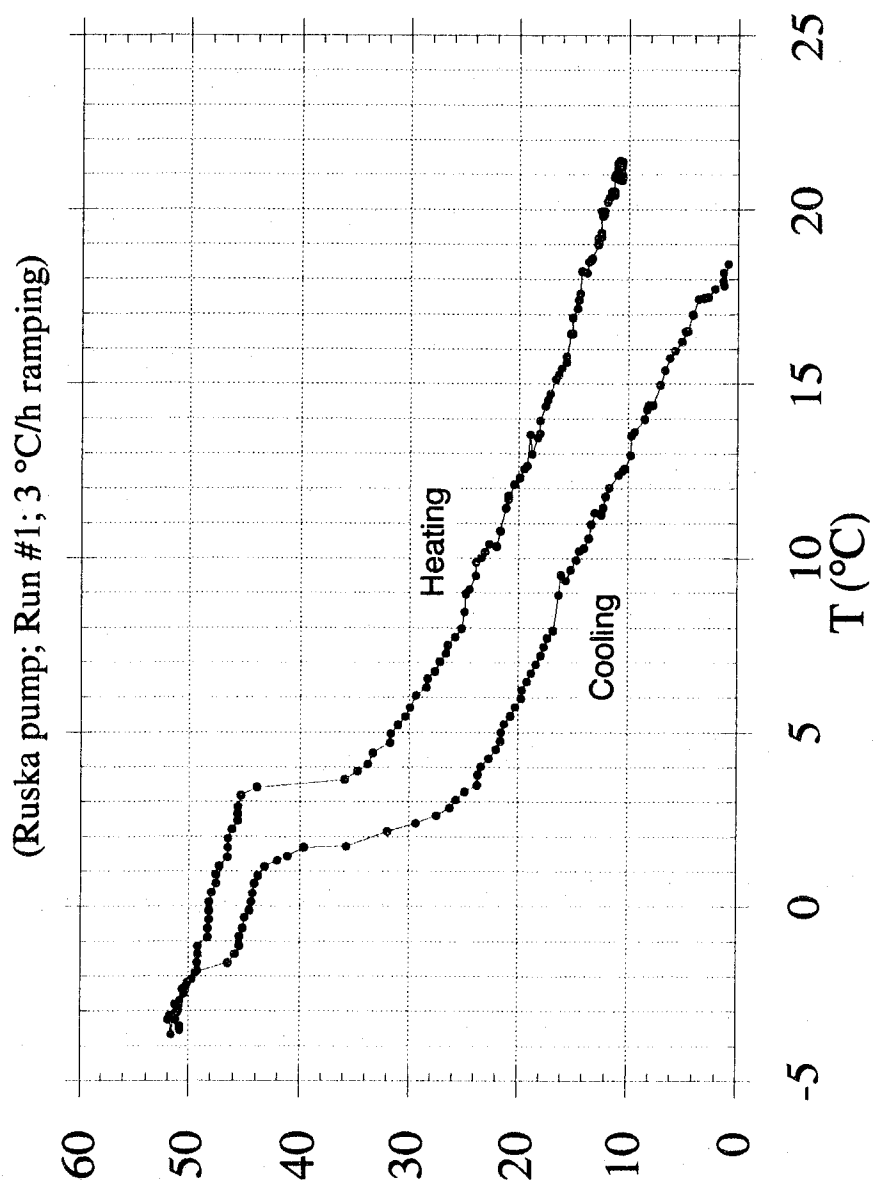


Fig. 4-2 Hydrate Run of a Mixture of CH_4 and C_3H_8 (19.98 mol %)
in a pH 5 Buffer Solution
 (Ruska pump; Run #1; 3 °C/h ramping)

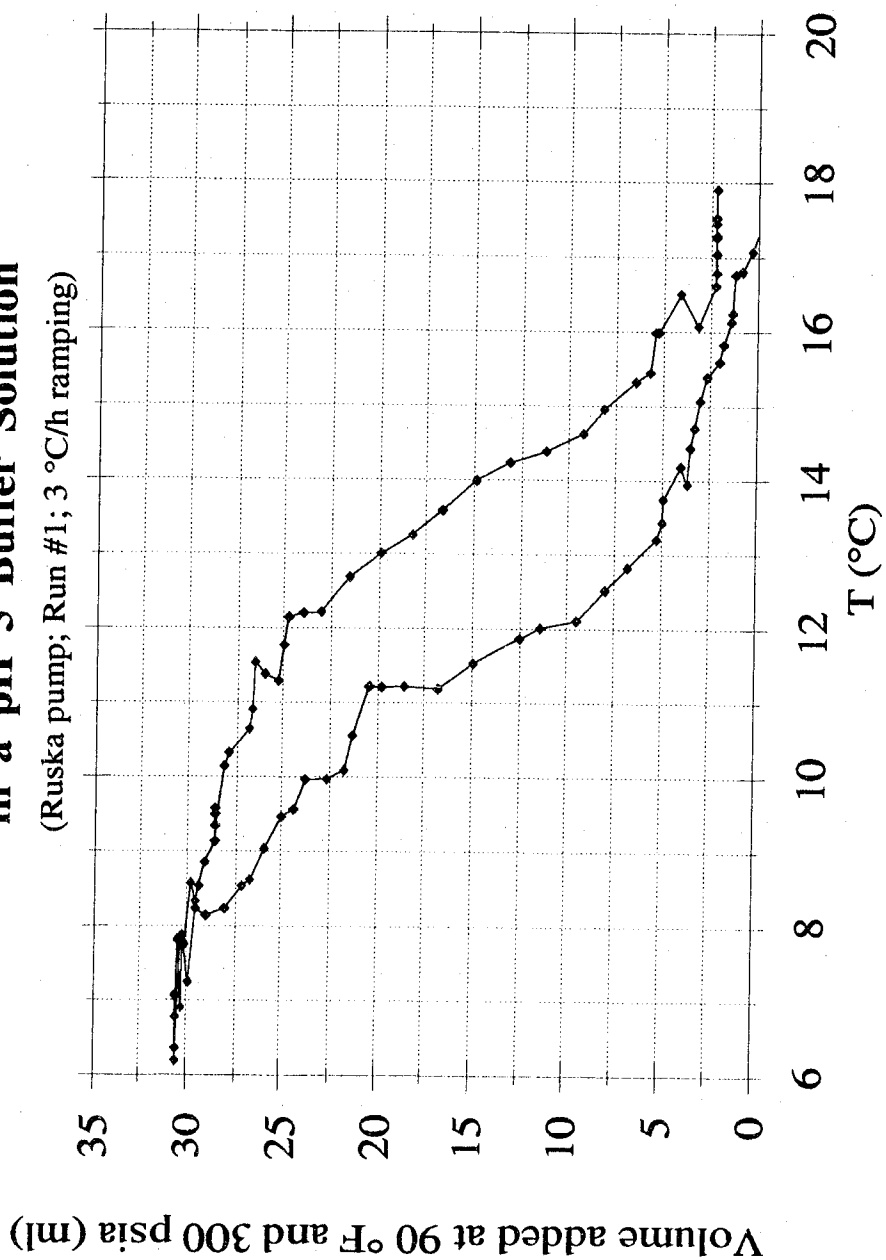
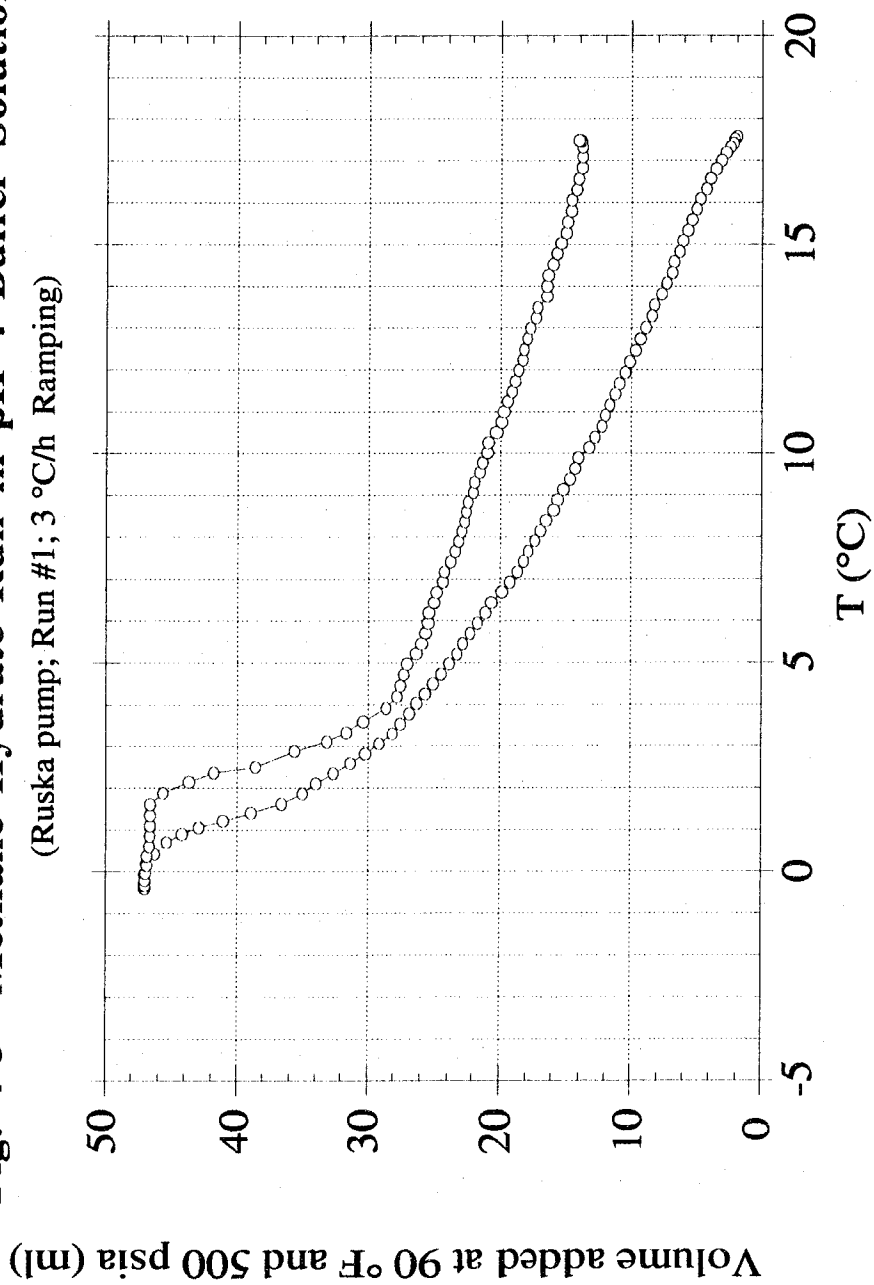
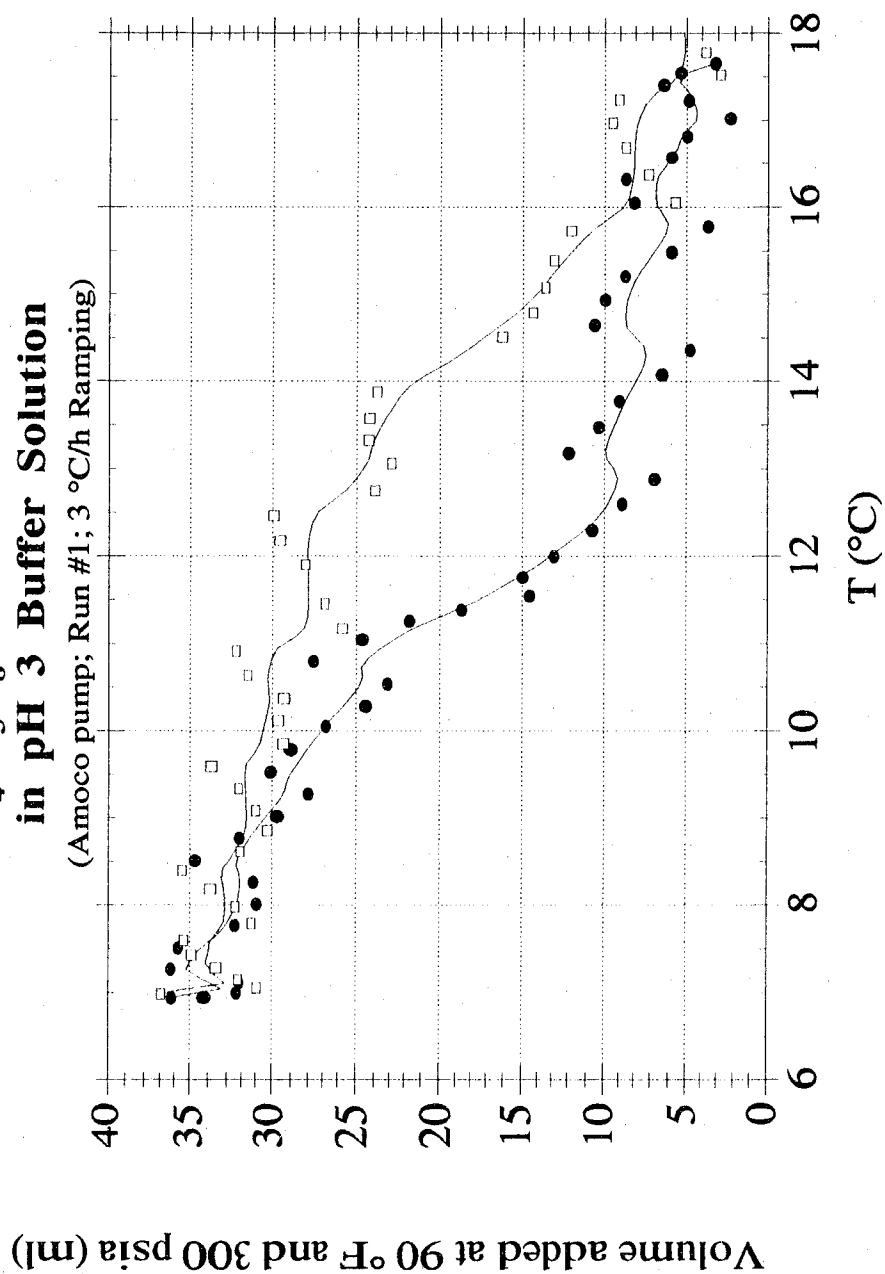


Fig. 4-3 Methane Hydrate Run in pH 4 Buffer Solution
(Ruska pump; Run #1; 3 °C/h Ramping)



**Fig. 4-4 CH₄-C₃H₈ (19.98 mol %) Hydrate Run
in pH 3 Buffer Solution**

(Amoco pump; Run #1; 3 °C/h Ramping)



**Fig. 4-5 CH₄-C₃H₈ (19.98 mol %) Hydrate Run
in a pH 5 Buffer Solution**

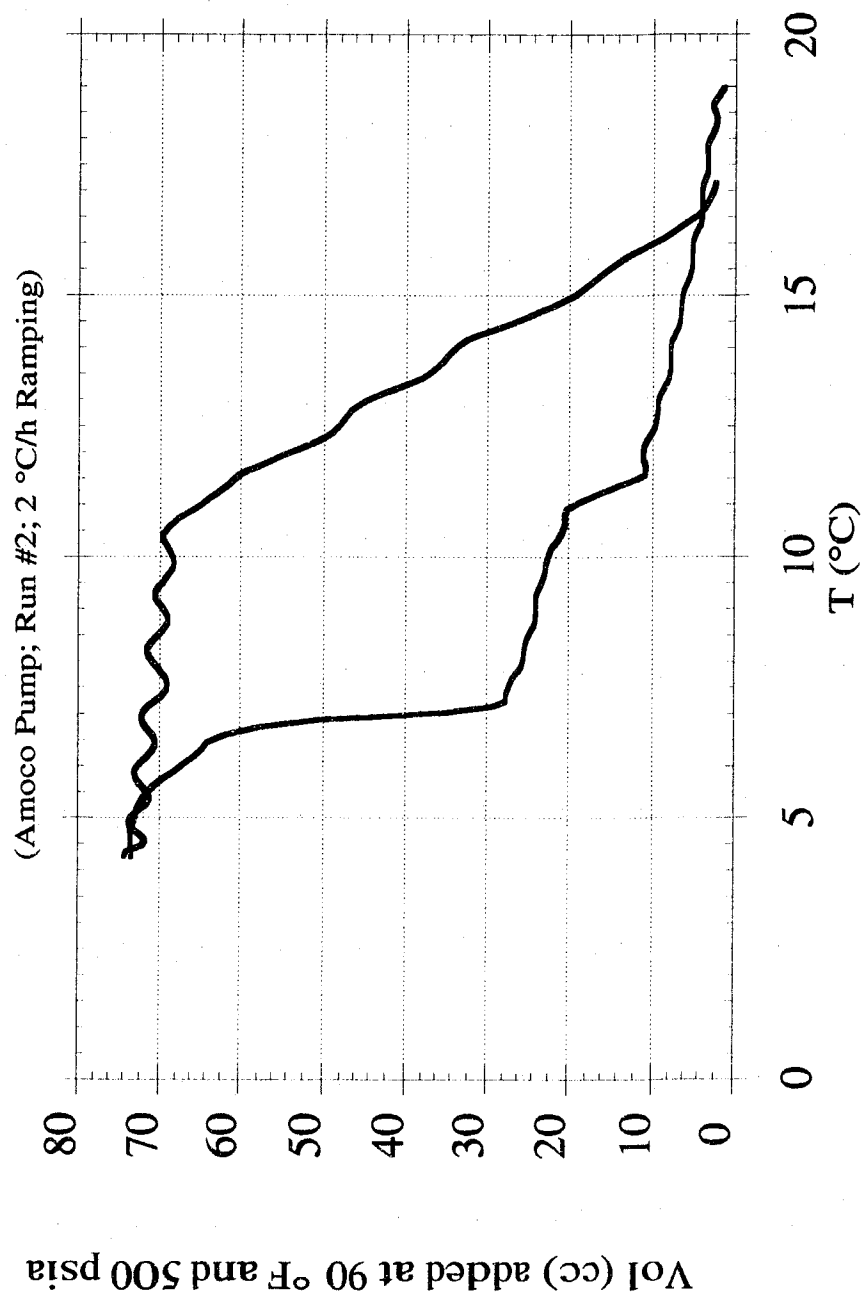


Fig. 4-6 $\text{CH}_4\text{-C}_3\text{H}_8$ (19.98 mol %) Hydrate Run in pH 3
Buffer Solution
(Amoco Pump; Run #2; 3°C/h Ramping)

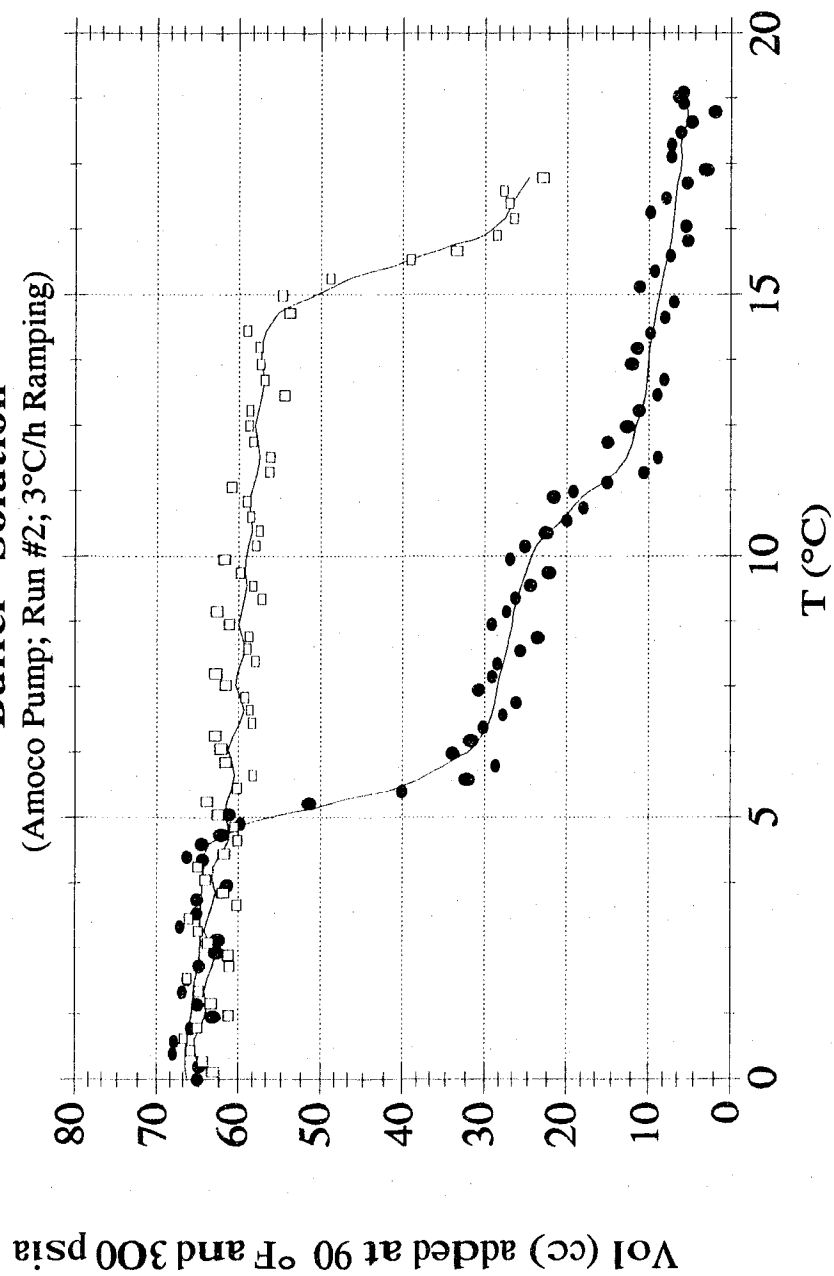


Table 4-3 Catastrophic Temperatures in Various pH Solutions (°C)

GAS	RUN #	pH 7	pH 5	pH 5 (2 nd set)	pH 4	pH 3
CH ₄	1	2.9*	2.3*	3.1*	2.7*	2.8*
	2	3.4	/		3.4	
	3		1.5 [#]		2.8	
	4		2 ^{###}		/	
	5		2		2 [#]	
	6				3 [#]	
CH ₄ -C ₃ H ₈	1	11.7*	12.6*	12.2*	12.9* ^{###}	11.8*
	2	11.7	12.4	11.7	11.5	11.5
	3			11* ^{##}	11.4	
	4				11.5	

* From fresh solution

Ramping at 5°C/h

Ramping at 4°C/h

Ramping at 1.5°C/h

Otherwise, ramping rate is 3°C/h.

Table 4-4 Final Hydrate Decomposition Temperatures in Various pH Solutions (°C)

GAS	RUN #	pH 7	pH 5	pH 5 (2nd set)	pH 4	pH 3
CH₄	1	15.5*	15.5*	16*	14.3* ###	15.8*
	2		15.2	/	15.5	16.5
	3			/	15.7	
	4			16.6*	15	
	5			16.5		
CH₄-C₃H₈	1	3.8*	/	/	4*	3.7*
	2	4.2	/	4*	/	
	3		/		4	
	4		/		3.8 [#]	
	5		3.8		3.3 [#]	

* From fresh solution

Ramping at 5°C/h

Ramping at 4°C/h

Ramping at 1.5°C/h

Otherwise, ramping rate is 3°C/h.

Fig. 4-7 Catastrophic Temperatures of CH₄-Buffer Solutions

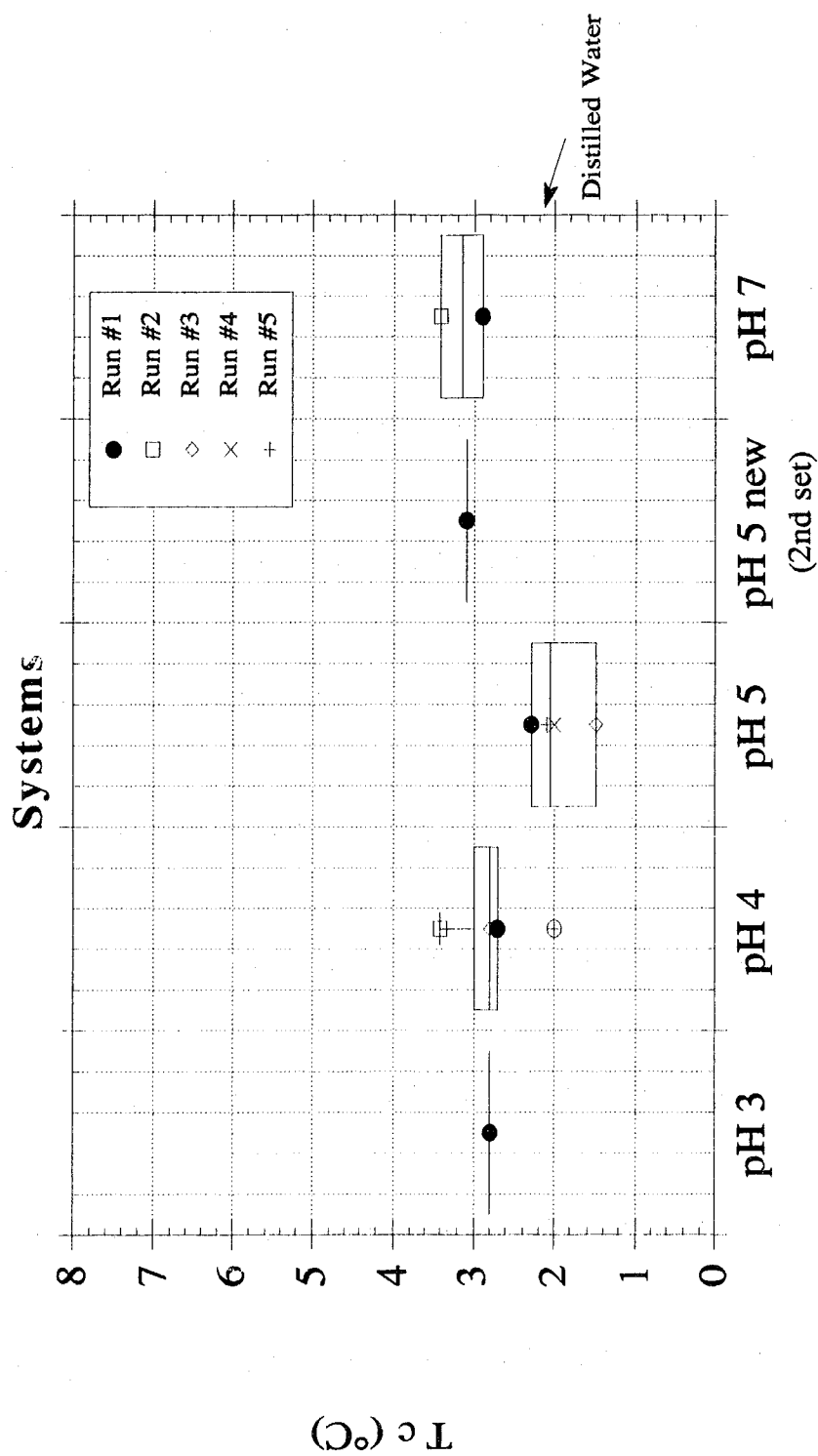


Fig. 4-8 FHDT of CH₄-Buffer Solutions Systems

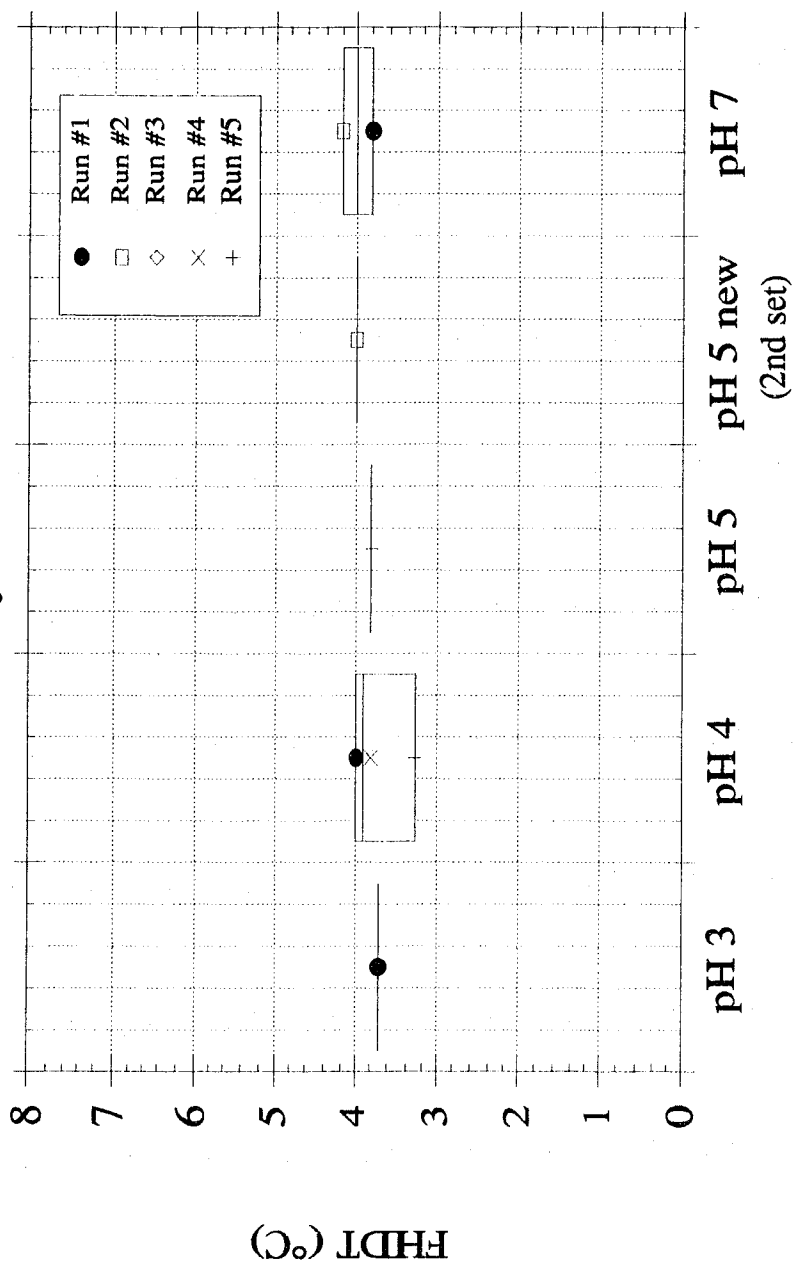


Fig. 4-9 Catastrophic Temperatures of $\text{CH}_4\text{-C}_3\text{H}_8$ -Buffer Solutions Systems

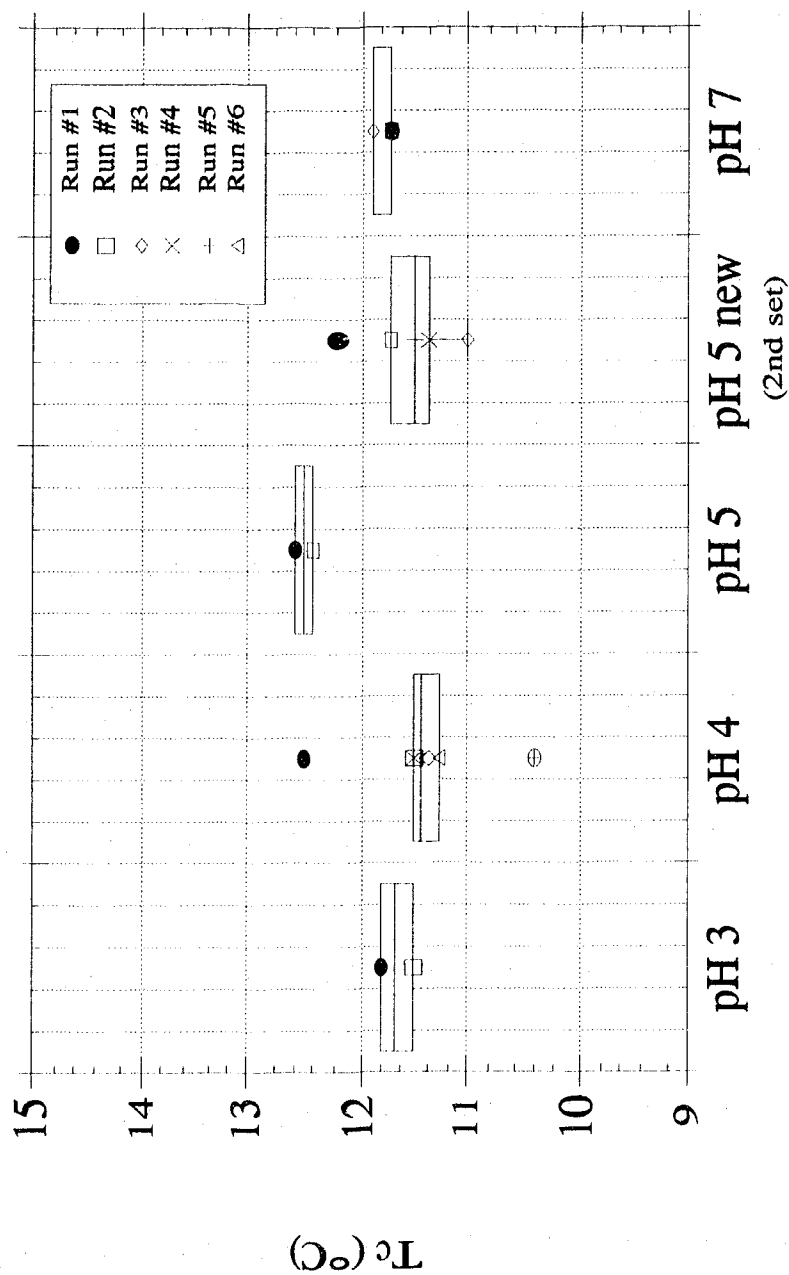
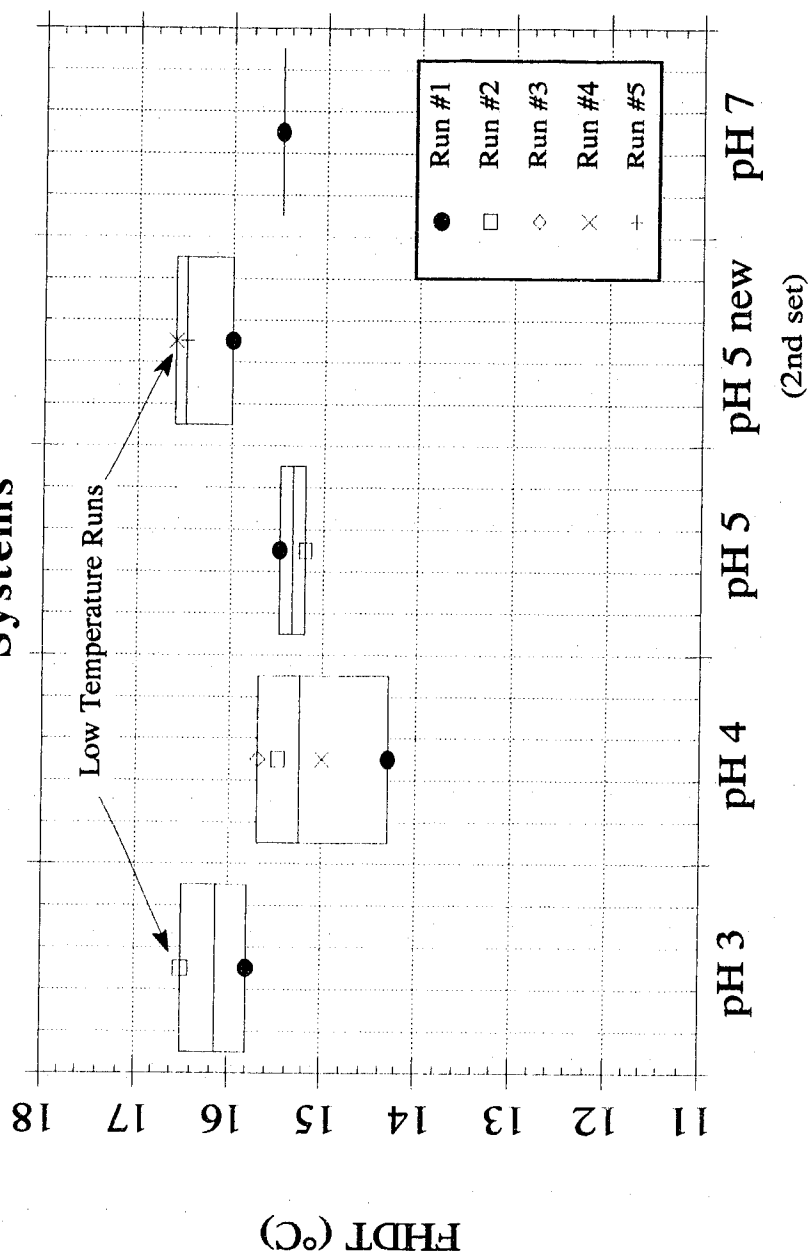


Fig. 4-10 FHDT of $\text{CH}_4\text{-C}_3\text{H}_8$ -Buffer Solutions Systems



4.2. TC AND FHDT AS A FUNCTION OF THE pH OF WATER

4.2.1. Comparisons of Tc and FHDT

The reported Tc and FHDT are carefully obtained by graphical interpolation and direct visual observation. For both gas systems, no conclusive relationship exists between the pH of the aqueous solution used and the catastrophic and final hydrate temperatures other than a minor effect of pH on those results. On the contrary, very consistent catastrophic temperatures are found between the different pH solutions. If runs carried out with fresh liquid solutions are taken into consideration, then we can give an estimate of the mean catastrophic temperature: $T_c = 2.7^\circ\text{C} \pm 0.4^\circ\text{C}$ for CH_4 hydrate and $T_c = 12.3^\circ\text{C} \pm 0.6^\circ\text{C}$ for $\text{CH}_4\text{-C}_3\text{H}_8$ hydrate. These values are, in addition, in good agreement with the catastrophic temperatures of the distilled water runs previously reported [Chapters 2 and 3].

FHDT are again very reproducible, particularly for CH_4 systems. The average FHDT value is 3.84°C with 0.26°C standard deviation. Yet, this value is above the CSMHYD temperature prediction that is very close to our Tc. In $\text{CH}_4\text{-C}_3\text{H}_8$ systems, the average FHDT is 15.6°C .

Experiments have been carried out at several ramping rates ranging from 1.5°C/h to 5°C/h . These reveal once again that hydrate formation and decomposition are independent of the ramping rate, providing that good mixing of the gas and liquid phases was achieved.

Temperatures are in very good agreement when fresh buffer solutions are used in the experiment. T_c and FHDT become more scatter when several cycles are carried out successively. Up to 6 continuous cycles are performed in these experiments. After a first run, the liquid solution is seeded with hydrate precursors. Upon dissociation of hydrates, the guest molecules are freed, but many of the hydrogen bonds remain. These remaining water clusters, or micro-crystals, modify the temperature at which the "assembling" process takes place [Chapter 5]. According to a study by Y.F. Makogon, the "remembered hydrate" structure of the water is almost completely eroded when the water is heated above 30°C (86°F). It should be easier to form hydrates the second time than from fresh solutions initially when substantial cooling is required. Our results do not clearly prove such a statement. Other factors may influence the nucleation process which are not rigorously controlled in this work. When the solution was carefully evacuated before ramping the temperature a second time, the resulting T_c and FHDT are very close to that from fresh solution temperatures, which confirms the existence of micro-crystals in the liquid water just after hydrate decomposition.

Finally, the predicted hydrate stability temperatures with CSMHYD lie slightly below our experimental FHDT. These predictions are based on the statistical thermodynamic theory as well as a correlation of empirical data [Appendix C]. These data are obtained from P-T measurements at a fixed temperature. Therefore it is not surprising if there is a small kinetic lag in the hydrate decomposition

in our experiments in comparison with previous work. Moreover, CSMHYD predicts a 3 phases hydrate temperature corresponding to a 80 mol%-20 mol% $\text{CH}_4\text{-C}_3\text{H}_8$ gas mixture. The formation of a hydrate phase from a gas-liquid system was shown to act as a gas separation process. Thus, the exact gas composition in equilibrium with the liquid at T_c or FHDT is not known and the CSMHYD predictions are not completely reliable. In the near future, gas chromatographic analyses should estimate the gas composition and state to show whether or not CSMHYD is in good agreement with our experimental results.

Nevertheless, the consistency of the measured FHDT of several systems confirm the reliability of the data obtained in our experiments.

4.2.2. Phase Rule

According to the Phase Rule, if the pH of the water is the only variable taken into account, the number of degrees of freedom remains the same between pH 7 and pH 3 for instance. In a $\text{CH}_4\text{-pH 7}$ buffer system, two components are present as well as in a $\text{CH}_4\text{-pH 3}$ buffer system. Therefore hydrate formation conditions should be identical between any pH solution system.

But if the salt added in the solution to change the pH is chemically involve in the hydrate formation process, then it must be taken into account. The number of components is then changed as well as the variance. This is the case when NaCl is added to water.

The salt ionizes in solutions and interacts with the dipoles of the water molecules with a much stronger bond than the van der Waals forces which cause clustering around the apolar solute molecule. A decrease in the solubility of potential hydrate guest molecules in the water takes place, known as a "salting out effect". Thus, the CH_4 -salted water system is a ternary system and bivariant¹² at hydrate formation conditions. The exact salt concentration has to be specified in order to define the state.

The pH-buffer solutions used in these measurements have unknown salts compositions which probably differ between solutions. Thus the measured T_c and FHDT are consistent within a pH system but differ between pH-buffer solutions according to their respective salt compositions. It is not the influence of the pH of the water on the catastrophic temperature that has to be researched but rather the effect of the salt concentration on the hydrate formation and decomposition conditions.

4.3. GAS SOLUBILITY AT T_c

The catastrophic temperature is the point at which a critically sized nucleus is achieved and crystal growth starts. One may expect that a certain amount of gas in solution is required at T_c to end the nucleation process. Given the solubility data of hydrocarbon gases in several aqueous solutions, the moles of gas added to the liquid phase from 17°C to T_c are computed. The exact concentration of gases is not known from our measurements. So only an increase in gas

¹² $F=3+2-3=2$

solubility starting at 17°C can be calculated. However, the solubility at 17°C should be very low in comparison to the lower temperature solubilities. Table 4-5 reports the computed number of mole of gas in the liquid phase at T_c from different aqueous solutions. A unique concentration for each gas is not clearly obtained from our results. The problem lies in the error resulting from a slight inaccuracy in the chosen catastrophic volumes and temperatures.

A change in T_c of $\pm 0.3^\circ\text{C}$ leads to a change in the gas solubility of $\pm 5\%$. But a change in the catastrophic volume V_c of only 0.1 ml at a given catastrophic temperature can lead to an error as high as 25 percent. In addition, the catastrophic concentration in the CH_4 -methanol system is low if T_c is read from the plot but gets as high as 6.2×10^{-3} mol if the volume added corresponds to the first crystal visually observed, since in that case the crystal is observed 1°C lower than T_c . Also, these values represent the added number of moles from 17°C and not the absolute concentration at T_c . Therefore, since not all the results are from fresh liquid solutions, the 17°C solubility may vary between the systems.

Nevertheless, these results show a range of gas solubility at which the catastrophic conditions occur. The solubility data obtained with CO_2 are the most consistent. Even when T_c is lowered by more than 2°C as in methanol systems, the concentration is roughly the same as with pure water. These are the first reported values of low temperature solubilities when the temperature is ramped down to the nucleation point.

Table 4-5 Gas Concentration in the Liquid Phase at T_c for Several Systems

SYSTEM	CONCENTRATION (mol*1000)	±25% (mol*1000)
CH ₄ -H ₂ O	4.5	±1.125
CH ₄ -Methanol	0.86/6.2 at T when first crystal is observed	
CH ₄ -PVP	7.6	±1.9
CH ₄ -pH 7	5.77	±1.44
C ₂ H ₆ -H ₂ O	1.21	±0.3
C ₂ H ₆ -Methanol	4.4	±1.1
C ₂ H ₆ -PVP	0.456	±0.11
C ₂ H ₆ -PVP	0.00	
CO ₂ -H ₂ O	20.6	±5.15
CO ₂ -Methanol	20.09	±5.02
CO ₂ -Methanol	19.98	±5.00
CO ₂ -Methanol	13.35	±3.34
CO ₂ -PVP	17.39	±4.35
CO ₂ -pH 7	18.52	±4.63
CO ₂ -pH 7	9.72	±2.43

4.4. LOW TEMPERATURE CH₄-C₃H₈ RUNS

As previously mentioned, the solubility of a CH₄-C₃H₈ gas mixture was measured at temperatures lower than 5°C in five distinct runs. The resulting plots [Fig. 4-5 and 4-6] exhibit very remarkable features. The first catastrophic increase in gas consumption was followed by a second jump. Yet, the heating part shows only one decomposition process. In addition, the catastrophic volumes and temperatures are very similar as shown in the following table.

Table 4-6 Second Catastrophic Increase in CH₄-C₃H₈ Runs

pH-buffer	Temperature (°C)	Volume (ml)
pH 7	5.3	33
pH 5	6.5	29
pH 5	7	24
pH 5	7.2	26
pH 3	6.7	24
Error	±0.5	±2

The volumetric data imply that the volume is set at zero at 17°C. Since these values come from smoothed data, the error in reading the catastrophic point must be taken into account.

While the first catastrophic conditions take place around 12°C and 10 ml, the second occur around 6.5°C with a 0.74°C standard

deviation. In all three runs, the second step is twice as big as the first one and the added volume increases by 30 ml in less than 1°C. The FHDT are all very close to 16.5°C.

A hydrate phase was observed visually during the first catastrophic increase in volume. Yet, a large amount of liquid water is assumed to be present along with the hydrate phase. Throughout the run the magnetic pump was still recirculating the gas phase, so that a large gas-liquid contact area remained. This, along with the good agreement in the conditions at which the second catastrophic temperature is obtained in several runs, leads us to believe that a second hydrate phase is forming. Pure methane does not form hydrate above 4°C at pressures lower than 700 psia. At 300 psia, methane hydrate forms below -6°C. The maximum quadrupole temperature of propane is 5.4°C when liquid and gas propane coexist with liquid and hydrate phases. Thus, a catastrophic temperature equal to 6.5°C can only occur when a mixture of CH₄ and C₃H₈ forms hydrate.

Statistical thermodynamics predicts that a 98 mol%-2 mol% CH₄-C₃H₈ mixture will form hydrate at 6.4°C at 300 psia. This second step may then be due to a second step in the formation of a structure II hydrate crystal from a different CH₄-C₃H₈ gas mixture. A 80 mol%-20 mol% CH₄-C₃H₈ gas mixture forms a 58 mol%-42 mol% CH₄-C₃H₈ structure II hydrate where 66 % of the small cages and 98.5 % of the large cages are occupied by methane and propane respectively.

The unique decomposition point observed tends to confirm that the whole hydrate phase is formed by the same structure. Again, future gas analyses will throw light on this phenomena.

5. MOLECULAR INSIGHTS ON THE DISSOLUTION OF HYDROCARBON GASES IN LIQUID WATER

The solubility of non-polar gases—such as methane, ethane and propane—in liquid water has been extensively studied and measured at ambient temperatures and pressures. Some authors [Kobayashi 1951, Culberson 1950 and 1951, Wiebe 1940, Schulze 1981] have reported high pressure solubility data at temperatures above 25°C and found that the solubility of hydrocarbons in water remained very low.

Nevertheless, our experimental results gain support from more recent studies conducted by Bishnoi et al. and molecular simulations.

High solubility data combined with the concepts of nucleation of a supercooled liquid and the metastability of liquid water appear to be part of a single phenomena taking place in the liquid water at low temperature. A better understanding of the structure of the liquid water may then result from our experimental measurements.

5.1. PRIMARY NUCLEATION, CRYSTAL GROWTH AND METASTABILITY

Most of the data dealing with the phase equilibria or the kinetics of natural gas hydrates are based on thermodynamic measurements upon hydrate dissociation. On the other hand, accurate kinetics of hydrate formation are scarce due to the difficulty of controlling the system when forming gas hydrate from liquid water.

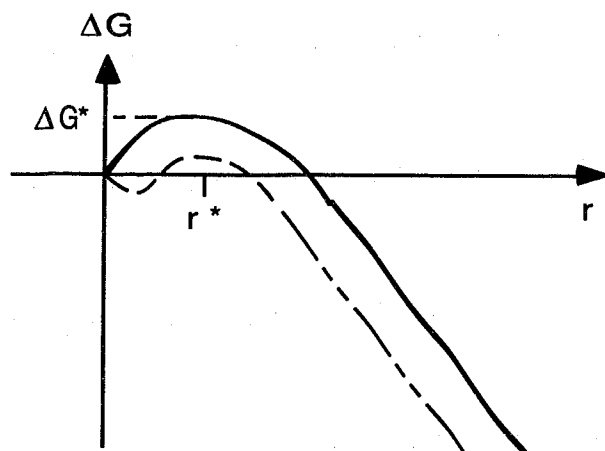
Hydrate formation is a crystallization process similar to that of ice formation from liquid water. When a quantity of water is cooled, freezing does not occur as soon as the thermodynamic freezing point is reached. Instead, water may easily be supercooled to -10°C before anything happens, then suddenly a certain amount of the water freezes. Supercooled water has a free energy higher than the state of minimum energy and thus is metastable. Nucleation is then the initiation of the transformation of an unstable mixture to a more stable phase, but is not bound to occur at a fixed temperature.

Experimentally, the nucleation temperature is always found to be lower than the melting point of ice. An explanation of the "barrier" to nucleation is in terms of the effect of surface energy on the total energy of very small particles.

Consider a system consisting of supercooled liquid and a small, spherical crystal of radius r . By analysis of the Gibbs free energy of the system, ΔG as a function of an increase in the radius of the crystal Δr is in the form shown in Fig. 5-1.

The maximum free energy increase is in growth from zero radius, or a small radius, to the critical radius r_{cr} . The quantity ΔG^* is called the free-energy barrier of nucleation and its existence is the reason why liquids supercool. Due to local temperature and pressure fluctuations in the liquid phase, nucleation occurs as a result of a chance fluctuation in free energy of sufficient magnitude to surmount the free-energy barrier. Once a crystal grows to this size further growth as well as dissolution decreases the free energy of the system and is thus thermodynamically favored.

Fig 5-1 Gibbs Free Energy as a Function of the Crystal Radius



— classic theory

-- proposed form for crystallization from salt solutions [Larson 1986]

Kinetics of hydrate formation are very similar in a way that a primary nucleation process during which the hydrate nuclei grows and disperses in an attempt to achieve critical size is followed by a sudden crystal growth process. Our data reveal this two steps process. During primary nucleation, the solubility of hydrocarbon gases remains low, though higher than predicted by Henry's law. At T_c , a critical size nucleus is achieved and crystal growth starts as evidenced by a tremendous increase in gas solubility.

Before crystal growth, the liquid water contains many transitory groupings of molecules. These assemblies are subcritical nuclei with radii less than the critical radius. They form when free-energy fluctuations occur and quickly disperse, since in this way they lower the free energy of the system. At the hydrate dissociation point

(FHDT), we can assume that the free-energy barrier is very large, thus the rate of nucleation is close to zero. At the absolute temperature, 0 K, the molecules have no kinetic energy so the rate of nucleation is also zero. There must necessarily be a maximum of the rate of nucleation as a function of temperature. Under the light of our experimental data, the range of the catastrophic temperature for a given system is the approximate temperatures at which the rate of nucleation is a maximum.

5.2. PREVIOUS INVESTIGATIONS ON HYDRATE NUCLEATION

Due to the high degree of metastability in the primary nucleation region, there are a real paucity of reproducible data.

Barrer and Ruzika have studied the formation of hydrates from ice using a non-agitated chamber at temperatures below the ice point.

A decade later, Falabella determined both the equilibrium and kinetic properties of hydrates of methane, ethane, ethylene, acetylene, carbon dioxide, argon and krypton at temperatures from 148 K to 240 K and pressures below atmospheric.

More recently, Bishnoi, Englezos et al. have carried out several experiments pertaining to the kinetics of methane and ethane hydrate formation and decomposition. The kinetics were investigated by using a semi-batch, opened stirred tank reactor at isothermal and isobaric conditions. The temperature investigated range from 274.2 K to 284.0 K over a pressure range of 30 to 100 bars. The experiment was designed to measure the volumetric

consumption rate of gas during hydrate formation. Table 5-1 reports the volume of methane gas consumed at 274.3 K and 55 bars in 300 ml of distilled water and after a few hydrate crystals were visually observed.

The experiments were run for approximately 15 min or until about 5 percent of the available water had reacted to form hydrates, at several mixing rates. For comparison, our calculations showed that 6 percent of water was transformed in hydrate after 90 min of crystal growth [Appendix A]. The results indicate that at 600 cycles per minute of the stirrer, the mol fraction of methane in the liquid phase is approximately 4 times higher than the predicted Henry's law solubility.

Table 5-1 Consumption of Methane Gas at 55 bars and 274.3 K from Bishnoi et al. [Vysniauskas 1983]

Mixing Rate (rpm)	Time (min)	X_{CH_4}
300	15	1.85×10^{-3}
400	15	2.64×10^{-3}
500	15	5×10^{-3}
600	7	5×10^{-3}

From our measurements, at 276.5 K and 500 psia (34.47 bars), the methane mol fraction is 4.7×10^{-3} . At 273.65 K, the mol fraction increases to 15.2×10^{-3} . Assuming that a 2.5°C change doesn't affect

the rate of crystal growth, our results show a consumption rate of methane equal to 0.140×10^{-3} mol of CH_4 per mol of H_2O per min. At 34.4 bars and 274.2 K, Bishnoi obtains a 0.089×10^{-3} mol of CH_4 per mol of H_2O per min consumption rate.

In later effort, Englezos and Bishnoi obtained, at 274 K and 506 psia, a 4.49×10^{-3} mol fraction of methane 75 minutes after the turbidity point occurred. A similar comparison can be made concerning ethane. At 275 and 95 psia (6.68 bars), the rate of ethane consumption was 27×10^{-6} mol of C_2H_6 /mol H_2O /min while in our experiments this rate is 68.9×10^{-6} mol of C_2H_6 /mol H_2O /min at 273.15 K and 95 psia. Since the temperature is continuously decreasing during crystal growth, lower consumption rates in constant temperature kinetics are not surprising.

Bishnoi also reports data on methane hydrate decomposition. At 600 rounds per minute, the methane hydrate phase he obtained decomposed with a rate of 0.180×10^{-3} mol of CH_4 /mol of H_2O /min at 274.3 K and 26.9 bars. Around 276 K and 500 psia, our methane hydrate runs show a 0.175×10^{-3} mol of CH_4 /mol of H_2O /min decomposition rate.

In more recent study, Bishnoi et al. [Englezos 1988] studied the methane solubility in liquid water in the primary nucleation region prior to crystal growth. His data indicate a mol fraction of methane equal to 1.3×10^{-3} at the nucleation point of a system maintained at

34.9 bars and 274 K. Approximately 40 percent more than the two phase Lw-V equilibrium value of methane was dissolved in liquid water before the appearance of nuclei. The spinodal point at the same conditions is also computed from the thermodynamic relation:

$$\frac{\partial^2 \Delta G_{\text{mix}}}{\partial x_w^2} = \frac{\partial \ln f_w}{\partial x_w} = 0 \quad (5-1)$$

The value obtained is 32.6×10^{-3} mol fraction of methane and gives information about the appearance of a new methane-rich liquid phase.

As a result, our experimental data are the second reported case of hydrocarbon gas supersaturation before the appearance of a hydrate phase. The rocking of the cell where the balls roll back and forth along with the magnetic pump achieve a very good mixing. Thus the hydrate formation takes place in the bulk of the liquid and not at the liquid-vapor surface as it probably happened in the previous investigations. The higher supersaturation observed in our work is therefore not surprising. During crystal growth, our results are in good qualitative agreement with Bishnoi's data concerning both the amount of methane consumed and the rates of methane consumption and decomposition.

5.3. THE STRUCTURE OF WATER UPON COOLING AND HYDROCARBON DISSOLUTION

5.3.1. The Structure of Liquid Water

Many studies have been performed in order to clarify the structure of water. But a uniform theory capable of interpreting all the properties of water unambiguously and completely has not yet been developed. Some of these properties are unique among liquids, indicating that there is a fundamental difference in structure between water and most other liquids. Such properties are the high melting and boiling points, the unusually high heat capacity, the decrease of the molar volume on melting and the subsequent contraction between 0°C and 4°C. Also, aqueous solutions of non-polar substances, particularly hydrocarbons, show an apparently anomalous thermodynamic behavior as discussed in chapter 5.3.2.

Nevertheless, agreement is complete regarding the fact that the structure of water cannot be considered independently of the crystalline ice structure.

On the basis of investigations of Bernal and Fowler and Samoilov, Pauling stated that water may have a structure based largely upon a complex of 21 water molecules, twenty of which lie at the corners of a pentagonal-dodecahedron, each of them forming three hydrogen-bonds with the adjacent neighbors in the dodecahedron, and the twenty-first forming no hydrogen-bond and occupying the central position in the dodecahedron [Pauling 1957]. In addition, other water molecules may be present, forming or not hydrogen-bonds. The resulting "buckyballs" are then very similar to

hydrate cavities, with the difference that a non-polar guest molecule such as a hydrocarbon molecule replaces a water molecule in the center of the cage.

More recently, this structure has been confirmed with the exception that the H_2O molecule is actually observed to be an H_3O^+ ion [Castleman 1989].

Frank and Evans and later Nemethy and Sheraga provided a model of liquid water where short-lived—"flickering"—hydrogen-bonded clusters coexist with non-hydrogen-bonded water molecules. As the temperature is decreased, the number of clusters will increase and aggregate. The formation and dissolution of the "flickering clusters" is governed by local energy fluctuations.

Based on recent X-ray data and molecular simulations, some authors [Stillinger 1980] described water as a "macroscopically connected random network of hydrogen-bonds, with frequent strained and broken bonds, that is continuously undergoing topological reformation".

However, the results definitely establish that water molecules link through hydrogen-bonding to form a quasi-crystalline—"ice-like"—structure in the liquid state.

5.3.2. Dissolution of Non-polar Gases in Water: A Molecular Mechanism for Gas Hydrate Nucleation ?

Enthalpy and entropy of solution of non-polar solutes in water diverge strikingly from the normal behavior established for regular solutions. The enthalpy of solution is negative and is counter-balanced by a very large negative entropy of solution. Thus, the free energy of solution is small and positive, resulting in a small solubility of non-polar gases in water.

Following the studies on liquid water, several authors [Frank 1945, Claussen 1952, Nemethy 1962, Ben-Naim 1980, Englezos 1988, Sloan 1991] have come to the conclusion that the solutes increase the structure of the solvent and enhances the aggregation of BuckyBalls already taking place in pure supercooled water. The large entropy of solution along with the high critical nucleation temperature measured, T_c , are thus considered as evidence of an "ordering" process taking place when dissolving non-polar molecules in water.

Experimental work as well as molecular simulations [Swaminathan 1978] demonstrate that an "iceberg" of submicroscopic dimensions is formed around the apolar solute molecule as shown in Fig 5-1. Fujihara et al. report a clear increase in hydrocarbon gas solubility as the temperature is lowered due to the iceberg formation of water [Shinoda 1968].

Supercooled water, iceberg formation and hydrate nucleation may then be part of a unique structural change taking place in the liquid water at low temperature. The similarity between the pure

water, the aqueous solutions and the hydrate phase structures appear therefore evident.

Following the work conducted by Sloan et al., a mechanism for Gas Hydrate nucleation can be hypothesized based on solubility and crystal diffraction data.

Our solubility data report a very large negative entropy of solution before hydrate formation. The enthalpies and entropies of solution obtained must not be taken as very precise values since they assume that the Gibbs-free energy of solution is zero. Nevertheless, the order of magnitude of the change of enthalpy and entropy with temperature indicates an increase in the ordering process before the catastrophic crystal growth. The negative entropy of solution originates in the strengthening of hydrogen-bonds in the imperfect clathrate-like cage formed around the non-polar solute; it is also related to the fact that H_2O molecules have reduced orientational preferences and rearrange around the hydrocarbon guest by pointing one of the four tetrahedral directions outwards which permits bonding to other water molecules.

A possible scenario of gas hydrate formation from liquid water may then be hypothesized.

As temperature is lowered, the ordering of the liquid water statistically increases through the hydrogen-bonding of the water molecules. The resulting "buckyballs" are stabilized by the presence of non-polar guest molecules and hence the solubility increases. For small hydrocarbon solute molecules, "buckyballs" form with a 5^{12} structure which is most favored because it maximizes the number of

bonds to molecules relative to similar cavities [Plummer 1987]. When buckyballs are stabilized with bigger hydrocarbon molecules such as propane molecules, the hydrogen-bonds are distorted further and a bigger cavity, such as a Tetrakaidecahedron or a Hexakaidecahedron, forms around the solute molecule.

In addition, the ordering decreases the entropy which is thermodynamically unfavorable. Buckyballs share faces and edges, and aggregate to minimize negative entropy through "hydrophobic bonding" [Ben-Naim 1980] and form subcritical crystals. At one point, which we term T_c , the density of subcritical crystals is very high due to a high gas solubility. A local density fluctuation provokes the formation of a critically sized nucleus. The measured enthalpies and entropies of solution are very high at temperatures slightly higher than T_c . Microscopically, the ordering of the liquid phase may not be perfectly uniform. A slight increase in the entropy leads to a large and positive Gibbs-free energy of sufficient magnitude to surmount the free-energy barrier of nucleation. Nucleation and rapid crystal growth then occur.

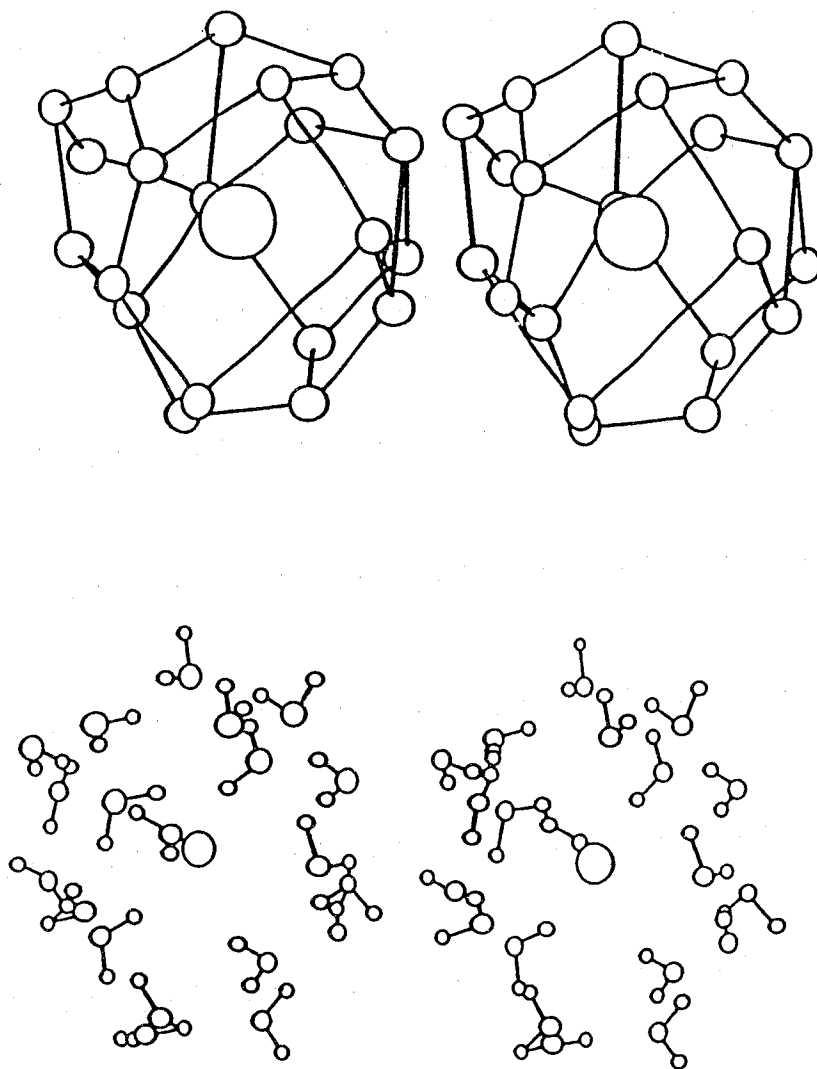


Fig. 5-1 Water Cluster Formation around a Dissolved Apolar Molecule (Large Circles)
(source: Swaminathan et al., 1978)

CONCLUSIONS AND FUTURE WORK

The data reported in this work are the first high pressure hydrocarbon gas solubility data in liquid water obtained by temperature ramping in the primary hydrate nucleation region as well as in the three phase Lw-V-H region where crystal growth occurs.

A striking divergence from Henry's law solubility data is found at temperatures below 20°C. At low temperatures and high pressures, the system exhibit a high level of supersaturation before hydrate formation, and high gas consumption rates upon crystal growth. The results agree qualitatively with the constant temperature and pressure kinetic experiments performed by Bishnoi et al.

Hydrocarbon solubilities in the liquid phase at the catastrophic temperature of hydrate formation, T_c , have been obtained for several hydrocarbon-aqueous solution systems. Even though the gas solubility at this temperature seems independent of the aqueous solution used, more work needs to be carried out with several solutions.

A 10 weight percent methanol solution inhibits hydrate formation by lowering the catastrophic temperature by $2.8^\circ\text{C} \pm 0.8^\circ\text{C}$. On the other hand, a small inhibition by a 0.5 weight percent PVP aqueous solution is measured.

The pH of the water is not a sufficient variable in the hydrate formation and decomposition process. The concentrations of the

electrolytes present in the solution need to be specified prior to the investigation of the pH-induced change of the catastrophic conditions.

Cooling of a $\text{CH}_4\text{-C}_3\text{H}_8$ aqueous solution system, at 300 psia, is of particular interest since our results show a two-step increase in gas solubility upon cooling the system. The first one corresponds to the formation of a first hydrate phase from liquid water around 12°C while the second one takes place around 6.5°C .

Finally, a mechanism of hydrate nucleation is hypothesized with the help of the enthalpies and entropies of solution derived from the experimental data and the current knowledge of the structure of liquid water. This mechanism suggests that hydrate formation is another facet of the aggregation of hydrogen-bonded structures taking place in pure supercooled water.

Future gas chromatographic analyses of the gas phase above the hydrate phase and calorimetric measurements upon ramping the temperature should provide an even better understanding of the hydrate formation and decomposition process.

APPENDIX A: SAMPLE CALCULATIONS OF MASS BALANCES, HYDRATE DENSITIES AND EXPERIMENTAL ACCURACY

Calculation of the number of moles of propane added to the liquid phase when the cell temperature is cooled down to 15.004 °C.

The propane gas is at 90°F and 60 psia inside the pump.

Density of pure propane at 90°F and 60 psia=0.17409 mol/l.

Volume of gas added assuming zero volume at 16.905°C=6.12 ml

So the pump has added 0.0010654 mol to the system.

From Kobayashi [1951], there is $0.00025 \times N_{H_2O}$ mol of gas in the liquid phase at 60°F and 100 psia. The water density at 22°C and 1 atm is 55.384 mol/l. So 23 ± 0.1 ml of water at ambient pressure and temperature correspond to 1.274 ± 0.0055 moles of water. This is the total amount of water present in the cell at any time. So there is 0.00032 mol of propane in the liquid phase initially.

The propane density at 16.905°C is 0.18570 mol/l from DDMIX and reference tables [Goodwin 1977].

Estimation of the total system volume:

- reservoir bottle=450 ml
- magnetic pump=9.63 ml
- cell=91.5 ml
- tubing=3 ml

So the total system volume inside the air bath is 554.13 ml.

The maximum change in the volume of water in the cell with temperature is computed: $\Delta V_W = 0.039$ ml. This change corresponds to the cooling of 1.274 mol of water from 20°C to 1.5°C. ΔV_W is lower than 0.1 ml resulting from experimental inaccuracy in the volume measurements. Therefore, the water volume is assumed constant: $\Delta V_W = 23$ ml. The vapor system volume is then 531.2 ml.

Thus, the number of moles of propane gas initially present in the vapor phase is 0.09865 mol. At 15.004°C, the propane density is 0.18738 mol/l. The number of moles of propane gas in the vapor phase is then 0.09954 mol.

Finally the propane solubility is estimated from Eq. 2-16:

$$(n_{C_3H_8}^L)_{15^\circ C} = 0.00107 + 0.09865 + 0.00032 - 0.09954 = 0.0005 \text{ mol}$$

After Hydrate Formation:

The only difference is the change in the volume of the condensed phase after hydrate formation.

G = moles of gas in the condensed phase after hydrate formation and above ice point

W = total (and initial) moles of water in the system

$$S = \text{solubility in the liquid phase} = n_G^L / n_W^L \quad (A-1)$$

$$N = \text{theoretical hydration number} = n_W^H / n_G^H \quad (A-2)$$

$$G = n_G^H + n_G^L \quad (A-3)$$

$$w = n_W^H + n_W^L \quad (A-4)$$

From Eq. (A-1) to (A-4):

$$n_W^L = (N.G - W) / (N.S - 1) \quad (A-5)$$

$$\text{and } n_W^H = W - n_W^L \quad (A-6)$$

Example with propane.

The extrapolated solubility at 1.5°C from our data is:

$$S = 1.3e-4 / 1.274 = 1.02e-4$$

The cavity occupancy of a propane hydrate at 60 psia is [from CSMHYD]: 0.9993

So $N = 136 / (0.9993 \times 8) = 17.01$ mol of water/mol of propane in the hydrate phase

Take $G = 4.8e-3$ mol at 1.5°C, then:

$$n_W^L = 1.1944 \text{ moles of free water from Eq. (A-5).}$$

That is: only 6.2 mol% of the initial liquid water is transformed in hydrate. The volume of the (hydrate+liquid) phase is then:

$$(1.1944 / 0.0555) + (1.274 - 1.194) / 0.0454 = 23.28 \text{ ml.}$$

0.0555 mol/ml is the water molar density and 0.0454 mol/ml the propane hydrate molar density as calculated in the next section.

And the total gas phase volume = $554.13 - 23.28 = 530.85$ ml.

Nevertheless, the calculations are made with a constant vapor system equal to 531.2 ml since the resulting error is lower than 0.2%.

Propane Hydrate Density:

Propane forms a structure II hydrate. The mass of water in a unit cell is then:

$$\begin{aligned} m_W^H &= (136 \text{ water molecules}) (18.016 \text{ g/mol}) / (6.022e23 \text{ molec/mol}) \\ &= 406.87e-23 \text{ g} \end{aligned}$$

$$\text{Volume of a unit cell} = (17.4 \text{ \AA})^3 = 526.80e-23 \text{ ml}$$

The hydrate cavity occupation number is 0.9993 at 60 psia [from CSMHYD]

So the propane mass in the hydrate is:

$$m_{C_3H_8}^H = (0.9993)(8 \text{ large cavities})(44.095/6.022e23) \\ = 58.538e-23 \text{ g}$$

The propane hydrate density is then:

$$\rho_{C_3H_8}^H = (58.538 + 406.870)/526.80 = 0.8835 \text{ g/ml}$$

$$\text{Or: } \rho_{C_3H_8}^H = (1.3275 + 22.584)/526.90 = 0.0454 \text{ mol/ml}$$

So propane hydrate is a little less dense than liquid water.

APPENDIX B: THERMODYNAMIC RELATIONS FOR ENTHALPIES AND ENTROPIES OF SOLUTION

Gibbs-Helmoltz equation:

$$\left(\frac{\partial \mu_i / RT}{\partial T} \right)_{P,x} = - \frac{\bar{h}_i}{RT^2} \quad (\text{B-1})$$

Also:

$$d\mu_i = RT d \ln \bar{f}_i \quad \text{at } T \quad (\text{B-2})$$

$$d(\mu_i - \mu_i^{ig}) = RT d \ln(\bar{f}_i / \bar{f}_i^{ig}) \quad (\text{B-3})$$

where T is no longer fixed.

$$\left(\frac{\partial (\mu_i - \mu_i^{ig}) / RT}{\partial T} \right)_{P,x} = \left(\frac{\partial \ln \bar{f}_i}{\partial T} \right)_{P,x} - \left(\frac{\partial \ln \bar{f}_i^{ig}}{\partial T} \right)_{P,x} \quad (\text{B-4})$$

\bar{f}_i^{ig} is only a function of P and x . So, from Eq. (B-1) and (B-4):

$$\left(\frac{\partial \ln \bar{f}_i}{\partial T} \right)_{P,x} = \frac{-\bar{h}_i + h_i^{ig}}{RT^2} \quad (\text{B-5})$$

From Henry's law: $\bar{f}_i = x_i H_i$ which is equivalent to assuming infinite dilution. Since x_i is fixed in the derivative:

$$\left(\frac{\partial \ln H_i}{\partial T} \right)_{P,x} = \frac{-\bar{h}_i^\infty + h_i^{ig}}{RT^2} \quad (\text{B-6})$$

With $P = P_{\text{solvent}}^{\text{sat}}$ since x_i tends to zero.

For a vapor and a liquid in equilibrium: $\bar{f}_i^V = \bar{f}_i^L = x_i H_i$

$$\text{So: } \frac{d \ln x_i}{dT} = \left(\frac{\partial \ln f_i}{\partial T} \right)_{P, x} - \left(\frac{\partial \ln H_i}{\partial T} \right)_{P, x} = \frac{-\bar{h}_i^V + \bar{h}_i^{\infty L}}{RT^2}$$

Or:

$$R \left(\frac{d \ln x_i}{d(1/T)} \right) = \bar{h}_i^V - \bar{h}_i^{\infty L} \quad (\text{B-7})$$

Which is the heat associated with the dissolution of hydrocarbon
i in water. For a nearly pure vapor: $\bar{h}_i^V = \bar{h}_i^{\circ L}$

Given that ΔG is almost zero: $\Delta S = \Delta H/T$. And:

$$R \left(\frac{d \ln x_i}{d \ln T} \right) = -\bar{s}_i^V + \bar{s}_i^{\infty L} \quad (\text{B-8})$$

APPENDIX C: IMPACT OF NEW SOLUBILITY DATA ON STATISTICAL THERMODYNAMICS PREDICTIONS

The CSMHYD predictions are based on the following equations derived from statistical thermodynamics considerations.

The fractional filling of cavity i by a type k molecule is:

$$Y_{k_i} = \frac{C_{k_i} P_k}{1 + \sum_J C_{J_i} P_J} \quad (C-1)$$

This equation is similar to a Langmuir isotherm. The constants C_{k_i} are function of the temperature only and are a direct function of the particle partition function within the cavity q_{k_i} . As derived by van der Waals and Platteeuw, the Langmuir constants can be expressed in terms of the particle potential within the cavity:

$$C_{k_i} = \frac{4\pi}{kT} \int_0^R \exp(-w(r)/kT) r^2 dr \quad (C-2)$$

$w(r)$ is an average of the pair potentials between the solute and each water molecules.

The chemical potential of the water in the hydrate in terms of that for the empty hydrate is:

$$\frac{\mu_W^H}{kT} = \frac{\mu_W^{MT}}{kT} + kT \sum_i v_i \ln(1 - \sum_k Y_{k_i}) \quad (C-3)$$

At equilibrium, $\mu_W^H = \mu_W^L$. The change in the chemical potential difference with temperature and pressure may then be obtained from [Holder 1980]:

$$\frac{\Delta\mu_w}{RT} = \frac{\Delta\mu_w^o}{RT_o} - \int_{T_o}^T \frac{\Delta h_w}{RT^2} dT + \int_0^P \frac{\Delta v_w}{RT} dP - \ln(\gamma_w x_w) \quad (C-4)$$

The particle potential within the cavity can be derived from Kihara potential parameters. However, these parameters need to be fitted to experimental hydrate formation data for each component. The Langmuir constants may then be evaluated at a given temperature. By numerical calculation, computer programs such as CSMHYD provide the fractional cavity filling, the chemical potential difference and eventually the temperature and pressure of hydrate stability. The water activity coefficient γ_w is taken as unity for pure water hydrate prediction. To take into account the inhibition effect provided by solutes in the water-rich phase such as methanol, this activity coefficient is modified.

Nevertheless, Eq. (C-4) requires the solubility of the component in water as well as the activity coefficient of the water in the liquid phase. One may then evaluate the impact of our new solubility measurements on the hydrate prediction scheme.

Following the work of Marshall, the chemical potential difference for the methane gas-water-methane hydrate system can be written as:

$$\Delta\mu = -\Delta H + C_2 RT + 0.039P - RT \ln x_w \quad (C-5)$$

where ΔH is the heat required to transform one mol of liquid water into one mol of the empty hydrate lattice, C_2 is a constant that

appears in the integration of the chemical potential with temperature.

From the solid solution theory, the chemical potential is also:

$$\Delta\mu = RT[v_1 \ln(1 + C_{M1}P_M) + v_2 \ln(1 + C_{M2}P_M)] \quad (C-6)$$

In structure I, $v_1 = 1/23$ and $v_2 = 3/23$. Marshall determined the two Langmuir constants for methane in the range 260 K-300 K. Once x_w is chosen, the only unknowns are then ΔH and C_2 for a given set of hydrate equilibrium pressure and temperature.

Using two hydrate equilibrium points, (297.6 K, 408.2 atm) and (288.6 K, 136.1 atm), and the corresponding methane solubility values reported by Culberson and McKetta (3.26×10^{-3} and 1.55×10^{-3}), Marshall obtained $\Delta H = 2406.3$ cal/mol and $C_2 = 4.697$.

Calculations are performed using the same first equilibrium point and methane solubility value as previously (297.6 K, 408.2 atm, $x_{CH_4} = 3.257 \times 10^{-3}$) but with a second equilibrium point (278.2 K, 500 psia = 34.023 atm) where the solubility value is $x_{CH_4} = 4 \times 10^{-3}$ as measured in this work. The results give $\Delta H = 2526$ cal/mol and $C_2 = 4.900$.

The values obtained differ from the initial calculations. However, it is difficult to evaluate the effect of the new solubility measurements on the hydrate prediction accuracy until the hydrate equilibrium pressure and temperature are recalculated and compared to the initial predictions and to the experimental values.

BIBLIOGRAPHY

- Barrer, R. M., Edge, A. V. Jr., *Proc. Roy. Soc. London.* **A300**, 1 (1967)
- Barrer, R. M., Ruzicka, D. J. *Trans. Far. Soc.* **58**, 2239,2253,2262 (1962)
- Ben-Naim, A. *Hydrophobic Interaction*. Plenum Press (1980)
- Berecz, E., Balla-Achs, M. *Gas Hydrates. Studies in Inorganic Chemistry.* **4** (1983)
- Castleman, A. W. Jr., Yang, X. *J. Am. Chem. Soc.* **111**, 6845 (1989)
- Claussen, W. F., Polgase, M. F. Solubilities and Structures in Aqueous Aliphatic Hydrocarbon Solutions. *J. Am. Chem.* **74**, 4817 (1952)
- Coulson, C. A. *The Hydrogen Bond. Hydrogen Bonding*. Hadzi, D. Pergamon Press (1959)
- Cox, J. L., *Natural Gas Hydrates: Properties, Occurrence and Recovery*. (1983)
- Culberson, O. L., McKetta, J. Jr. The Solubility of Ethane in Water at Pressures to 10,000 psia. *Petrol. Trans, AIME.* **189**, 319 (1950)
- Culberson, O. L., McKetta, J. Jr. The Solubility of Methane in Water at Pressures to 10,000 psia. *Petrol. Trans, AIME.* **192**, 223 (1951)
- Culberson, O. L., McKetta, J. Jr. Vapor-Liquid Equilibrium Constants in the Methane-Water and Ethane-Water Systems. *Petrol. Trans, AIME.* **192**, 297 (1951)
- Davidson, D. W. *Clathrate Hydrates.. Water: A Comprehensive Treatise.* **2**, Chapter 3 (1973)
- Davy, H. *Phil. Trans. Roy. Soc. London.* **101**, 1 (1811)
- de Forcrand, R. *Compt. Rend.* **95**, 129 (1882)
- Deaton, W. M., Frost, E. M. Jr. *Gas Hydrates and their Relation to the Operation of Natural Gas Pipelines*. Monograph 8. U. S. Bureau of Mines (1946)
- Dholabhai, P. D., Kalogerakis, N., Bishnoi, P. R. *Can. J. Chem. Eng.* **71**, 68 (1993)
- Dodds, W. S., Stutzman L. F., Sollami, B. J. Carbon Dioxide Solubility in Water. *Ind. Eng. Chem.* **1** 92 (1956)
- Dyadin, Y. A., Boudaryuk, I. V., Shurko, F. V. Clathrate Hydrates at High Pressure. *Inclusion Compounds*. Oxford U. Press., Atwood, J. L., Davies J. E. D., MacNichol D. D., **5**, 213 (1991)
- Englezos, P., Bishnoi, P. R. Gibbs Free Energy Analysis for the Supersaturation Limits of Methane in Liquid Water and the Hydrate-Gas-Liquid Water Phase Behavior. *Fluid Phase Equilibria.* **42**, 129 (1988)

- Englezos, P., Kalogerakis, N., Dholabhai, P. D., Bishnoi, P. R. Kinetics of Formation of Methane and Ethane Gas Hydrates. *Chem. Eng. Sci.* **42**, 2647 (1987)
- Englezos, P., Kalogerakis, N., Dholabhai, P. D., Bishnoi, P. R. Kinetics of Gas Hydrate Formation from Mixtures of Methane and Ethane. *Chem. Eng. Sci.* **42**, 2659 (1987)
- Falabella, B. J. *A Study of Natural Gas Hydrates*. Dissertation. U. Mass. (1975)
- Fleyfel, F., Song, K. Y., Kook, A., Martin, R., Kobayashi, R. Interpretation of ^{13}C NMR of Methane/Propane Hydrates in the Metastable/Nonequilibrium Region. *J. Phys. Chem.* **97**, 6722 (1993)
- Frank, H. S., Evans, M. W. *J. Chem. Phys.* **13**, 507 (1945)
- Franks, F., Editor, *Water: A Comprehensive Treatise*. Plenum, **1-7** (1973)
- Galloway, T. J. *The Comparison of Experimental and Theoretical Hydrate Numbers*. Master Dissertation. Rice U. (1968)
- Glew, D. N. Aqueous Solubility and the Gas-Hydrates. The Methane-Water System. *J. Phys. Chem.* **66**, 605 (1962)
- Goodwin, R. D. *Provisional Thermodynamic Functions of Propane from 85 to 300 K at Pressures up to 700 bar*. National Bureau of Standards (1977)
- Goodwin, R. D. *The Thermophysical Properties of Methane from 90 to 500 K at Pressures to 700 bar*. National Bureau of Standards. Technical Note 653 (1974)
- Gunton, J. D., Droz, M. *Introduction to the Theory of Metastable and Unstable States*. Lecture Notes in Physics, Springer-Verlag, **183** (1983)
- Haar, L., Gallagher, J. S., Kell, G. S. *Steam Tables*. National Bureau of Standards (1984)
- Hammerschmidt, E. G. Formation of Gas Hydrates in Natural Gas Transmission Lines. *Ind. Eng. Chem.* **26**, 851 (1934)
- Handa, Y. P. *J. Phys. Chem.* **90**, 5497 (1988)
- Handbook of Gas Hydrate Properties and Occurrence. Office of Scientific and Technical Inf. U.S. Dept of Energy (1983)
- Hildebrand, *The Solubility of Non-Electrolytes*. (1964)
- Himmelblau, D. M. Partial Molal Heats and Entropies of Solution for Gases Dissolved in Water from the Freezing to Near the Critical Point. *J. Phys. Chem.* **63**, 1803 (1959)
- Holder, G. D., Grigoriou, G. C. *J. Chem. Thermo.* **12**, 1093 (1980)
- Holder, G. D., *Multi-Phase Equilibria in Methane-Ethane-Propane-Water Hydrate Forming Systems*. Dissertation. U. Mich. (1976)

- Holder, G. D., Zetts, S. P., Pradhan, N. Phase Behavior in Systems Containing Clathrate Hydrates. *Reviews in Chemical Engineering*. 5, 1 (1988)
- Holland, P. M., Castleman, A. W. Jr. A Model for the Formation and Stabilization of Charged Water Clathrates. *J. Chem. Phys.* 72, 5984 (1980)
- IUPAC. *Carbon Dioxide*. International Thermodynamic Tables of the Fluid State. Pergamon Press. 3 (1973)
- Jeffrey, G. A. *Inclusion Compounds*. Oxford U. Press., Atwood, J. L., Davies J. E. D., MacNichol D. D., 1, 135 (1984)
- Katz, D. L. *Trans. AIME*. 160, 140 (1945)
- Katz, D. L., Cornell, D., Kobayashi, R., Poettmann, F. H., Vary, J. A., Elenbaas, J. R., Weinaug, C. F. *Handbook of Natural Gas Engineering*. McGraw-Hill (1959)
- Kim, H. C., Bishnoi, P. R., Heidemann, R. A., Rizvi, S. S. H. Kinetics of Methane Hydrate Decomposition. *Chem. Eng. Sci.* 42, 1645 (1987)
- Knight, C. A. *The Freezing of Supercooled Liquids*. Van Nostrand (1967)
- Kobayashi, R. *Vapor-Liquid Equilibria in Binary Hydrocarbon-Water Systems*. Dissertation. U. Mich. (1951)
- Kobayashi, R., Katz, D. L. Methane Hydrate at High Pressure. *Petrol. Trans. AIME*. 186, 66 (1949)
- Kobayashi, R., Song, K. Y., Sloan, E. D. Jr. Phase Behavior of Water/Hydrocarbon Systems. *Petroleum Engineering Handbook*. Chapter 25 (1987)
- Larson, M. A., Garside, J. J. *Crystal Growth*. 76, 88 (1986)
- Lederhos, J. P., Mehta A. J., Nyberg G. B., Warn, K. J., Sloan, E. D. Jr. Structure H Hydrate Equilibria of Methane and Adamantane. *AIChE J.* 38, 1045 (1992)
- Lekvam, K., Ruoff, P. A Reaction Kinetic Mechanism for Methane Hydrate Formation in Liquid Water. *J. Am. Chem. Soc.* 115, 8565 (1993)
- Lievois, J. S. *Development of an Automated, High Pressure Heat Flux Calorimeter and its Application to Measure the Heat of Dissociation of Methane Hydrate*. Dissertation, Rice U. (1987)
- Makogon, Y. F. *Hydrates of Natural Gas*. Moscow, Nedra, Izdatelstro (1974). Translated from the Russian by W. J. Cieslesicz. Pennwell Books (1981)
- Makogon, Y. F. *Perspectives for the oil and gas industry in the World*. Gazovaya Promyshlennost (Gas Industry). 8 (1984)
- Marshall, D. R. *Gas Hydrates at High Pressures*. Dissertation. Rice U. (1962)

- Mehta, A. P., Sloan, E. D. Jr. Structure H Hydrates: the State-of-the-Art. *Presented at the 75th Annual GPA Convention.* (1996)
- Nemethy, G., Sheraga, H. A. A Model for the Thermodynamic Properties of Liquid Water. *J. Chem. Phys.* **36**, 3382 (1962)
- Nemethy, G., Sheraga, H. A. Model for the Thermodynamic Properties of Aqueous Solutions of Hydrocarbons. *J. Chem. Phys.* **36**, 3401 (1962)
- Neuman, R. C. Jr., Kauzmann, W., Zipp, A. Pressure Dependence of Weak Acid Ionization in Aqueous Buffers. *J. Phys. Chem.* **77**, 2687 (1973)
- Pauling, L. *The Structure of Water.* Hydrogen Bonding. Hadzi, D. Pergamon Press (1959)
- Plummer, P. L. M., Chen, T. S. *J. Chem. Phys.* **86**, 7149 (1987)
- Rettich, T. R., Handa, Y. P., Battino, R., Wilhelm, E. Solubility of Gases in Liquids:13. High-Precision Determination of Henry's Constants for Methane and Ethane in Liquid Water at 275 to 328 K. *J. Phys. Chem.* **85**, 3230 (1981)
- Ripmeester, J. A., Tse, J. S., Ratcliffe, C. I., Powell, B. M. A New Clathrate Hydrate Structure. *Nature.* **325**, 135 (1987)
- Rueff, R. M., Sloan E. D., Yesavage, V. F. *AIChE J.* **34**, 1468 (1988)
- Saito, S., Marshall, D. R., Kobayashi, R. Hydrates at High Pressure: Part II. Application of Statistical Mechanics to the Study of the Hydrates of Methane, Argon and Nitrogen. *AIChE J.* **10**, 734 (1964)
- Schulze, G., Prausnitz, J. M. Solubilities of Gases in Water at High Temperatures. *Ind. Eng. Chem. Fundam.* **20**, 175 (1981)
- Shinoda, K., Fujihira, M. The Analysis of the Solubility of Hydrocarbons in Water. *Bull. Chem. Soc. Japan.* **41**, 2612 (1968)
- Sloan, E. D. Jr. *Clathrate Hydrates of Natural Gases.* Dekker (1990)
- Sloan, E. D. Jr. Conference Overview. *Ann. N.Y. Acad. Sci.* **715** (1994)
- Sloan, E. D., Fleyfel, F. A Molecular Mechanism for Gas Hydrate Nucleation from Ice. *AIChE J.* **37**, 1281 (1991)
- Song, K. Y., Kobayashi, R. Final Hydrate Stability Conditions of a Methane and Propane Mixture in the Presence of Pure Water and Aqueous Solutions of Methanol and Ethylene Glycol. *Fluid Phase Equil.* **47**, 295 (1989)
- Song, K. Y., Kobayashi, R. The Water Content of Ethane, Propane and their Mixtures in Equilibrium with Liquid Water or Hydrates. *Fluid Phase Equil.* **95**, 281 (1994)
- Stillinger, F. H. Water Revisited. *Science.* **209**, 451 (1980)
- Swaminathan, S., Harrison, S. W., Beveridge, D. L. *J. Am. Chem. Soc.* **100**, 5705 (1977)

- van der Waals, J. H., Platteeuw, J. C. Clathrate Solutions. *Adv. Chem. Phys.* **2**, 1 (1959)
- Villard, P. *Compt. Rend.* **106**, 1602 (1888)
- von Stackelberg, M. Solid Gas Hydrates. *Naturwiss.* **36**, 327,359 (1949)
- von Stackelberg, M., Muller, H. R. On the Structure of Gas Hydrates. *J. Chem. Phys.* **19**, 1319 (1951)
- Vysniauskas, A., Bishnoi, P. R. A Kinetic Study of Methane Hydrate Formation. *Chem. Eng. Sci.* **38**, 1061 (1983)
- Vysniauskas, A., Bishnoi, P. R. Kinetics of Ethane Hydrate Formation. *Chem. Eng. Sci.* **40**, 299 (1985)
- Wiebe, R., Gaddy, V. L. The Solubility of Carbon Dioxide in Water at Various Temperatures from 12 to 40° and at Pressures to 500 atm. Critical Phenomena. *J. Am. Chem. Soc.* **62**, 815 (1940)
- Yousif, M. H., Dorshow, R. B., Young, D. B. Testing of Hydrate Kinetic Inhibitors Using Laser Light Scattering Technique. *Ann. N.Y. Acad. Sci.* **715** (1994)